

การแตกตัวเชิงแรงพอลิโพรพิลีนและพอลิเอทิลีนแรงปฏิกิริยาด้วยเซอร์โคเนียมออกไซด์ฟิลลาร์
เคลย์



นางสาว มัทพู่เซาะห์ มะสาละ

สถาบันวิทยบริการ จุฬาลงกรณ์มหาวิทยาลัย

วิทยานิพนธ์นี้เป็นส่วนหนึ่งของการศึกษาตามหลักสูตรปริญญาวิทยาศาสตรมหาบัณฑิต


สาขาวิชาปิโตรเคมีและวิทยาศาสตร์พอลิเมอร์

คณะวิทยาศาสตร์ จุฬาลงกรณ์มหาวิทยาลัย

ปีการศึกษา 2551

ลิขสิทธิ์ของจุฬาลงกรณ์มหาวิทยาลัย

CATALYTIC CRACKING OF POLYPROPYLENE AND POLYETHYLENE USING ZIRCONIUM/ALUMINIUM OXIDE-
PILLARED CLAY



Miss Mahfuzah Masalaeh

สถาบันวิทยบริการ
จุฬาลงกรณ์มหาวิทยาลัย

A Thesis Submitted in Partial Fulfillment of the Requirements
for the Degree of Master of Science Program in Petrochemistry and Polymer Science

Faculty of Science

Chulalongkorn University

Academic Year 2008

Copyright of Chulalongkorn University

Thesis Title CATALYTIC CRACKING OF POLYPROPYLENE AND POLYETHYLENE
 USING ZIRCONIUM/ALUMINIUM OXIDE-PILLARED CLAY


By Miss Mahfuzah Masalaeh

Field of Study Petrochemistry and Polymer Science

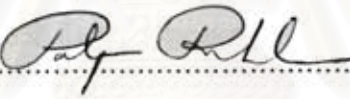
Advisor Nipaka Sukpirom, Ph.D.

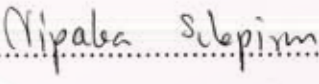
Co-Advisor Assistant Professor Soamwadee Chaianansutcharit, Ph.D.


Accepted by the Faculty of Science, Chulalongkorn University in Partial
Fulfillment of the Requirements for the Master 's Degree


.....Dean of the Faculty of Science
(Professor Supot Hannongbua., Dr.rer.nat.)

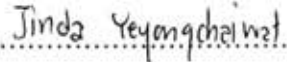
THESIS COMMITTEE

.....Chairman
(Professor. Pattarapan Prasassarakich, Ph.D.)

..... Advisor
(Nipaka Sukpirom, Ph.D.)

.....Co-Advisor
(Assistant Professor Soamwadee Chaianansutcharit, Ph.D.)

..... Examiner
(Associate Professor Wimonrat Trakarnpruk, Ph.D.)

.....External Examiner
(Assistant Professor Jinda Yeyongchaiwat, Ph.D.)

มหัพพะระห์ มะสาและ:การแตกตัวเชิงเร่งพอลิโพรพิลีนและพอลิเอทิลีนเร่งปฏิกิริยาด้วยเซอร์โคเนียม อะลูมิเนียมออกไซด์ฟิลลาร์เคลย์. (CATALYTIC CRACKING OF POLYPROPYLENE AND POLYETHYLENE USING ZIRCONIUM/ALUMINIUM OXIDE-PILLARED CLAY) อ. ที่ปรึกษา วิทยานิพนธ์หลัก : คร.นิปกา สุขภิรมย์, อ. ที่ปรึกษาวิทยานิพนธ์ร่วม : ผศ. ดร.ไสมวดี ไชยอนันต์สุจริต, 106หน้า.

อะลูมิเนียมออกไซด์ฟิลลาร์เคลย์เตรียมโดยการแทรกโมเลกุลของอะลูมิเนียมสปีซีเข้าไประหว่างชั้นของเคลย์ซึ่งเป็นสารตั้งต้นที่ผ่านการทำให้บริสุทธิ์ จากนั้นไปเผาที่อุณหภูมิที่อุณหภูมิ 500 องศาเซลเซียส เป็นเวลา 1 ชั่วโมง และทำการอิมเพกเนคเซอร์โคเนียมลงไปโดยจะทำการเปลี่ยนแปลงในช่วง 0 ถึง 5 เปอร์เซ็นต์ แล้วนำไปเผาที่อุณหภูมิ 450 องศาเซลเซียส เป็นเวลา 4 ชั่วโมง ค่า d_{001} , พื้นที่ผิว, ปริมาณของอะลูมิเนียมและการสั่นของพันธะในสภาวะแวดล้อมที่ต่างกันจะทำการวิเคราะห์โดยใช้เทคนิค การเลี้ยวเบนของรังสีเอกซ์, การดูดซับในโครเจน, ไอซีทีเออีเอสและเอฟทีไออาร์ตามลำดับ สำหรับค่า d_{001} และพื้นที่ผิวของอะลูมิเนียมออกไซด์ฟิลลาร์เคลย์เท่ากับ 16.3 องศาและ 189 ตารางเมตรต่อน้ำหนักสาร 1 กรัม ได้ทดสอบความว่องไวของปฏิกิริยาของตัวเร่งปฏิกิริยาดังกล่าวโดยการแตกย่อยเม็ดพลาสติกชนิดพอลิโพรพิลีนและ โพลีเอทิลีน อุณหภูมิที่ใช้ในการทำปฏิกิริยาจะทำในช่วง 350 ถึง 450 องศาเซลเซียส และจะทำการศึกษาภาวะต่างๆที่มีผลต่อปฏิกิริยา เช่น เวลาของการเกิดปฏิกิริยา อุณหภูมิที่ใช้ในการเกิดปฏิกิริยา เปอร์เซ็นต์ของเซอร์โคเนียมที่อิมเพกบนตัวเร่งปฏิกิริยา และอัตราส่วนของตัวเร่งปฏิกิริยาต่อปริมาณของพอลิเมอร์ ภาวะที่เหมาะสมสำหรับการแตกย่อยพอลิโพรพิลีนคือเวลาที่ทำปฏิกิริยา 1 ชั่วโมง อุณหภูมิที่ใช้เท่ากับ 380 องศาเซลเซียส เปอร์เซ็นต์ของเซอร์โคเนียมเท่ากับ 2 เปอร์เซ็นต์และอัตราส่วนระหว่างตัวเร่งปฏิกิริยากับเม็ดพลาสติกเท่ากับ 10 เปอร์เซ็นต์ ผลิตภัณฑ์ที่เป็นแก๊สจะมีความจำเพาะเจาะจงต่อ C_5 , และโพรพินส่วนผลิตภัณฑ์ที่เป็นของเหลวมีความจำเพาะเจาะจงต่อ C_7 ถึง C_{10} ซึ่งมีจุดเดือดอยู่ในช่วงของแก๊สอินมาทรฐาน และภาวะที่เหมาะสมสำหรับการแตกย่อยพอลิเอทิลีนคือเวลาที่ทำปฏิกิริยา 1 ชั่วโมง 30 นาที อุณหภูมิที่ใช้เท่ากับ 410 องศาเซลเซียส เปอร์เซ็นต์ของเซอร์โคเนียมเท่ากับ 2 เปอร์เซ็นต์และอัตราส่วนระหว่างตัวเร่งปฏิกิริยากับเม็ดพลาสติกเท่ากับ 10 เปอร์เซ็นต์ ผลิตภัณฑ์ที่เป็นแก๊สจะมีความจำเพาะเจาะจงต่อ C_5 , นอร์มอลบิวเทน, อีเทน, มีเทนและโพรพินส่วนผลิตภัณฑ์ที่เป็นของเหลวมีความจำเพาะเจาะจงต่อ C_7 ถึง C_{10} ซึ่งมีจุดเดือดอยู่ในช่วงของแก๊สอินมาทรฐาน

สาขาวิชา.....ปิโตรเคมีและวิทยาศาสตร์พอลิเมอร์.....ลายมือชื่อนิสิต.....*ณัฐพร วัฒน*.....*ณัฐพร วัฒน*.....

ปีการศึกษา.....2551.....ลายมือชื่อ อ.ที่ปรึกษาวิทยานิพนธ์หลัก.....*ดร.นิปก*.....
ลายมือชื่อ อ.ที่ปรึกษาวิทยานิพนธ์ร่วม.....*ดร.ไสมวดี ไชยอนันต์สุจริต*.....

4872418423: MAJOR PETROCHEMISTRY AND POLYMER SCIENCE

KEY WORDS: aluminium oxide-pillared clay / zirconium/aluminium oxide-pillared clay / CATALYTIC CRACKING / PE / PP

MAHFUZAH MASALAEH: CATALYTIC CRACKING OF POLYPROPYLENE AND POLYETHYLENE USING ZIRCONIUM/ALUMINIUM OXIDE-PILLARED CLAY. ADVISOR :NIPAKA SUKPIROM, Ph.D. COADVISOR :ASST. PROF. SOAMWADEE CHAIANANSUTCHARIT, Ph.D., 106 pp.

Aluminium oxide-pillared clay was prepared by intercalation between ionic precursors and raw clay suspensions with any previous purification and homoionisation of clay prior to pillaring. The intercalated product was calcined at 500°C for 1h. And then was impregnated with various amounts of zirconium (from 0.0 to 5.0 wt%) by slurry method and calcined at 450°C for 4h. The basal spacing, the surface area, the aluminium contents and the vibrational of chemical bonds in different environments were determined by XRD, N₂-BET, ICP-AES and IR respectively. The synthesized aluminium oxide-pillared clay had a basal spacing and surface area of 16.3 Å and 189 m²g⁻¹. The basal spacings of zirconium doped aluminium oxide-pillared clays (zirconium/aluminium oxide-pillared clays) at 15.6 Å were lower than aluminium oxide-pillared clay. Increasing amount of zirconium, the surface area decreased from 188 to 131 m²g⁻¹. When compared catalytic cracking reaction between two type of polymer observed that polyethylene more difficult than polypropylene. When aluminium oxide-pillared clay and zirconium/aluminium oxide-pillared clays were used as catalysts, the conversions of both polymers greatly increased compared to that in the absence of a catalyst. The cracking reaction was carried out in a semi-batch reactor with a mixture of catalyst and plastic at 350–450°C. The effects of reaction temperature, reaction time, type of catalyst and catalyst per plastic ratio were discussed. The activity and selectivity of catalysts modified by impregnation of zirconium were higher than the original clay catalyst. Gaseous and liquid hydrocarbon products were analysed by GC. The optimal condition for PP cracking was reaction time of 1.0 h, reaction temperature of 380°C, 2.0wt% zirconium/aluminium oxide-pillared clay as a catalyst and 10.0 wt% catalyst per plastic ratio. The major components of gas fraction were C₅₊ and C₃ (propene). Liquid fractions were in the range of C₇ to C₉ with the boiling point range compared to that of standard gasoline. The optimal condition for PE cracking was reaction time of 1.5 h, reaction temperature of 410 °C, 2.0wt% zirconium/aluminium oxide-pillared clay and 10.0 % catalyst per plastic ratio. The major components of gas fractions were C₅₊, C₄(n-butane), C₃ (propene), C₂(ethane) and C₁(methane). Liquid fractions were in the range of C₇ to C₁₀.

สถาบันวิทยบริการ
จุฬาลงกรณ์มหาวิทยาลัย

Field of Study: Petrochemistry and Polymer Science Student's Signature : Mahfuzah MasalaeH
Academic Year:2008..... Advisor's Signature : Nipaka Sukpirom
Co-Advisor's Signature : Soamwadee Chaiansutcharit

ACKNOWLEDGEMENTS

The success of this thesis can be attributed to the extensive support and assistance from Dr. Nipaka Sukpirom and Assistant Professor Dr. Soamwadee Chaianansutcharit, my thesis advisor and thesis committee. I deeply thank them for their valuable advice and guidance in this research and their kindness throughout this study.

I would like to gratitude to Professor Dr. Pattarapan Prasassarakich and Associate Professor Dr. Wimonrat Trakarnpruk as the chairman and member of this thesis committee, respectively, for all of their kindness and useful advice in the research.

I would like to gratefully thank PTT Chemical Public Company Limited for supporting the standard mixtures for GC analysis. I would like to gratefully thank CERNIC INTERNATIONAL CO., LTD for supporting bentonite clay. Moreover, I would like to thank Department of Chemistry and Program of Petrochemistry and Polymer Science, Faculty of Science, Chulalongkorn University for the valuable knowledge and experience. I would like to thank the Graduate School Chulalongkorn University for supporting a research fund. In addition, Thailand Japan Technology Transfer Project supported a loan by Japan Banks for International Cooperation (TJTTP-JBIC) for instrument support. Furthermore, I would like to thank the member of Materials Chemistry and Catalysis Research Unit for consideration and generosity.

For all of my friends, I greatly appreciate help and encouragement throughout the course of my research and study.

สถาบันวิทยบริการ
จุฬาลงกรณ์มหาวิทยาลัย

CONTENTS

	Page
ABSTRACT IN THAI.....	iv
ABSTRACT IN ENGLISH.....	v
ACKNOWLEDGEMENTS.....	vi
CONTENTS.....	vii
LIST OF TABLES.....	xi
LIST OF FIGURES.....	xiii
LIST OF SCHEMES.....	xvii
LIST OF ABBREVIATIONS.....	xviii
CHAPTER I INTRODUCTION.....	1
1.1 Background.....	1
1.2 Literature Review.....	6
1.3 Objective.....	10
CHAPTER II THEORY.....	12
2.1 Clay.....	12
2.2 Structural Feature of Clay.....	12
2.2.1 Tetrahedral Sheets.....	12
2.2.2 Octahedral Sheets.....	13
2.3 Classification.....	13
2.4 Smectite Clay.....	14
2.5 Bentonite.....	14
2.6 Properties of Clay.....	16
2.6.1 Ion Exchange.....	16
2.6.2 Swelling.....	17
2.6.3 Acidity.....	17
2.7 Intercalation.....	18
2.8 Pillaring.....	18
2.9 Pillaring Agent.....	19
2.10 Pillared Clay.....	19

	Page
2.11 Impregnation.....	20
2.12 Dialysis.....	20
2.13 Characterization of Clay Catalyst.....	21
2.13.1 Powder X – ray Diffraction.....	21
2.13.2 Inductively Coupled Plasma-Atomic Emission Spectroscope (ICP-AES).....	22
2.13.3 Nitrogen Adsorption – Desorption Isotherm.....	23
2.13.4 FTIR Spectroscopy.....	25
2.14 The Refining Process.....	26
2.15 Catalytic Cracking Mechanisms.....	29
2.15.1 General Cracking Mechanisms.....	29
2.15.2 Reactions of Olefins.....	30
2.15.3 Reaction of Paraffins.....	31
 CHAPTER III EXPERIMENTS.....	 33
3.1 Equipment and Apparatus.....	33
3.2 Chemical and Starting Materials.....	38
3.2.1 Clays.....	38
3.2.2 Chemicals.....	38
3.3 Homoionic Clays.....	39
3.4 Synthesis of Aluminium Oxide– Pillared Clay.....	40
3.5 Synthesis of Zirconium/Aluminium Oxide– Pillared Clay.....	41
3.6 Sample Preparation for ICP-AES.....	41
3.7 Activity of Aluminium Oxide-Pillared Clay Catalysts in PP Cracking.....	41
3.7.1 Effect of Reaction Time.....	41
3.7.2 Effect of Reaction Temperature.....	43
3.7.3 Effect of Zirconium Doped Aluminium Oxide-Pillared Clay (Zirconium/Aluminium Oxide-Pillared Clay).....	43
3.7.4 Effect of Catalyst per Plastic Ratio.....	45
3.8 Activity of Various Aluminium Oxide-Pillared Clays Catalyst in PE Cracking.....	45

	Page
3.8.1 Effect of Reaction Time.....	45
3.8.2 Effect of Reaction Temperature.....	45
3.8.3 Effect of Zirconium Doped Aluminium Oxide-Pillared Clay(Zircinium/Aluminium Oxide-Pillared Clay).....	45
3.8.4 Effect of Catalyst per Plastic Ratio.....	45
 CHAPTER IV RESULTS AND DISCUSSION.....	 47
4.1 The Characterization of Clay Catalysts.....	47
4.1.1 X – Ray Diffraction (XRD).....	47
4.1.1.1 The Characterization of Raw Clay.....	47
4.1.1.2 The Purification of Purified-Clay.....	47
4.1.1.3 The Preparation and Characterization of Na-Clay.....	47
4.1.1.4 The Characterization of Aluminium Oxide-Pillared Clay by XRD.....	48
4.1.1.5 The Preparation and Characterization of Zirconium/Aluminium Oxide-Pillared Clay.....	50
4.1.2 Fourier Transform Infrared Spectroscopy (FT-IR).....	53
4.1.3 Inductively Coupled Plasma-Atomic Emission Spectroscopy (ICP-AES).....	54
4.1.4 Nitrogen Adsorption-Desorption (BET).....	55
4.2 Activity of Aluminium Oxide-Pillared Clay and Zirconium/Aluminium Oxide-Pillared Clay Catalysts in PP Cracking.....	57
4.2.1 Effect of Reaction Time.....	57
4.2.2 Effect of Reaction Temperature.....	62
4.2.3 Effect of Zirconium Doped Aluminium Oxide-Pillared Clay (Zirconium/Aluminium Oxide-Pillared Clay).....	66
4.2.4 Effect of Catalyst to Plastic Ratio.....	69
4.3 Activity of Aluminium Oxide-Pillared Clay and Zirconium/Aluminium Oxide-Pillared Clay Catalysts in PE Cracking.....	73
4.3.1 Effect of Reaction Time.....	73

	Page
4.3.2 Effect of Reaction Temperature.....	77
4.3.3 Effect of Zirconium Doped Aluminium Oxide -Pillared Clay (Zirconium/Aluminium Oxide -Pillared Clay).....	81
4.3.4 Effect of Catalyst to Plastic Ratio.....	84
 CHAPTER V CONCLUSIONS.....	 88
5.1 Conclusions.....	88
5.2 Suggestions for Future Work.....	89
 REFERENCES.....	 90
APPENDICES.....	95
VITAE.....	106



สถาบันวิทยบริการ
จุฬาลงกรณ์มหาวิทยาลัย

LIST OF TABLES

Table	Page
2.1 Features of adsorption	24
2.2 IUPAC classification of pores	24
3.1 Bentonite composition	38
4.1 The d_{001} spacing of aluminium oxide-pillared clay and 1.0wt% zirconium/aluminium oxide-pillared clay to 5.0wt% zirconium/aluminium oxide-pillared clay	51
4.2 FTIR frequencies of major bands in raw clay, Na-clay and aluminium oxide-pillared clay	53
4.3 The aluminium contents in clay and aluminium oxide-pillared clay	55
4.4 The BET specific surface area of raw clay, purified-clay, Na-clay, aluminium oxide-pillared clay, ZrO_2 and Al_2O_3	56
4.5 The BET specific surface area of Al_2O_3 , ZrO_2 , aluminium oxide-pillared clay and 1.0wt% zirconium/aluminium oxide-pillared clay to 5.0wt% zirconium/aluminium oxide-pillared clay	57
4.6 %Conversion, %yield and %selectivity of liquid fraction obtained by thermal and catalytic cracking of PP over aluminium oxide-pillared clay catalyst with various reactions times	58
4.7 %Conversion, %yield and %selectivity of liquid fraction obtained by thermal and catalytic cracking of PP over aluminium oxide-pillared clay with various reaction temperatures	63
4.8 Conversion, %yield and %selectivity of liquid fraction obtained by thermal and catalytic cracking of PP over zirconium/aluminium oxide-pillared clay with various percent zirconium	67
4.9 %Conversion, %yield and %selectivity of liquid fraction obtained by thermal and catalytic cracking of PP over Al/2.0wt%Zr-pillared clay with various	70
4.10 %Conversion, %yield and %selectivity of liquid fraction obtained by thermal and catalytic cracking of PE over aluminium oxide-pillared clay catalyst with various	74

Table	Page
4.11 %Conversion, %yield and %selectivity of liquid fraction obtained by thermal and catalytic cracking of PE over aluminium oxide-pillared clay with various reaction temperatures.....	77
4.12 %Conversion, %yield and %selectivity of liquid fraction obtained by thermal and catalytic cracking of PE over zirconium/aluminium oxide-pillared clay with various percent zirconium.....	81
4.13 %Conversion, %yield and %selectivity of liquid fraction obtained by thermal and catalytic cracking of PE over 2.0wt% zirconium/aluminium oxide-pillared clay with various percent catalyst per plastic ratios.....	84



สถาบันวิทยบริการ
จุฬาลงกรณ์มหาวิทยาลัย

LIST OF FIGURES

Figure	Page
1.1 Global consumer packaging split by material.....	1
1.2 Global plastic consumption.....	2
1.3 Distribution of the thermoplastic demand in South East Asia 2004.....	2
1.4 Demand for thermoplastic in South East Asia 2004.....	3
2.1 (1) A single tetrahedral silica unit, and a (2) sheet structure	12
2.2 (1) A single octahedral alumina unit, and a (2) sheet structure	13
2.3 1:1 Layer and 2:1 layer type formed by linked tetrahedral and octahedral sheets.....	14
2.4 The structure of bentonite.....	15
2.5 The exchange properties of cations with clays.....	16
2.6 The principle of pillaring a clay with oxide particle.....	18
2.7 Simple Design of Pillared and Pore.....	19
2.8 Diffraction of X-ray by regular planes of atom.....	21
2.9 ICP-AES spectrometer.....	23
2.10 The IUPAC classification of adsorption isotherms.....	24
2.11 This simplified drawing shows many of a refinery's most important processes.....	27
3.1 Apparatus for catalytic activity test in polymer degradation.....	37
3.2 Dialysis apparatus.....	39
3.3 Apparatus for catalytic cracking.....	43
3.4 Apparatus for vacuum distillation.....	44
4.1 XRD pattern of raw clay.....	48
4.2 XRD patterns of raw clay and purified-clay.....	49
4.3 XRD patterns of purified-clay and Na-clay.....	49
4.4 XRD patterns of Na-clay and aluminium oxide-pillared clay.....	50
4.5 XRD patterns of Al ₂ O ₃ , ZrO ₂ , aluminium oxide-pillared clay and 1.0wt% zirconium/Aluminium oxide-pillared clay to 5.0wt% zirconium/aluminium oxide-pillared clay.....	52

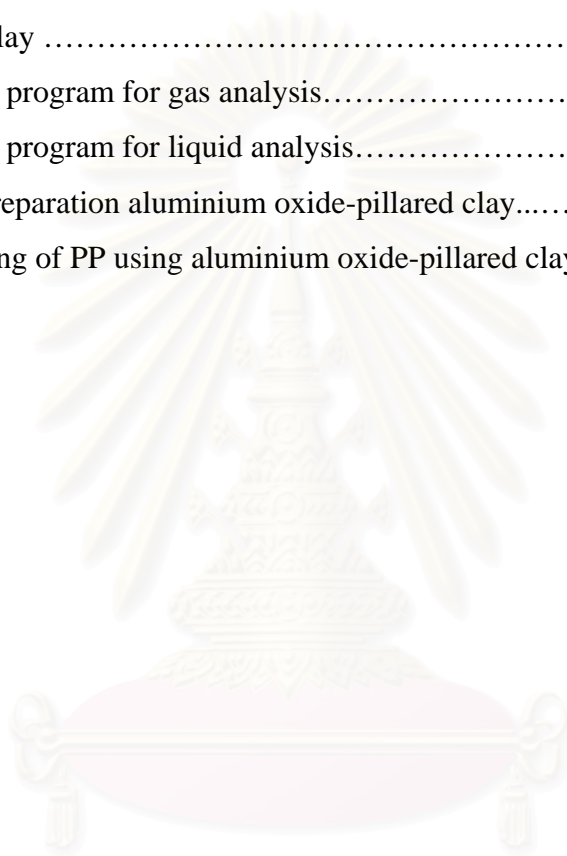
Figure	Page
4.6 FTIR spectra of (a) raw clay, (b) Na-clay and (c) aluminium oxide-pillared clay.....	54
4.7 N ₂ adsorption-desorption isotherm of Na-clay.....	56
4.8 Accumulative volume of liquid fraction obtained by thermal and catalytic cracking of PP over aluminium oxide-pillared clay catalyst with various reaction times.....	59
4.9 Distribution of gas fraction obtained by the thermal and catalytic cracking of PP with various reaction times.....	60
4.10 Carbon number distribution of distillate oil obtained by thermal and catalytic cracking of PP over aluminium oxide-pillared clay catalyst with various reaction times.....	61
4.11 Carbon number distribution of commercial SUPELCO standard gasoline fraction.....	62
4.12 Accumulative volume of liquid fractions obtained by thermal and catalytic cracking of PP over aluminium oxide-pillared clay catalyst with various reaction temperatures.....	64
4.13 Distribution of gas fractions obtained by the thermal and catalytic cracking of PP over aluminium oxide-pillared clay with various reaction temperatures.....	65
4.14 Carbon number distribution of distillate oil obtained by thermal and catalytic cracking of PP over aluminium oxide-pillared clay with various reaction temperatures.....	66
4.15 Accumulative volume of liquid fraction obtained by thermal and catalytic cracking of PP over zirconium/aluminium oxide-pillared clay with various percent zirconium.....	68
4.16 Distribution of gas fractions obtained by the thermal and catalytic cracking of PP over zirconium/aluminium oxide-pillared clay with various percent zirconium.....	68

Figure	Page
4.17 Carbon number distribution of distillate oil obtained by catalytic cracking of PP over zirconium/aluminium oxide-pillared clay with various percent zirconium.....	69
4.18 %Conversion at various percent catalyst to plastic ratio.....	71
4.19 Accumulative volume of liquid fraction obtained by thermal and catalytic cracking of PP over 2.0wt%zirconium/aluminium oxide-pillared clay with various percent catalyst per plastic ratio.....	72
4.20 Distribution of gas fraction obtained by the thermal and catalytic cracking of PP over 2.0wt%zirconium/aluminium oxide-pillared clay with various percent catalyst per plastic ratio.....	72
4.21 Carbon number distribution of distilled oil obtained by catalytic cracking of PP over 2.0wt%zirconium/aluminium oxide-pillared clay with various percent catalyst per plastic ratio.....	73
4.22 Accumulative volume of liquid fraction obtained by thermal and catalytic cracking of PE over aluminium oxide-pillared clay catalyst with various reaction times.....	75
4.23 Distribution of gas fraction obtained by the thermal and catalytic cracking of PE with various reaction times.....	76
4.24 Accumulative volume of liquid fractions obtained by thermal and catalytic cracking of PE over aluminium oxide-pillared clay catalyst with various reaction temperature.....	78
4.25 Distribution of gas fractions obtained by the thermal and catalytic cracking of PE over aluminium oxide-pillared clay with various reaction temperatures.....	79
4.26 Carbon number distribution of distillate oil obtained by thermal and catalytic cracking of PE over aluminium oxide-pillared clay with various reaction temperatures.....	80
4.27 Accumulative volume of liquid fraction obtained by thermal and catalytic cracking of PE over 2.0wt%zirconium/aluminium oxide-pillared clay with various percent zirconium.....	82

Figure	Page
4.28 Distribution of gas fractions obtained by the thermal and catalytic cracking of PE over 2.0wt% zirconium/aluminium oxide-pillared clay with various percent zirconium	82
4.29 Carbon number distribution of distillate oil obtained by catalytic cracking of PE over 2.0wt% zirconium/aluminium oxide-pillared clay with various percent zirconium.....	83
4.30 %Conversion at various percent catalyst to plastic ratio.....	85
4.31 Accumulative volume of liquid fraction obtained by thermal and catalytic cracking of PE over 2.0wt% zirconium/aluminium oxide-pillared clay various percent catalyst per plastic ratio.....	86
4.32 Distribution of gas fraction obtained by the thermal and catalytic cracking of PE over 2.0wt% zirconium/aluminium oxide-pillared clay with various percent catalyst per plastic ratio.....	86
4.33 Carbon number distribution of distilled oil obtained by catalytic cracking of PE over 2.0wt% zirconium/aluminium oxide-pillared clay with various percent catalyst per plastic ratio.....	87

LIST OF SCHEMES

Scheme	Page
3.1 The heating program used for calcinations of aluminium oxide-pillared clay.....	34
3.2 The heating program used for calcinations of zirconium/aluminium oxide-pillared clay	34
3.3 The GC heating program for gas analysis.....	36
3.4 The GC heating program for liquid analysis.....	36
3.5 Main step for preparation aluminium oxide-pillared clay.....	40
3.6 Catalytic cracking of PP using aluminium oxide-pillared clay as catalyst..	44



สถาบันวิทยบริการ
จุฬาลงกรณ์มหาวิทยาลัย

LIST OF ABBREVIATIONS

BET	Brunauer-Emet-Teller
XRD	X-ray Diffraction
GC	Gas chromatography
ICP-AES	Inductively Coupled plasma-Atomic Emission Spectroscopy
FT-IR	Fourier Transform Infrared Spectroscopy
PP	Polypropylene
HDPE	Polyethylene
°C	degree Celsius
G	gram (s)
h	hour (s)
mg	milligram (s)
min	minute (s)
M	molar
%	percent
CEC	Cation Exchange Capacity
cm ⁻¹	Unit of wave number
meq	milli equivalent
FID	Frame Ionization Detector
Å	Angstrom

สถาบันวิทยบริการ
จุฬาลงกรณ์มหาวิทยาลัย

CHAPTER I

INTRODUCTION

1.1 Background

Plastic waste is raising very fast because of the increase in polymer product. This problem is serious to social and environment. Food and beverage packagings are the huge amount of plastic waste. Figure 1.1 shows materials use for packaging. Plastic packaging shows the highest amount for around 39% because of cover a wide variety of designs and extremely durable. Therefore, plastics are used in several applications and in substitute of previous material.

Figure 1.2 shows distribution of polymer consumption in the world. Polyethylene (PE) are the highest amount and follow by polypropylene (PP).

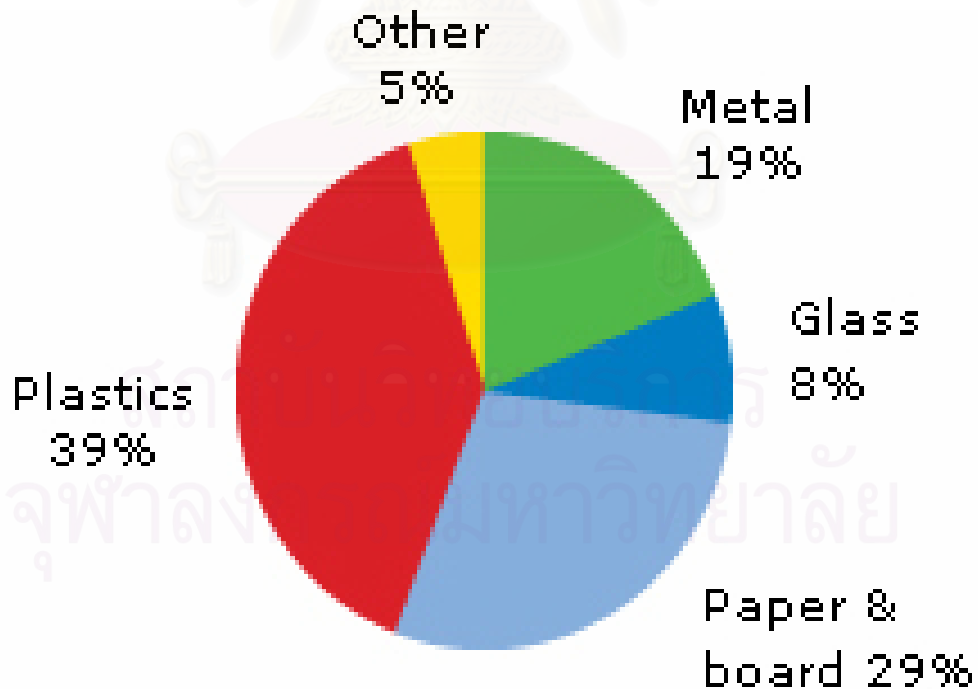


Figure 1.1 Global consumer packaging split by material [1].

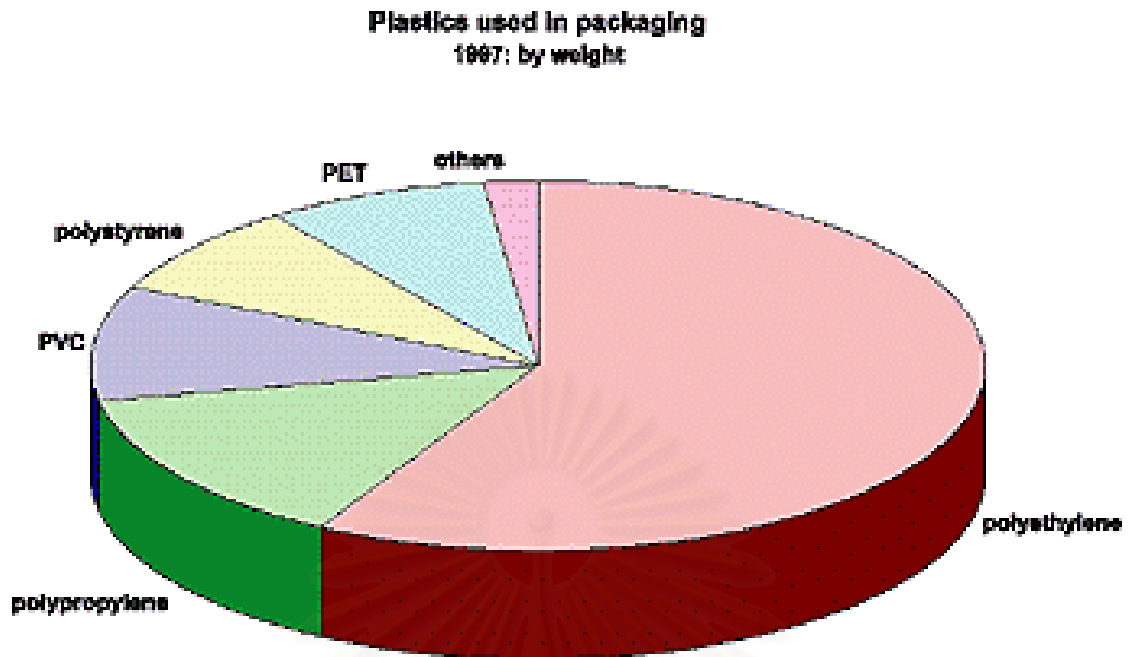


Figure 1.2 global polymer consumption [2].

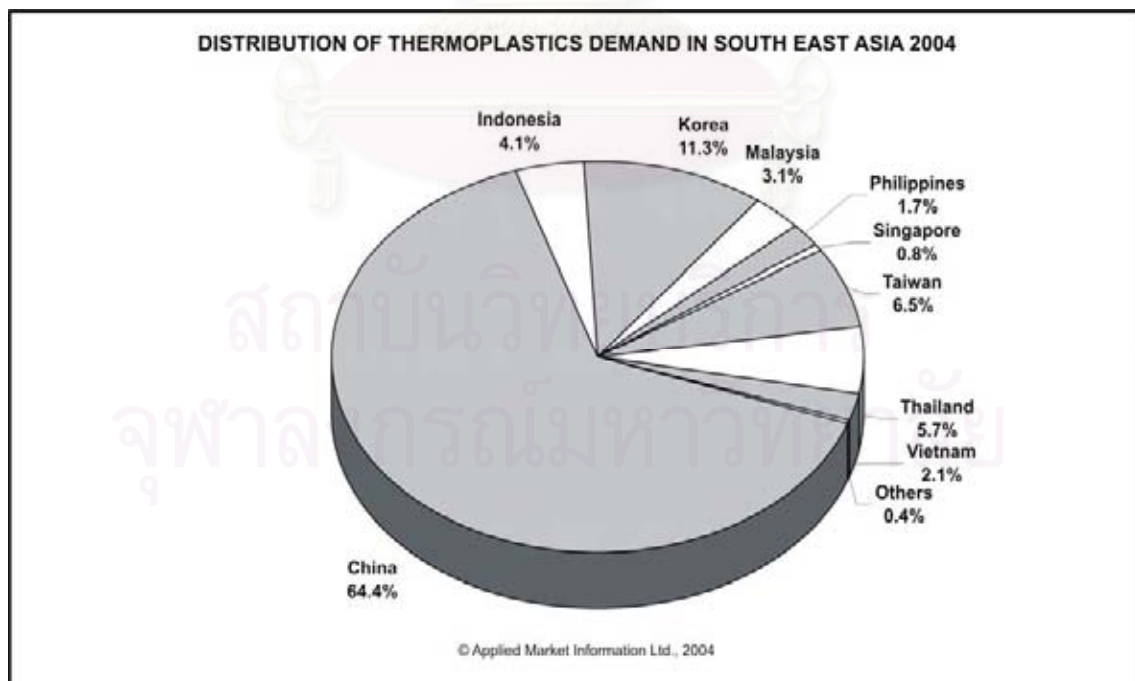


Figure 1.3 Distribution of the thermoplastic demand in South East Asia 2004 [3].

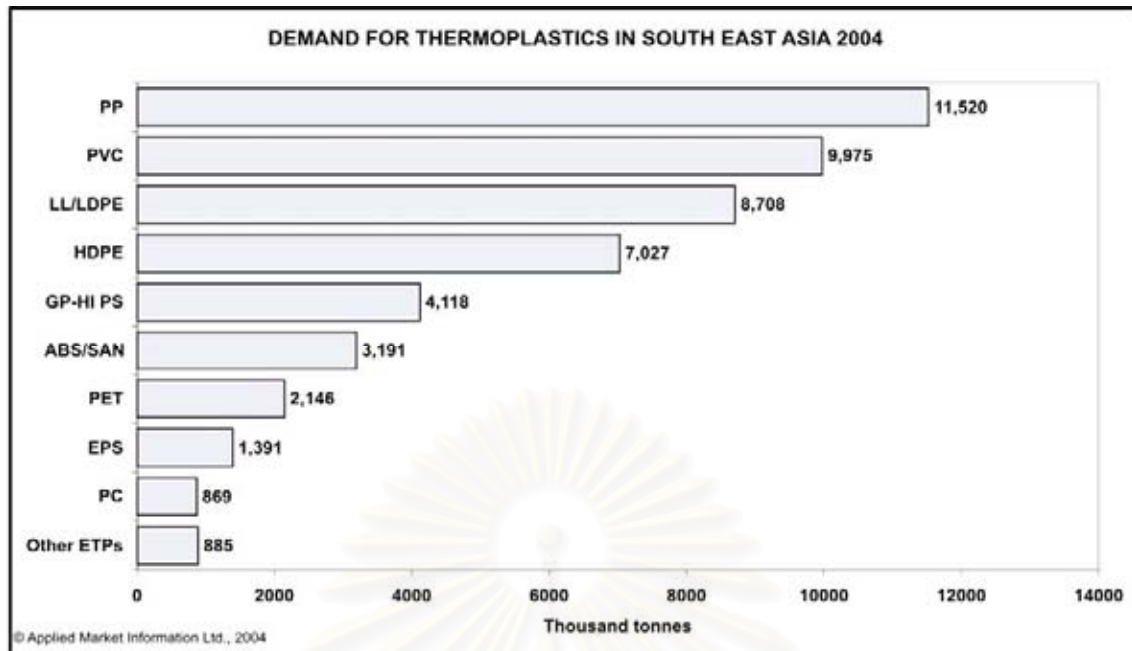


Figure 1.4 Demand for thermoplastic in South East Asia 2004 [3].

Demand for thermoplastics in South Asia

In 2004, Applied Market Information Ltd (AMI's) reported that, South Asia was the leader in global thermoplastic market. It was growing over 6%. Figure 1.3 shows distribution of the thermoplastic demand in South East Asia 2004. China showed the highest demand thermoplastic. Their showed around 65% of all polymer demand. Indonesia and Philippine confronted economic crisis and polymer price was high. Effect decreased polymer demand. Thailand and Malaysia increased import final product from China, effect increased polymer demand. South Korea, Taiwan and Singapore showed markets mature and a trend for plastics processing to move into China, Vietnam and other lower cost locations.

Figure 1.4 showed demand of all major thermoplastic in South Asia in 2004. Demand of three major thermoplastic increased in the order PP>PVC>PE. PP showed the highest demand from the powerful demand of commodity polymer such as the automotive and home appliances sectors. Demand of PVC increased, effect from increased in construction and manufacturing for a wide range of general household and consumer products. PVC market was China but also Malaysia and Indonesia. When demand of film applications was grewed, effect PE demand increased.

Government and environment foundations required to solution of large amount of plastic waste, because there is important point to environment pollution. There are many ways such as by landfill [4]. But nowadays, the consumption of plastic materials has been growing steadily and plastic waste being more voluminous than the organic waste. The problems are plastics used more time for degrade and landfill space is becoming scarce and expensive. Incineration is a new to solve this problem [4]. But there is disadvantage, as toxic gases are produce and solid waste problem becomes air pollution. The only sustainable way for solution is plastic recycling. There are four types of recycling processes such as : primary, secondary, tertiary and quaternary.

The primary recycling

This process is not widely used. It's only clean up the recycling material and ready for utilization. The recycling materials and products keep similar features of the original product.

Secondary recycling

The secondary process occurs by combination of plastic with other composition. The products from this recycling method shows low mechanical properties. That is the reason why the above products are created. Fence, posts and others are product from this process that can replacing previous materials such as ; wood, concrete and metal.

Tertiary recycling

Nowadays, tertiary recycling is favor because of need to rising worth of waste plastic. This process converts plastic waste into basic chemicals and fuel such as cracking reaction.

Quaternary recycling

Quaternary recycling converts waste plastic into energy by burning process at high temperature as 900 to 1000°C. The high heat content from burning method is the reason wildely use in this process. Disadvantage of this method is occurred air pollution such as ; toxic gases and solid waste. For the benefit of the environment the new techniques being used with the incinerators have decreased the amount of air pollutants being released. The use of incineration in the quaternary process is most beneficial because through the high temperature heating process the incoming waste is reduced by 80% in weight and 90% in volume. The remaining materials from this process are placed in landfills.

An alternative strategy is that of chemical recycling, which has attracted much interest recently with the aim of converting polymer waste into basic petrochemical is tertiary recycling. Two main chemical recycling routes are the thermal and catalytic cracking of plastic waste.

1. Thermal cracking involves the degradation of the polymeric materials by means of temperature when it is applied under inert atmosphere conditions [5]. In term of mechanism, it precedes a radical chain reaction pathway with hydrogen transfer step. Normally, no rearrangement reactions occur, while branched products are only formed in secondary reactions as result of the interaction two radicals. As a consequence, it produces a broad product range and required high operating temperature, typically more than 500°C and even up to 900°C.

2. Catalytic cracking involves several advantages over a purely thermal process. First, catalyst promotes the degradation reaction to occur at lower temperatures with lower energy consumptions. Second and most importantly, the shape selectivity allows the formation of narrower distribution of products, which may be directed towards light and aromatic hydrocarbons with higher market values. It provides to control the product distribution and reduce the reaction temperature. In such a catalytic cracking system, mainly zeolites have been used so far as acidic solid catalysts. Previous studies have suggested that the initial polyolefin degradation occurs mainly on the external surface of the catalyst. Only smaller fragments formed by this initial cracking can then enter the zeolite pore structure, where the majority of the active sites are located, to undergo further reactions. Because of the strong zeolitic acidity, severe over cracking takes place resulting into the formation of small molecules that are collected mainly in the gaseous fraction, increasing its yield. Hence the yield to liquid fuel decreases, which we consider as the most saleable product. We recently introduced pillared clays as well as their original analogues as catalysts for a polymer catalytic degradation process. Clay based catalysts possess much milder acidity than zeolites and have a bimodal pore structure including mesopores as well as micropores. Plastic catalytic cracking over these catalysts results in much less degree of overcracking and higher liquid yield.

The researchers have contributed to the theory and practice of thermal degradation (with or without catalyst) of polymers. Mainly polyolefins, polyethylene (PE) and polypropylene (PP) and polystyrene (PS), are the target polymer, because their cracking results in products with favourable properties for further application.

According to results the products of polyethylene, polypropylene and even polystyrene cracking have the most favourable properties for further energetic applications. PE derived fuel has very high cetane and octane number, because it is rich in linear paraffins and olefins. Linear paraffin content in the gas oil fraction is advantageous, because this hydrocarbon structure has the highest cetane rate, but also has the lowest octane number in the naphtha fraction. However, PE-derived naphtha like fraction has high octane number, which comes from the high content of the olefins. The liquid products of PP cracking contain primarily olefins and isoparaffins that resemble the molecular skeleton of PP. Both hydrocarbon structures are advantageous for further utilization. Neat PS feedstock will depolymerise in cracking processes to give predominately styrene monomer. Therefore, the fuel made from polystyrene feedstock will be high by aromatic character and have good energy content. The aromatic hydrocarbons have the highest octane number in the naphtha fraction [6].

1.2 Literature Review

K. Gobin *et al.* [7] studied the catalytic cracking of polyethylene over US-Y, ZSM-5, a 50-50 wt% US-Y/ZSM-5 mixture, two commercial cracking catalysts containing 20 and 40 % US-Y, saponite clay, montmorillonite clay, aluminium-pillared saponite and aluminium-pillared monmorillonite. The cracking reaction was performed in a semi-batch reactor. ZSM-5 zeolite produced gas fraction as a main product, low liquid fraction and no coking, that was explained by shape selectivity. Two commercial cracking catalysts containing 20 and 40 % US-Y showed higher liquid hydrocarbon and lower coke, comparing with parent US-Y. Two types of clay (saponite and montmorillonite) and their pillared clays were less active than zeolite. Cracking reaction under mild condition of clay and pillared clay catalyst gave high liquid hydrocarbon and low coke. Regeneration of two types of pillared clays (aluminium-pillared saponite and aluminium pillared montmorillonite) showed performance of catalyst be the same in fresh catalyst, but their original clays decomposed after removal of coke.

G. Manos *et al.* [8] studied the catalytic cracking of PE over two natural clays such as saponite and monmorillonite and their pillared clays such as aluminium-

pillared saponite (ATOS) and aluminium-pillared montmorillonite (AZA). Activity of clays and their pillared clays catalyst were less active than US-Y zeolite. But they were able to completely decomposed PE when slightly increased temperature. The yields to liquid product was around 70%, while US-Y zeolite showed less around 50%. The liquid product from clay catalyst was heavier than zeolite and distribution in range of gasoline. Attribution of this fact was by weaker acidity while strong acidity zeolite played overcracking. Furthermore, the high amount of alkenes as products over the clay catalyst was due to lower hydrogen-transfer secondary reaction. The milder acidity induced lower hydrogen-transfer secondary reactions compared to US-Y zeolite.

K. Gobin *et al.* [9] studied activation energy of PE cracking over montmorillonite, aluminium-pillared montmorillonite, aluminium-pillared saponite, two commercial cracking catalysts containing 20 and 40% US-Y respectively and US-Y zeolites. High density polyethylene (HDPE), linear low density polyethylene (LLDPE), low density polyethylene (LDPE) and polypropylene (PP) were used for studying the degradation of polymer in the absence of catalyst. LLDPE can be degraded at lower temperature when compared with other polymer. Commercial cracking catalysts showed higher activation energy than their parent US-Y zeolite as they contain only 20 and 40% of US-Y zeolite. The activation energy of polymer cracking over US-Y zeolite showed the lowest value due to the strongest acidity of this zeolite. The activation energy order was follows : US-Y zeolite < commercial cracking catalysts (20 and 40% US-Y) < clay and two pillared clays.

G. Manos *et al.* [10] studied the catalytic degradation of PE over Al pillared saponite, Al pillared montmorillonite, and their regenerated samples. Two types of pillared clays were completely cracking of PE. Gaseous and liquid fractions were product from catalytic cracking, with low amount of coke. The conversion over both fresh pillared clays were very high around 95% and selectivity to liquid was more than 70%. Regeneration of catalysts showed that conversion and selectivity were not different with fresh pillared clay samples. Furthermore, the hydrocarbons distribution were the same as the fresh samples. The boiling point distribution for the liquid fractions of Al pillared saponite, Al pillared montmorillonite and their regenerates showed in range of motor fuels.

J. Tae *et al.* [11] investigated the performance of acid-treated halloysite clay catalysts in the cracking of polystyrene (PS). The cracking temperature performed in

range of 400-450 °C. Acid-treated catalyst was varied for 1, 2, 3 and 4 M HCl at 400°C for 2h. Increasing HCl concentration, amount of liquid increased while residue decreased. All reactions showed liquid fraction as main products. Aromatic hydrocarbons were main products over 96 wt%. The increasing of HCl concentration from 1 to 3 M resulted as increase is ethylbenzene and the decrease of styrene. Increasing HCl concentration affected the specific surface area, pore volume and acidic sites.

H. Yang *et al.* [12] studied hydroprocessing of synthetic crude gas oil over Pt supported pillared clay and delaminated clays. This reaction was performed using a fixed-bed micro reactor between 260 and 380°C. Hydrocracking activity and selectivity to ring opening of Pt supported pillared clay and delaminated clays were compared. Under similar reaction conditions, Pt-supported pillared clays had higher hydrogenation and hydrocracking activities than Pt-supported delaminated clay. However, the delamination catalyst had a higher selectivity to diesel yield and less naphtha. Composition of liquid products also indicated that the Pt/pillared clay catalyst achieved ring opening of two- and three- ring naphthenes, while the Pt/delaminated clay converted only three-ring. Catalyst deactivation was evaluated by approximately 300 h time-on-stream. The surface area and pore size distributions measured by N₂-adsorption/desorption of fresh and used catalysts were compared to determine loss of micro porosity due to deposition of carbonaceous materials and possible changes on the catalyst structure.

George Manos *et al.* [13] explored the catalytic cracking of HDPE over ultrastable Y, Y, β zeolites, mordenite and ZSM-5 at 360°C. The structure of zeolite framework had shown a significant influence on the product distribution. Over large-pore such as USY, Y and β zeolites, alkanes are the main products with less amounts of alkenes and aromatics, and only very small amounts of cyclopalkanes and cycloalkenes. Medium-pore mordenite and ZSM-5 gave alkenes as major products. The hydrocarbons formed with medium-pore zeolites were lighter than those formed with large-pore zeolites. A order was found regarding the bond saturation: (more alkenes) ZSM-5 < mordenite < β < Y < USY (more alkanes).

F. Gonzalez [14] investigated preparation and characterization of Al- and Al/Ga-pillared clays. Activity test for both catalysts were cracking of heavy oil using a microactivity test (MAT). AlGa-pillared clay catalyst ($d_{001}=17.3 \text{ \AA}$; S_{BET} and V micropores remained around 85% at 700°C with respect to the pillared material)

showed property of higher thermal stability, surface area, micropore volume and surface acidity more than Al-pillared clay. The AlGa-pillared clay also showed higher gas oil cracking conversion and olefin production than the Al-pillared clay. The AlGa-pillared clay produced less gasoline and more gases and coke than the Al-pillared clay in all conversion range. This may be due to the dehydrogenating affected of Ga, which gave a higher amount of alkene. The gasoline of AlGa-pillared clay catalyst showed olefin content and the ratio butanes/butane (which was related to the octane number (RON)) higher than the Al-pillared clay.

S. Moreno [15] studied the textural, structural, and acidic properties of Zr- and Al/Zr-pillared clays by comparing with Al-pillared clay. Hydroconversion of heptane over platinum-doped samples was used to investigate the influence of the nature of the pillars and type of clay on the catalytic properties. The results were compared with Al-pillared clay forms of smectites. For the Zr-pillared clay, mixture of pillared and unpillared fractions were obtained in proportions depending on the preparation conditions. The pillared fractions exhibited poorer thermal resistance than the resemble Al-pillared forms. Mixed Al/Zr-pillared clay performed liked Al-pillared clay. The conversion of heptane over the Zr-pillared montmorillonite was substantially enhanced with respect to the Al-pillared analogues, due to the enhanced hydrogenolysis on platinum. Isomerisation activity drastically decreased. These change were less pronounced in the case of pillared saponites. Zr-pillared saponite with low tetrahedral charge showed an intermediated behavior.

Y. Sakata *et al.* [16] reported catalytic cracking of PE and PP using FSM, silica-alumina, ZSM-5, silicalite and silica gel as catalyst by batch operation at 430°C and 380°C. Comparison with thermal degradation, FSM catalyst accelerated the initial rate of degradation, increased the liquid product yield and promoted degradation into lower molecular weight products. Silicalite and silica-gel had very negligible effected on polymer degradation. When the batch reaction was repeated four times using FSM catalyst, the extent of the decline in the degradation rate was lower for PE and PP. Compared with the silica-alumina and ZSM-5, which turned completely black in the case of both PE and PP, the deposition of coke on the used FSM catalyst was related to the hexagonal pore structure system of FSM.

J. Aguado *et al.* [17] investigated the catalytic conversion of LDPE, HDPE and PP using Al-MCM-41, ZSM-5 and amorphous silica-alumina as catalyst. The catalytic cracking of HDPE and LDPE are investigated at 400°C in a batch reactor

with duration of 30 min. In the catalytic cracking of HDPE and LDPE, the highest activity was observed with ZSM-5 due to its stronger acidity. But in the catalytic conversion of PP, the Al-MCM-41 sample led to almost 100% conversion whereas the activity obtained with the ZSM-5 was very close to that of thermal cracking (11.3%). Moreover, for the cracking of LDPE, HDPE and PP, the selectivities toward hydrocarbons in the range of gasoline and middle distillates obtained over MCM-41 were clearly higher than those of ZSM-5. Therefore, MCM-41 was a potential catalyst for the conversion of polyolefinic plastic waste into liquid fuels.

In 2001, R. Van Grieken *et al.* [18] studied thermal and catalytic cracking of PE under mild conditions. The catalyst employed were n-HZSM-5, HY zeolite, amorphous silica-alumina, activated carbon, Pd charcoal and MCM-41. Thermal cracking between 360 °C and 420°C led to the solid yields. LDPE cracking was enhanced when catalyst was used. The high BET surface area, uniform mesoporosity and medium acid strength of MCM-41 promoted the polymer cracking according to a random scission mechanism, as well as, the hydrogen transfer reactions which reduced the olefinic character of the solid product. The use of HDPE yielded a solid with a higher homogeneity, and improved the properties of the waxy product for potential applications.

V. J. Fernandes, Jr. *et al.* [19] reported that thermal cracking of HDPE without catalyst gave rise to products distributed over a wide range of carbon atom numbers (C_5 - C_{26}), the main fraction was C_{10} - C_{15} (60.2%). The catalytic reaction led to lighter products (C_5 - C_{26}), predominantly in C_5 - C_9 (73.5%). This behavior was due to the strong acid sites of the ZSM-5 zeolite, which promoted the polymer chains cracking.

1.3 Objective

1. To synthesize and characterize aluminium oxide-pillared clay and zirconium/aluminium oxide-pillared clay catalyst
2. To comparison catalytic cracking reaction between polypropylene and polyethylene over aluminium oxide-pillared clay and zirconium/aluminium oxide-pillared clay
3. To study the effect of reaction time, reaction temperature, percent zirconium doped aluminium oxide-pillared clay and percent catalyst to plastic ratio in catalytic cracking of polypropylene and polyethylene

4. To study the optimal condition for catalytic cracking of polypropylene and polyethylene over aluminium oxide-pillared clay and zirconium/aluminium oxide-pillared clay catalyst



สถาบันวิทยบริการ
จุฬาลงกรณ์มหาวิทยาลัย

CHAPTER II

THEORY

2.1 Clay

Clay minerals occur abundantly in nature. They are the most common products of water-rock interaction under earth-surface conditions. The term of clay is generally defined as fine grained, crystalline and earthy material. The property of clays contain high surface area, high sorption, reversible ion-exchange and high acidity. Their structures consist of negatively charged layers with strong covalent bonding stacked in aggregates called tactoids and held together by electrostatic forces. The suspension of clay in aqueous solution contains particles with the average diameter of about 2 μm [20]. Clay shows two types of acid sites that are brønsted acid site and lewis acid site. The exploitation of clay acidity allows this materials to be use as catalysts.

2.2 Structural Feature of Clay

Clay minerals are aluminosilicates the negative charge layer structure and balancing cations in the interlayer space. Layer structure of clay is built from linked tetrahedral and octahedral sheets.

2.2.1 Tetrahedral Sheets

Tetrahedral sheet is formed by combining silica tetrahedral units. All the tops of the tetrahedra (the apical oxygen atoms) are at the same side of the sheet. This sheet extends infinitely in two dimension by each tetrahedron sharing three oxygen atom with three other tetrahedra to form hexagonal network. In tetrahedral sheet, the major cation is Si^{4+} but it is frequently substituted by Al^{3+} and occasionally by Fe^{3+} .

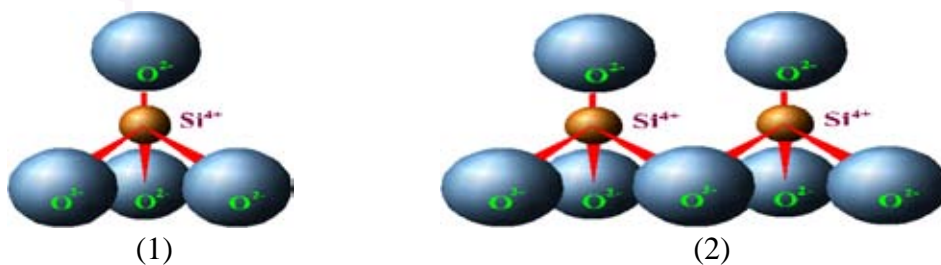


Figure 2.1 (1) A single tetrahedral silica unit, and a (2) sheet structure [21].

2.2.2 Octahedral Sheets

The tetrahedral layer is combined with an octahedral layer. Octahedral layer consists of alumina octahedral units. A positive cation is surrounded by six negative ions (Figure 2.2). The dominant cation is Al^{3+} but substituted frequently by Mg^{2+} and occasionally by Fe^{2+} and Fe^{3+} and the six corner negative charge ion are oxygen (O^{2-}) or hydroxyl groups (OH^-).

The octahedral units are combined in an octahedral layer just as in the case of tetrahedral sheet. The positive ion in the center of octahedral unit shares with the negative ones on the corners. The corner of each octahedron (thus each OH^- group or O^{2-} ion) in an octahedral layer is shared with 3 octahedral unit.

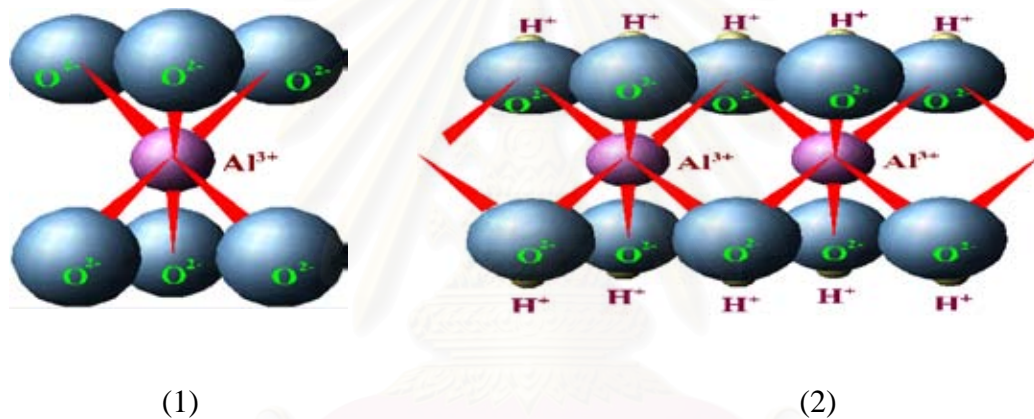


Figure 2.2 (1) A single octahedral alumina unit, and a (2) sheet structure [21].

2.3 Classification

The combination between tetrahedral and octahedral layers formed silicate sheets. Tetrahedral layer jointed with octahedral layer by sharing oxygen atom at the top of tetrahedral layer. So, O^{2-} at the corner of octahedral layer substitutes by OH^- . In this way, if one tetrahedral layer combines with one tetrahedral layer we called this minerals a 1:1 or t-o mineral (the open sandwich type) such as kaolinite. And if two tetrahedral layer combine with one octahedral layer we call this minerals a 1:2 or t-o-t minerals (hamburger type) such as bentonite, hectorite and monmorilonite. Thus we can divide clay minerals using the difference in layer structure into two types such as : t-o and t-o-t minerals as shown in Figure 2.3.

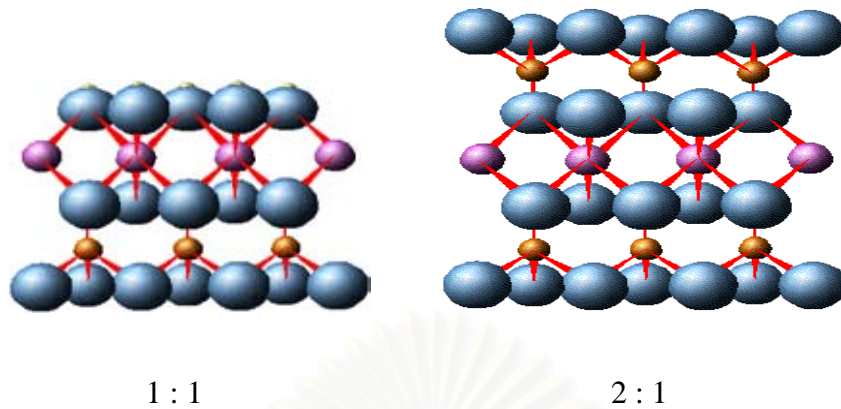


Figure 2.3 1:1 Layer and 2:1 layer type formed by linked tetrahedral and octahedral sheets [21].

2.4 Smectite Clay

Smectite clays are obtained from the mineral talc and pyrophyrite. The overlap of layer structure is composed of silica tetrahedral sheet ($\text{Mg}_6\text{Si}_8\text{O}_{20}(\text{OH})_4$) and alumina octahedral sheet ($\text{Al}_4\text{Si}_8\text{O}_{20}(\text{OH})$) [22]. Each layer of smectite clay consists of one octahedral sheet combined with two tetrahedral sheets (1 : 2 or t-o-t). Cation substitute in either the octahedral sheet (typically from the substitution of low charge species such as Mg^{2+} , Fe^{2+} , Mn^{2+} and Al^{3+}) or tetrahedral sheet (the substitute of Al^{3+} or occasionally Mn^{2+} substitutes for Si^{4+}) results in negative layered charge. The negative charge layer was balanced with cations in the interlayer space.

2.5 Bentonite

Bentonite clay is the member of smectite group. Beidellite, saponite and hectorite be the same in this group. The name “bentonite” is derived from the location of the first commercial deposits mined (Fort Benton), Wyoming U.S.A. Geologically bentonites are mainly of volcanic origin [23]. The outstanding of bentonite property is essentially a high swelling. Because attractive surfaces between the surface oxygen atoms of the silica tetrahedra and the hydrogen atoms of the water molecules develop.

This allows the hexagonal water structure to build up and form a rigid network made up of many water layers. The water structure extends outward from the platelet surface further increasing the separation of platelets. Bentonite principally consists of montmorillonite and impurities around 10 to 20 percent (such as feldspars, calcite, silica and gypsum). In the montmorillonite structure, the aluminium atoms are partially replaced by the substitution of either magnesium or iron atoms, causing the charge deficiency in the sheet structure. The charge is balanced by absorption of (exchangeable) cations between adjacent platelets. The natural balancing of cations between adjacent platelets of montmorillonites are calcium, sodium or magnesium as shown in Figure 2.4.

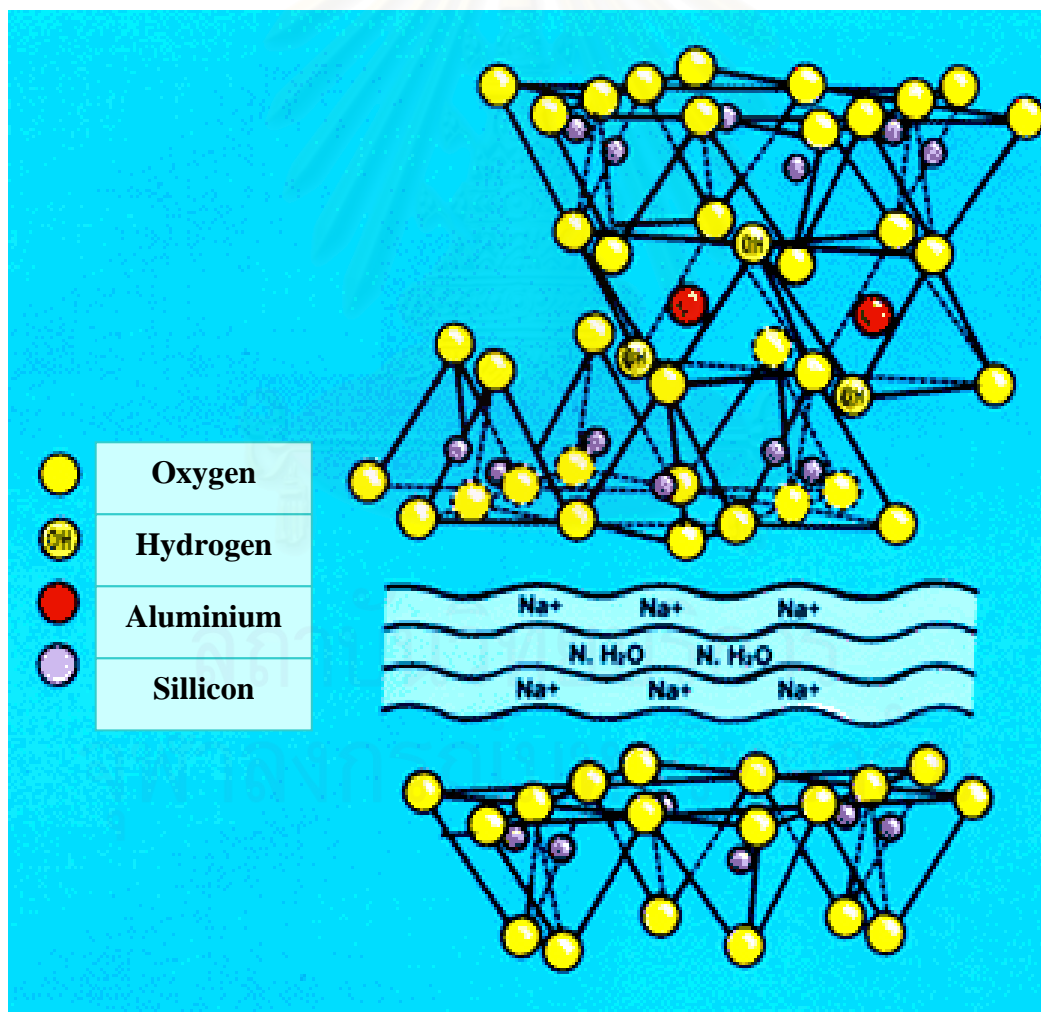


Figure 2.4 The schematic structure of bentonite [24].

2.6 Properties of Clay

2.6.1 Ion Exchange

Clays have the ability to adsorb and exchange cations from solution. In most clays, the ideal neutral structure is disrupted by introduction of charged imbalance into the clay sheets. Two main causes of these charged imbalance are (1) isomorphous substitution of cations in the lattice by lower valent ions, such as the substitution of aluminum cation for silicon in the tetrahedral layer, magnesium for aluminum or sometimes lithium for magnesium cations in the octahedral layer and crystal defects. The layers have an overall negative charge which is balanced by adsorption of metal cations into interlayer of the clay minerals. These balance cations can be readily replaced by other cations in aqueous solution. The property of ion exchange is great fundamental and practical importance in the investigation of clay minerals. In the application of clay mineralogy, it is important because the nature of the exchangeable ion may influence substantially the physical properties of the material.

Where a solution of a metal cation is used to exchange the interlayer cations of clay, it has been observed that the smaller the sized and the higher the charge of the exchange cation, the more powerful that cation at replacing the interlayer exchangeable cations. Similarly the ease of replacement of interlayer cations follows the reverse trend. The following series can be constructed:

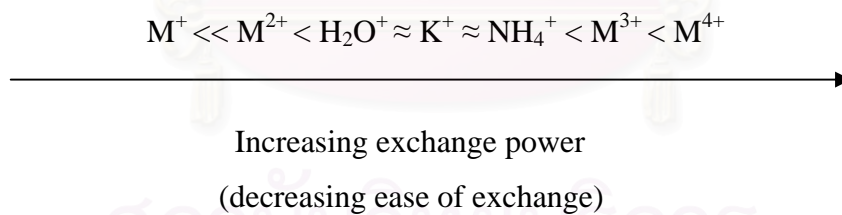


Figure 2.5 The exchange properties of cations with clays [23].

For the swelling clay minerals, such as smectites, the interlayer cations can be exchanged with cations from external solutions.

The concentration of exchangeable cations (CEC) is measured in milliequivalents per 100 g of dried clay. CEC is measured by uptake and release of ammonium ions from 1 M ammonium acetate solution, although other cations are sometimes used in place of NH_4^+ . Since smectites have the highest concentration of

interlayer cations, they have the highest cation exchange capacities (typically 70-120 mequic/100g). Structural defects at layer edges give rise to an additional CEC and a small amount of anion exchange capacity.

2.6.2 Swelling

Many clay minerals adsorb water between their layers, which move apart and the clay swells. The energy is released by the attractive forces, such as hydrogen bonding, between the adjacent layers from cations and/or layer salvation. Thus water forms strong hydrogen bonds with hydroxyl group on hydrophilic octahedral layers in 1 : 1 clay minerals (kaolinite), allowing swelling to occur [25].

With 2 : 1 clay minerals, the ability to swell depends on the salvation of interlayer cation and layer charge. Clay with 2 : 1 structure and low layer charge have very low concentration of interlayer cations and therefore do not swell readily. At the other extreme, those with very high layer charges have strong electrostatic forces holding alternate anionic layers and the interlayer cations together. For those with divalent, trivalent and polyvalent cations, swelling decrease accordingly. The extent of swelling can be observed by measuring interlayer separations using power X-ray diffraction.

2.6.3 Acidity

Clay minerals show both brønsted and Lewis acidity. The interlayer cations contribute to the acidity of clay minerals. Some of these cations may be protons or polarizing cations (*e.g.* Al^{3+}) which give rise to strong acidity. The higher electronegativity of M^+ , the strong acidic sites generated. Brønsted acidity also stems from the terminal hydroxyl group and from the bridging oxygen atoms. In addition, clay minerals have layer surface and edge defects, which would result in weaker brønsted and/or lewis acidity, generally at low concentrations.

A further source of acidity is associated with the $-\text{OH}$ groups of the octahedral layer which protrude into the interlayer region via the holes of the ring. The incidence of these protons may be increased by preparing a “proton exchange” clay [26]. This is achieved either a simply exchanging the clay with dilute acid, or less destructively to exchanging the clay with ammonium ions and calcining at 200-300°C to expel ammonia. The exchanged proton can migrate into vacancies on the octahedral layer where they protonate bridging oxygen.

2.7 Intercalation

Intercalation is the insertion of a guest species into the interlayer region of a layer solid, and the layer structure still remains. Intercalation compound was approved by the XRD pattern. The increasing of basal spacing reflects the expansion of inter layer structure.

2.8 Pillaring

Pillaring is the process, which made a layered compound is transformed into a pillared compound or a pillared layered solid. A pillared material is thermally stable, microporous and/or mesoporous with retention of the layer structure. A pillared derivative is distinguished from an ordinary intercalated by virtue of intercrystalline porosity made possible by the lateral separation of the intercalated compounds guest (see below; Figure 2.6).

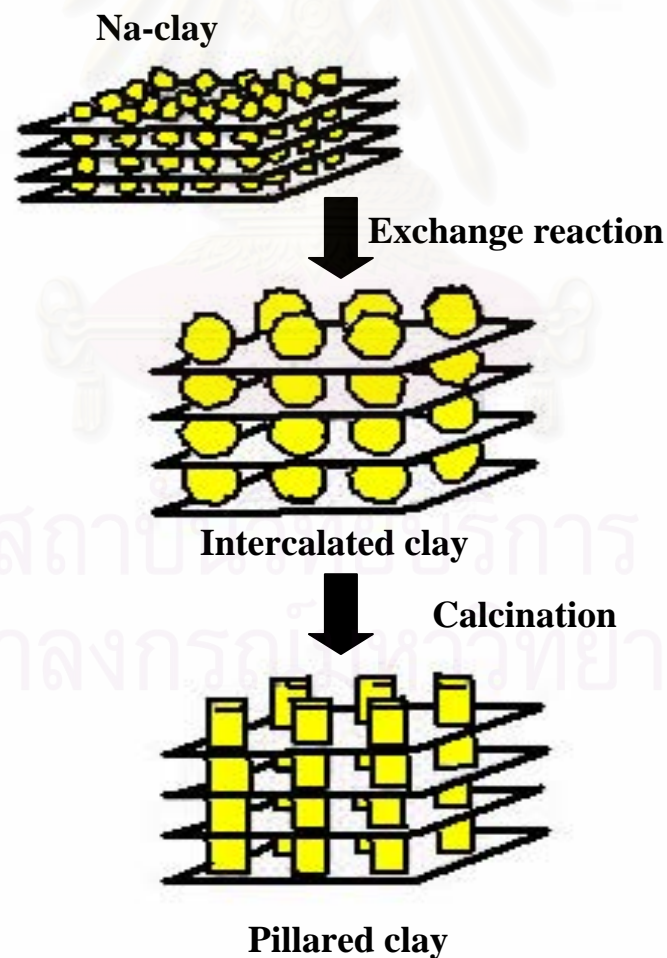


Figure 2.6 The principle of pillaring a clay with oxide particle [26].

2.9 Pillaring Agent

A pillaring agent is any compound, which can be intercalated between adjacent layers of a layered compound. It maintains the spacing between adjacent layers upon removal of the solvent and induce an experimentally observable pore structure between the layers.

2.10 Pillared Clay

Pillared clay is a microporous material. Its structure is based on the intercalation of metal complex cations in order to “prop open” the clay sheet, which when treated thermally generate pillars of the corresponding metal. This ensures uniform porosity with a high interlayer pore volume than that of natural clay. This microporous materials are commonly used as catalysts because they have good textural properties, such as high surface area and substantial micropore content (see below; Figure 2.7).

Pillared clays with aluminium (aluminium oxide-pillared clay) have been the most extensively studied, but commercial applications in catalysis are limited due to their low thermal stability. The introduction of mixed pillars in the clays presented two advantages: (1) it created a two-dimensional porosity in the inter layer spacing of the clay and (2) it generates thermal stability, increasing the application range of such solids to high temperatures. Depending on the final properties of the materials, they can be used in catalytic cracking reactions and the isomerisation of paraffin, among others.

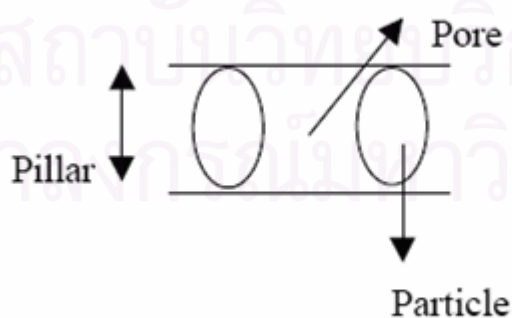


Figure 2.7 Simple Design of Pillared and Pore [27].

2.11 Impregnation

Impregnation is the easiest method of making a heterogeneous catalyst. A support or carrier, usually a porous material will be in contact with a solution of one or more suitable metallic compounds. The size and shape of the catalyst particle are those of the carrier. The impregnation technique requires less equipment since the filtering and forming steps are eliminated and washing may not be needed. It is the economically desirable method in preparing supported noble metal catalysts in order to spread out the metal in a highly dispersed form as possible. The noble metal is usually present in the order of 1% by weight or less of the total [28]. This makes maximum use of a very expensive ingredient; in contrast, in a precipitated catalysts some of the active ingredient will usually be enclosed by other material percent and thus unavailable for reaction.

Impregnation method can be divided into two types;

(a) Wet Impregnation

This method can be prepared by adding an excess amount of metal salt solution into supports. The composition of the solution will be changed slowly as the metal is absorbed on the surface. Thus, the metal content on the support will not be equal to the initial content in the solution. Besides, the release of support debris in the solution might form a mud, which makes it difficult to separate from the catalyst.

(b) Dry Impregnation or Impregnation to incipient wetness

This method is favored for industrial catalysts because the solution of metal salt will be dispersed by spraying on supports. The volume of solution should be equal to the pore volume of support in order to control the amount of active component. The required catalyst was obtained after drying and calcinations step.

2.12 Dialysis

Dialysis is a method for separation of substance in solution by means of their unequal diffusion through semipermeable membranes. The pores in the membrane allow molecules that are smaller than the pores to move freely across the membrane. Therefore, OH^- will cross out of the membrane into the deionized water [29]. Eventually, an equilibrium is achieved where the concentration of OH^- is equal inside and outside of the membrane.

2.13 Characterization of Clay Catalyst

2.13.1 Powder X – Ray Diffraction

X-ray diffraction (XRD) is an instrument technique for characterization of microporous and mesoporous materials, as well as other crystalline materials. When X-ray radiation is directed on a sample, the X-rays are scattered (diffracted) by electrons present in the material. If the atoms in the material are arranged in a regular structure, i.e. if the material is crystalline, this scattering results in maxima and minima in the diffracted intensity. The signal maxima follow Bragg's law equation [30];

$$n\lambda = 2d\sin\Theta.$$

Here n is an integer, λ is the X-ray wavelength, d is the inter planar spacing and Θ is the diffraction angle (see Figure 2.8). Thus, for each lattice d -spacing, Bragg's law predicts a maximum at a characteristic diffraction angle Θ . During an X-ray diffraction (XRD) measurement the angles of incidence and detection are scanned. When the intensity of detected X-rays is plotted as a function of angle Θ an X-ray diffraction pattern is obtained, which is characteristic for the sample material. The usual information depth of XRD measurements ranges from a few micrometers to a few hundred micrometers, depending on the density of the material.

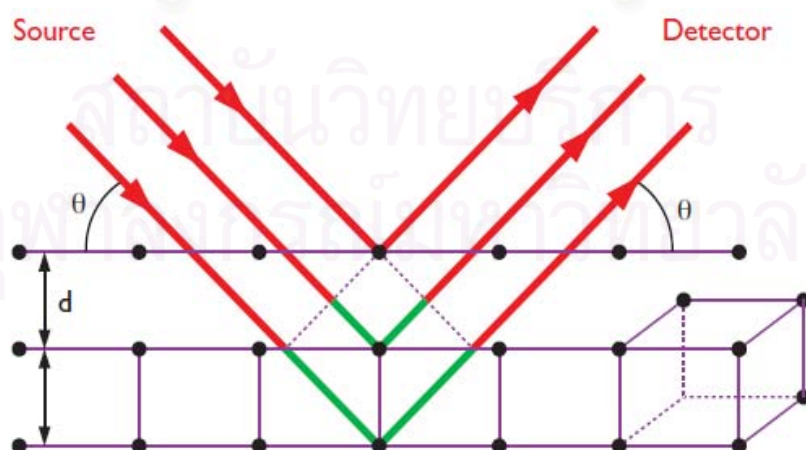


Figure 2.8 Diffraction of X-ray by regular planes of atom [31].

In an X-ray diffraction pattern the position and intensity of the maxima are characteristic for the crystallographic structure and the atomic composition of the material. In case of a multi-phase composition, the resulting pattern is a combination of the patterns of all structures present. Phase identification can be done by matching the XRD pattern with reference patterns of pure substances.

2.13.2 Inductively Coupled Plasma-Atomic Emission Spectroscopy (ICP-AES)

Inductively Coupled Plasma-Atomic Emission Spectrometry (ICP-AES) is one of the most common techniques for elemental analysis. Its high specificity, multi-element capability and good detection limits result in the use of the technique in a large variety of applications. All kinds of dissolved samples can be analyzed, varying from solutions containing high salt concentrations to diluted acids. A plasma source is used to dissociate the sample into its constituent atoms or ions, exciting them to a higher energy level. They return to their ground state by emitting photons of a characteristic wavelength depending on the element present. This light is recorded by an optical spectrometer. When calibrated against standards the technique provides a quantitative analysis of the original sample. In Figure 2.10 a schematic of an ICP-AES is shown. In the ICP-AES a plasma source is used to make specific elements emit light, after which a spectrometer separates this light in the characteristic wavelengths.

A solid sample is normally first dissolved and mixed with water. The technique is robust enough to allow direct analysis of liquids. The sample solution is transformed into an aerosol by a so-called nebuliser. The bigger droplets are separated from the smallest in a specially spray-chamber. The smallest droplets (1-10 μm) are transferred by an argon flow into the heart of the ICP-AES, the argon plasma. The bigger droplets (>90%) are pumped to waste.

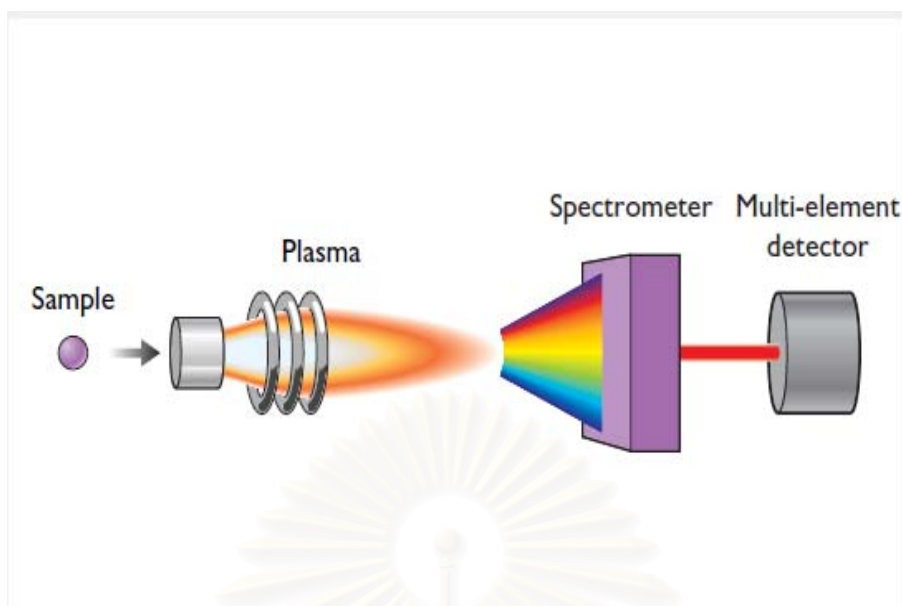


Figure 2.9 ICP-AES spectrometer [32].

2.13.3 Nitrogen Adsorption – Desorption Isotherm

The N_2 adsorption technique is used to determine the physical properties of mesoporous molecular sieves, such as the surface area, pore volume, pore diameter and pore-size distribution of solid catalysts. Adsorption of gas by a porous material is described by an adsorption isotherm, the amount of adsorbed gas by the material at a fixed temperature as a function of pressure. Porous materials are frequently characterized in terms of pore sized derived from gas sorption data. IUPAC conventions have been proposed for classifying pore sized and gas sorption isotherms that relationship between porosity and sorption. The IUPAC classification of adsorption isotherms is illustrated in Figure 2.15 Six types of isotherms are the characteristics of adsorbent that are microporous (type I) nonporous or macroporous (type II, III and VI) or mesoporous (types IV and V).

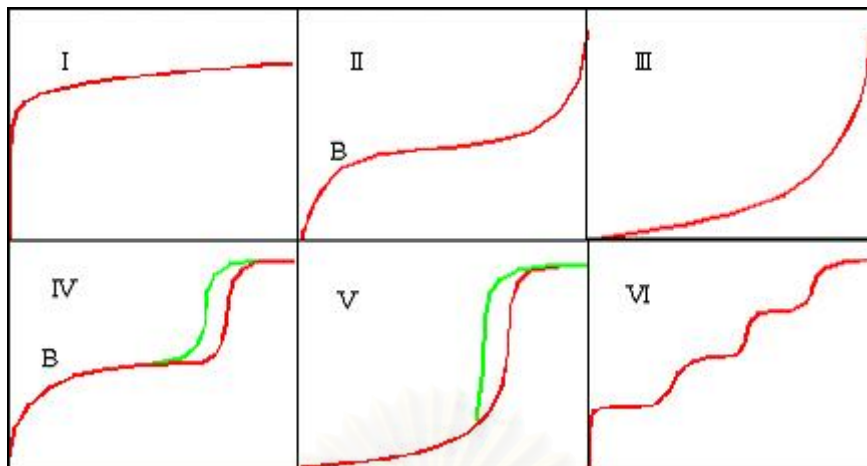


Figure 2.10 The IUPAC classification of adsorption isotherms [33].

Adsorption isotherms are described as shown in Table 2.1 based on the strength of the interaction between the sample surface and gas adsorbate, and the existence or absence of pores. Pore types are classified as shown in Table 2.2.

Table 2.1 Features of adsorption isotherms [34].

Type	Features	
	Intercalation between sample surface and gas adsorbate	Porosity
I	Relatively strong	Micropores
II	Relatively strong	Nonporous
III	Weak	Nonporous
IV	Relatively strong	Mesopore
V	Weak	Micropores or Mesopore
VI	Relatively strong sample surface has an even distribution of energy	Nonporous

Table 2.2 IUPAC classification of pores

Pore Type	Pore diameter (nm)
Micropore	Up to 2
Mesopore	2 to 50
Macropore	20 to up

Pore size distribution is measured by the use of nitrogen adsorption/desorption isotherm at liquid nitrogen temperature and relative pressure (P/P_0) ranging from 0.05-0.1. The large uptake of nitrogen at low P/P_0 indicates filling of the micropores ($<20 \text{ \AA}$) in the adsorbent. The linear portion of the curve represents multilayer adsorption of nitrogen on the surface of the sample, and the concave upward portion of the curve represents filling of mesopores and macropores.

The multipoint Brunauer, Emmett and Teller (BET) [35] method is commonly used to measure total surface area.

$$\frac{1}{W[(P_0/P)-1]} = \frac{1}{W_m C} + \frac{C-1}{W_m C} (P/P_0)$$

Where W is the weight of nitrogen adsorbed at a given P/P_0 , and w_m is the weight of gas to give monolayer coverage, and C is a constant that is related to the heat of adsorption. A linear relationship between $1/W[(P/P_0)-1]$ and P/P_0 is required to obtain the quantity of nitrogen adsorbed. This linear portion of the curve is restricted to a limited portion of the isotherm, generally between 0.05-0.30. The slope and intercept are used to determine the quantity of nitrogen adsorbed in the monolayer and calculate the surface area. For a single point method, the intercept is taken as zero or a small positive value, and the slope from the BET plot is used to calculate the surface area. The surface area reported depends upon the method used, as well as the partial pressures at which the data are collected.

2.13.4 FTIR Spectroscopy

Infrared (IR) spectroscopy is used to obtain information on the molecular structure of virtually all types of samples in any physical state (solid, liquid or gas). The technique is widely spread and is applied in the polymer, pharmaceutical, medical and chemical industry. The infrared spectrum is related to the vibrations of molecules and is unique for each compound, like a fingerprint for a person. Using an IR microscope samples with dimensions down to $10 \mu\text{m}$ can be measured with little or no sample preparation. Infrared spectroscopy is based on the fact that all molecules vibrate and can absorb energy in the infrared region. Most of the vibrational absorption states correspond to the wavelength in the order of 2.5 to $25 \mu\text{m}$ ($4000\text{-}400 \text{ cm}^{-1}$) [36]. For a

two atomic system consisting of two masses m_1 and m_2 , the vibrational frequency (ν) is related to the force constant (k) and the reduced mass (μ) by the following equation:

$$\nu = \frac{1}{2\pi} \sqrt{\frac{k}{\mu}}, \quad \mu = \frac{m_1 m_2}{m_1 + m_2}$$

An infrared spectrum shows transmission versus wave number (cm^{-1}). Absorption is only possible at specific frequencies at which higher vibrational states can be reached. If energy is absorbed by a molecule, the signal at this frequency decreases, leading to a peak in the spectrum. The formula showed that if the force constant (k) of the bond between two atoms is larger, the frequency of the vibration is higher. This means that a C=C bond will absorb at a higher frequency than a C-C bond, resulting in a peak at 1600 cm^{-1} and 1000 cm^{-1} respectively. The lighter the atoms involved in the vibration the higher the frequency will be. The stretching vibrations of the C-H bond can be found in the 3000 cm^{-1} region of the spectrum.

2.14 The Refining Process

Every refinery begins with the separation of crude oil into different fractions by distillation (Figure 2.14). The fractions are further treated to convert them into mixture of more useful saleable products by various methods such as cracking, reforming, alkylation, polymerization and isomerization. These mixtures of new compounds are then separated using methods such as fractionation and solvent extraction. Impurities are removed by various methods e.g. dehydration, desalting, sulphur removal and hydrotreating.

Refinery processes have develop in response to change market demands for certain products. With the advent of the internal combustion engine the main task of refineries became the production of petrol. The quantity of petrol available from distillation alone is insufficient to satisfy consumer demand. Refineries began to look for ways to produce more and better quality petrol. Two types of processes have been develop [38]:

- breaking down large, heavy hydrocarbon molecules.
- reshaping or rebuilding hydrocarbon molecules.

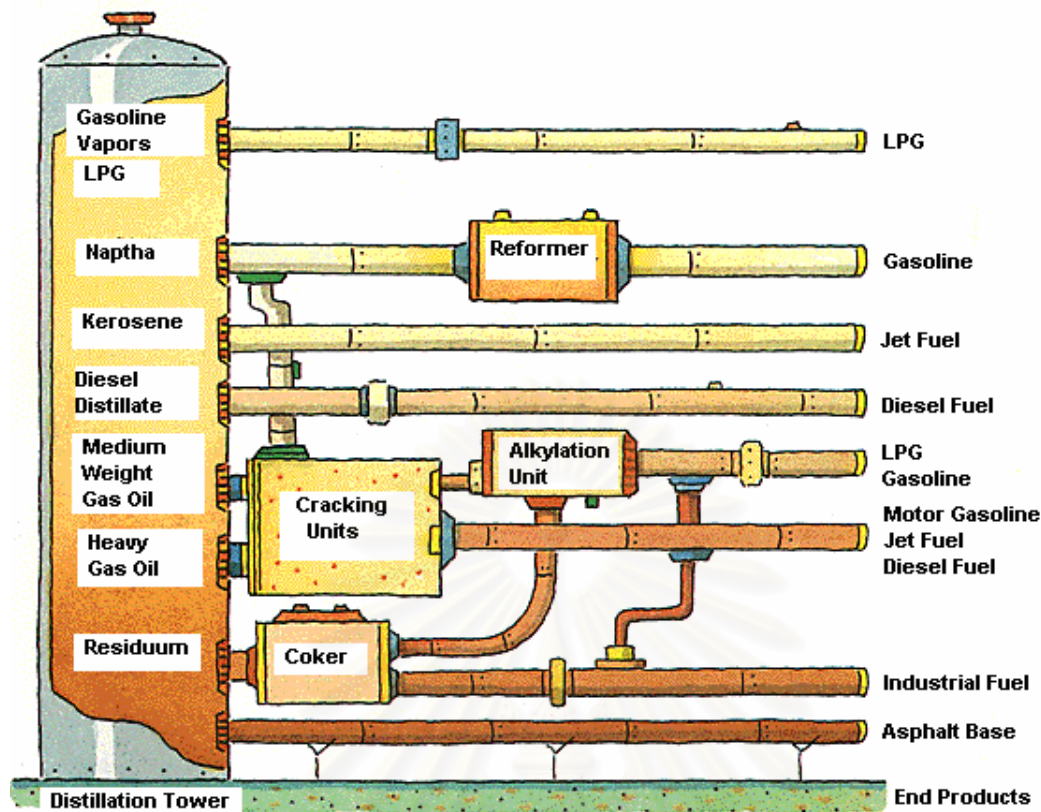


Figure 2.11 The simplified drawing of many of a refinery's most important processes [37].

Cracking processes break down heavier hydrocarbon molecules (high boiling point oils) into lighter products such as petrol and diesel. These processes include catalytic cracking, thermal and hydrocracking [39].

- **Catalytic cracking** [40] is used to convert hydrocarbon fractions obtained by vacuum distillation into a mixture of more useful products such as petrol and light fuel oil. In this process, the feedstock undergoes a chemical breakdown, under controlled heat (450°C - 500°C) and pressure. Small pellets of silica-alumina have prove to be the most effective catalysts. The cracking reaction yield petrol, LPG, unsaturated olefin compounds, cracked gas oil recycled to cause further breakdown and coke, which forms a layer of the catalyst is moved by burning. The other products are passed through fractionators to be separated and separately processed.

- **Thermal cracking**

In thermal cracking elevated temperature ($\sim 800^{\circ}\text{C}$) and pressure (~ 800 kPa) are used [41]. An overall process of disproportionation can be observed, where

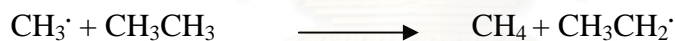
“light” hydrogen -rich products are formed at the expense of heavier molecules which condense and are depleted of hydrogen. The actual reaction is known as hemolytic fission and produces alkenes, which are the basis for the economically important production of polymer.

A large number of chemical reactions takes place during steam cracking. The main reactions that take place include:

1. Initiation reactions where a single molecule breaks apart into two free radicals. Only a small fraction of the feed molecules actually undergo initiation, but these reactions are necessary to produce the free radicals that drive the rest of the reactions. In steam cracking, initiation usually involves breaking a chemical bond between two carbon atoms, rather than the bond between a carbon and hydrogen atom.



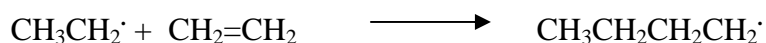
2. Hydrogen abstraction where a free radical removes a hydrogen atom from another molecule, turning the second molecule into a free radical.



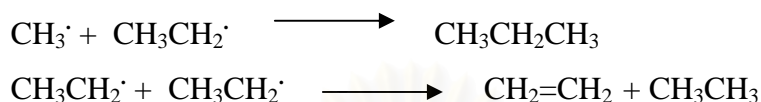
3. Radical decomposition where a free radical breaks apart into two molecules, one an alkene, the other a free radical. This is the process that results in the alkene products of steam cracking.



4. Radical addition, the reverse of radical decomposition, in which a radical reacts with an alkene to form a single, larger free radical. These processes are involved in forming the aromatic products that result when heavier feedstocks are used.



5. Termination reactions which happen when two free radicals react with each other to produce products that are not free radicals. Two common forms of termination are *recombination*, where the two radicals combine to form one larger molecule, and *disproportionation*, where one radical transfers a hydrogen atom to the other, giving an alkene and an alkane.



-**Hydrocracking** can increase the yield of petrol components, as well as being used to produce light distillates. It produces no residues, only light oils. Hydrocracking is catalytic cracking in the presence of hydrogen. The extra hydrogen saturates or hydrogenates the chemical bonds of the cracked hydrocarbons and process because the hydrogen combines with contaminants such as sulphur and nitrogen allowing them to be removed.

2.15 Catalytic Cracking Mechanisms

Pillared clay are catalysts that offer the advantage of mild acidity combined with stability at high temperature.

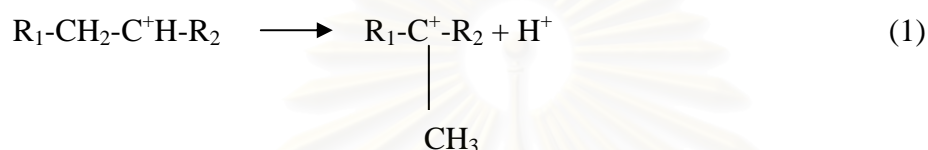
2.15.1 General Cracking Mechanisms

In general, for components with equal carbon numbers, the rate of cracking decrease in the order: i-olefins > n-olefins > i-paraffins = naphthenes > n-paraffins > aromatics [42]. The cracking mechanism can be seen as a chain mechanism that involves the intermediate formation of carbonations. Carbonations include both carbenium ions (e.g. $\text{R}_1\text{-CH}_2\text{-C}^+\text{H-R}_2$, $\text{R}_1\text{-CH=C}^+\text{-R}_2$) and carbonium ions (e.g. $\text{R}_1\text{-CH}_2\text{-C}^+\text{H}_3\text{-R}_2$, $\text{R}_1\text{-CH=C}^+\text{H}_2\text{-R}_2$). In carbenium ions, the charge carrying carbon atom can be di- or tri-coordinated, while in carbonium ions, the charge carrying carbon atom is tetra- or pentacoordinated. The stability of the carbocations decreases in the order tertiary > secondary > primary [43]. Cracking of hydrocarbons is a primary reaction that proceeds through adsorbed carbenium ion intermediates.

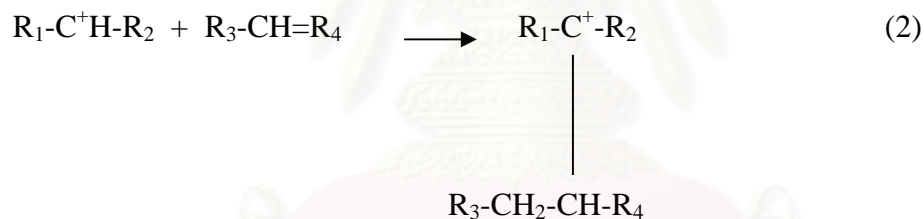
2.15.2 Reactions of Olefins

The formation of carbenium ions from olefins can easily proceed by additional of the proton from a brønsted acid site of the catalyst to the carbon-carbon double bond. Cracking of the adsorbed carbenium ion proceeds through the β -scission mechanism or through the protonated cyclopropane mechanism [44, 45]. Other reactions of the adsorbed carbenium ion are [46, 47]:

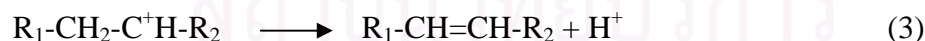
1. Isomerization to a more stable carbenium ion, for example, through a methyl shift:



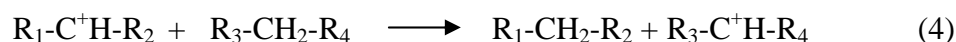
2. Oligomerization with olefin in a bimolecular reaction to form a larger adsorbed carbenium ion:



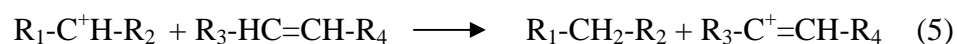
3. Desorption with deprotonation to form an olefin (the opposite of adsorption):



4. Desorption with hydride abstraction from a paraffin to form new paraffin from the carbenium ion from the paraffin (H-transfer reaction):



5. Desorption with hydride abstraction from (cyclic) olefins or coke (precursors) to form paraffin and a more aromatic compound (H-transfer reaction):



The bimolecular reaction (2), (4) and (5) can occur if the pore size of the catalyst is large enough to accommodate the reactive intermediates, or they should occur on the outer surface of the zeolite particles. If the pores are too small, as in the case of ZSM-5 (0.53 nm x 0.56 nm), these reactions cannot take place with the larger (gasoline) components, although oligomerization or dimerization of small (C₁-C₄) olefins could be possible. For example, in the Mobil olefins to gasoline and distillates process (MOGD) coupling of light hydrocarbons is catalyzed by ZSM-5.

With ZSM-5, cracking through dimeric intermediates has only been reported in the reactions of relatively small *n*-olefins (C₄-C₆). Abbot and Wojciechowski [45] have studied cracking of *n*-olefins from C₅ to C₉ at 678° K with ZSM-5 and found that cracking of pentene solely took place through a dimeric/disproportionation mechanism. Cracking of heptene and larger molecules proceeded mainly through monomolecular cracking and at 678° K, hexane represented the transition case of the two mechanisms and was cracked by both monomolecular cracking and through dimeric intermediates.

2.15.3 Reaction of Paraffins

Compared to olefins, paraffins have a lower reactivity towards cracking due to a more difficult formation of carbenium ions. This may proceed at Lewis acid sites or adsorbed carbenium ions can react with paraffins in a bimolecular-type of mechanism. The latter mechanism requires the presence of the adsorbed carbenium ions and can take place if the pore size of the catalyst is large enough to accommodate the necessary transition state.

Indirect formation of carbenium ions is proposed to proceed through the formation of carbonium ions; paraffins reacts with a proton from a Brønsted acid site and the resulting carbenium ion is cracked to an adsorbed carbenium ion and hydrogen or small olefins. The formation of a carbenium ion requires an energetically unfavorable transition state and has high activation energy. This mechanism for activation of paraffins will only be significant in the absence of olefins and is favored by high temperature, low hydrocarbon partial pressures and low conversions of the

paraffins. The occurrence is not expected to be significant when cracking a gasoline mixture that contains olefins. The olefins can easily form carbenium ions and cause cracking of paraffins through the bimolecular cracking mechanism as discussed above.



สถาบันวิทยบริการ
จุฬาลงกรณ์มหาวิทยาลัย

CHAPTER III

EXPERIMENTAL

3.1 Equipment and Apparatus

Ovens and Furnace

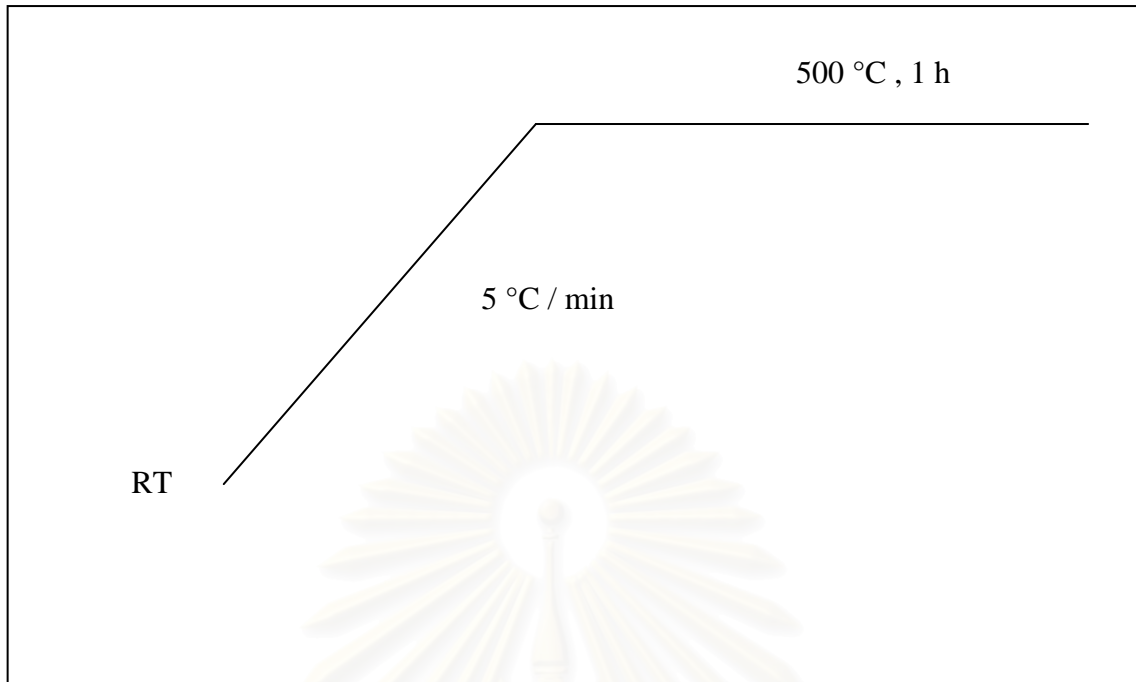
Raw clay was dried in a Memmert UM – 500 oven at 100 °C. All synthesized catalysts were dried using the same oven. The temperature was set between 70 to 120 °C for 24 h. Metal precursors in the interlayer of clay were converted to metal oxide by calcinations using a Carbolite RHF 1600 muffle furnace. The calcinations temperature was set between 450 – 500°C with the heating rate of 5°C/min. The heating program was show in Scheme 3.1 and 3.2.

X – ray Powder Diffractometer

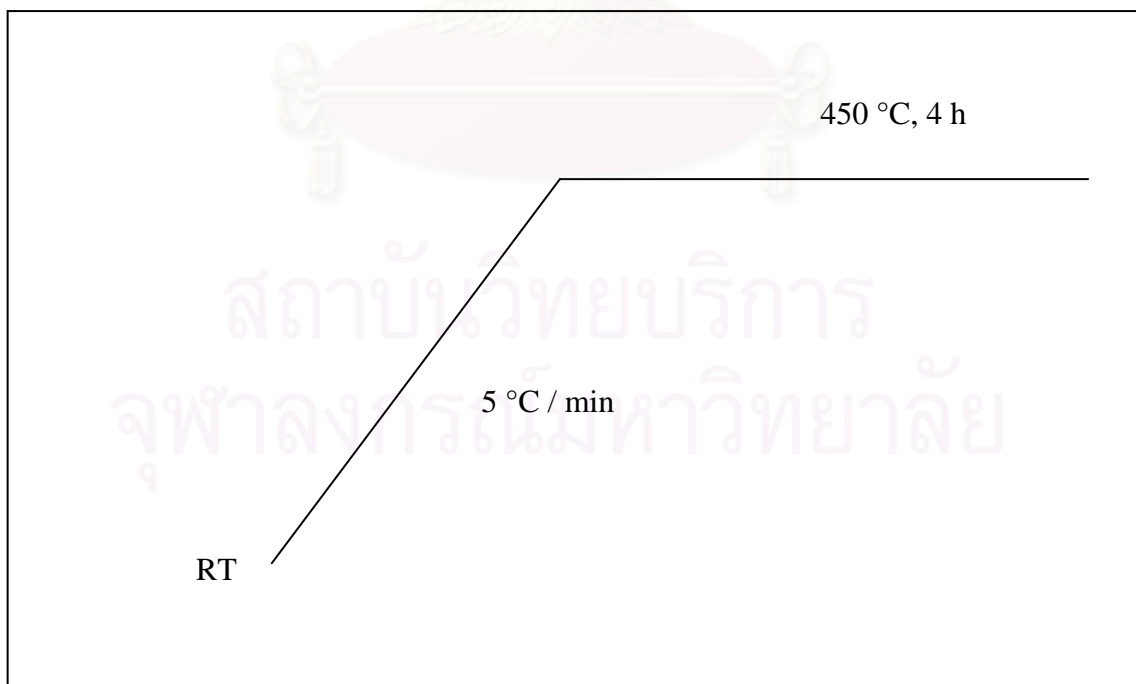
The structure of synthesized catalysts was identified using a Rigaku, Dmax 2200/Ultima plus X – ray powder diffraction (XRD) with a monochromater and Cu K_α radiation (40 kv. 30 mA) at an angle of 2 Θ range from 2 to 50 degree. The scan speed was 5 degree/min and the scan step was 0.02 degree. The three slits (scattering, divergent and receiving slits) were fixed at 0.5 degree, 0.5 degree and 0.15 nm respectively.

Centrifuge

A Centaur 2, Sanyo centrifuge was used to purify clays and collect the synthesized catalysts. The process of purification is aimed for removing quartz and other impurities at various centrifugal speeds.



Scheme 3.1 The heating program used for calcination of aluminium oxide– pillared clay.



Scheme 3.2 The heating program used for calcination of zirconium/aluminium oxide – pillared clay.

Nitrogen Adsorptometer

Characterization of catalyst porosity was studied term of nitrogen adsorption–desorption isotherm. BET specific surface area of the catalyst was carried out using a BELSORP-II instrument. The sample weight was near 40 mg and weight exactly pretreatment at 400°C 2.5 h before each measurement.

ICP-AES Spectrometer

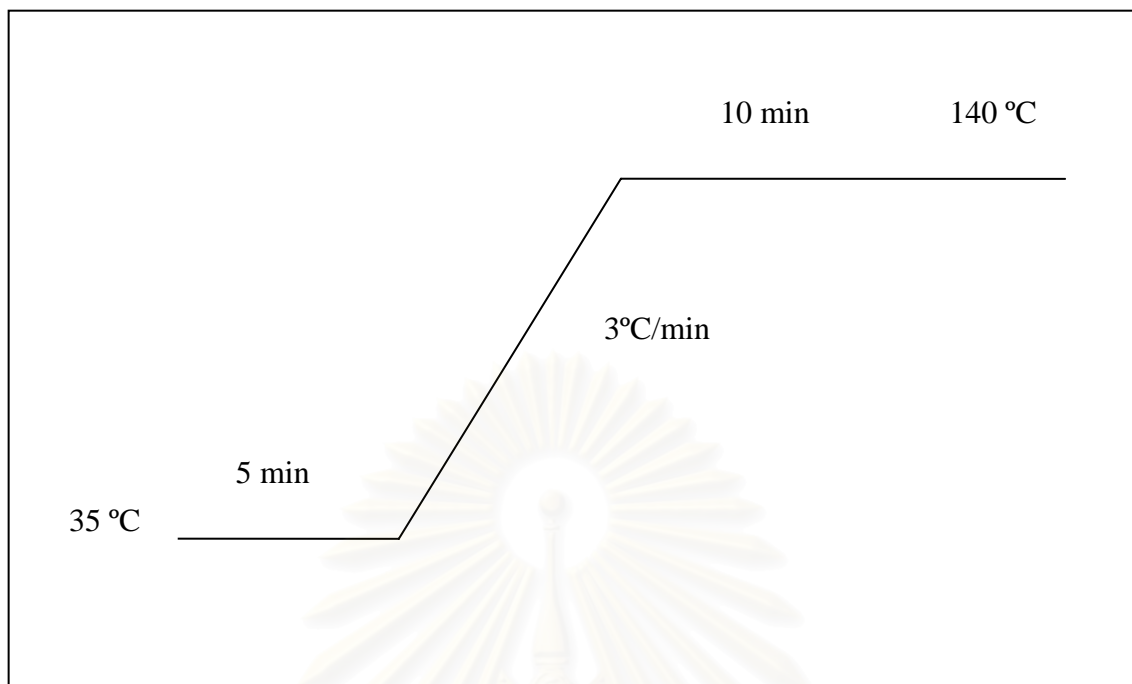
Aluminium content in the catalysts was analyzed using the Perkin Elmer PLASMA-1000 inductively couple plasma-atomic emission (ICP-AES) spectrometer at the Scientific and Technological Research Equipment Center of Chulalongkorn University.

FTIR Spectrometer

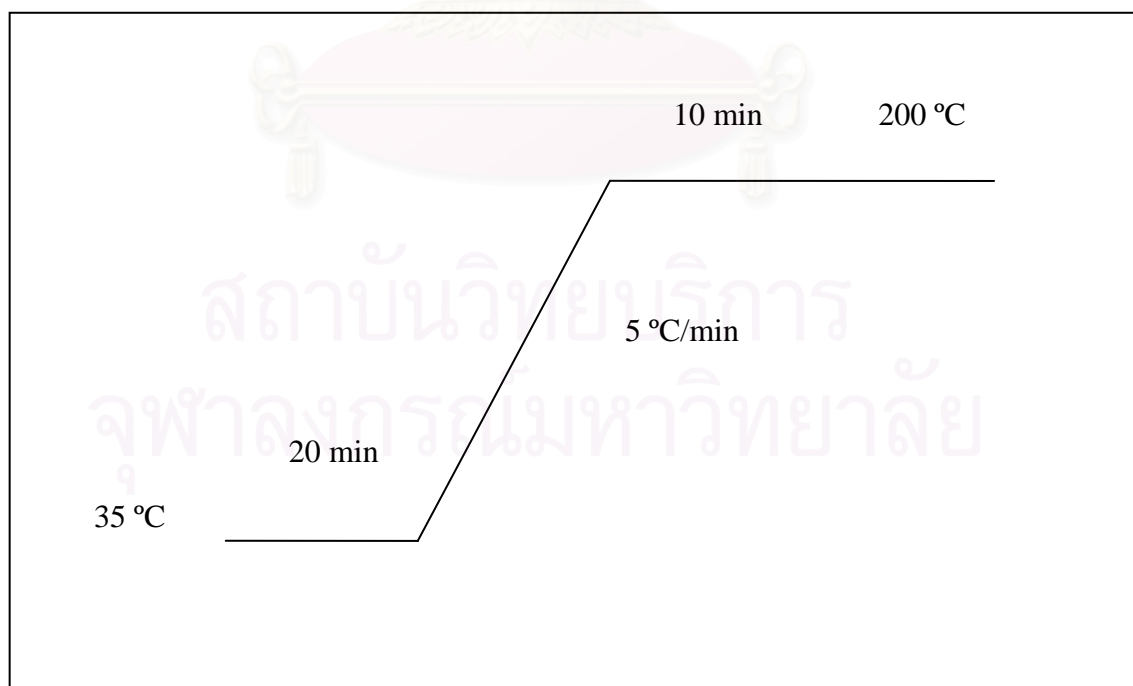
Vibrations of metal-oxygen bound in the catalysts were measured in the wave number range from 400 to 4000 cm^{-1} using a Nicolet Impact 410 Fourier transformed infrared (FTIR) spectrometer with the KBr pellet technique at Department of Chemistry, Faculty of Science, Chulalongkorn University.

Gas Chromatograph

Hydrocarbon gases were analyzed using a Varian CP-3800 gas Chromatograph equipped with a 50 – m long and 0.53-mm inner diameter Alumina-PLOT column. Liquid samples were analyzed using a Varian CP-3800 gas Chromatograph equipped with a 30-m long and 0.25-mm inner diameter CP-sil 5 (0.25 μm film thickness) column. All GC detectors were flame ionization detectors (FID). The GC heating programs for 3.00- μl gas and 1.00- μl liquid analysis were shown in Scheme 3.3 and 3.4 respectively.



Scheme 3.3 The GC heating program for gas analysis.



Scheme 3.4 The GC heating program for liquid analysis.

The Cracking Catalytic Apparatus

The cracking apparatus for cracking of polymer shown in figure 3.5 is comprised of ;

1. tube reactor
2. thermocouple
3. furnace
4. temperature programming controller
5. tedlar bag
6. a water-cooled condenser
7. receiving adaptor
8. bone
9. cylinder

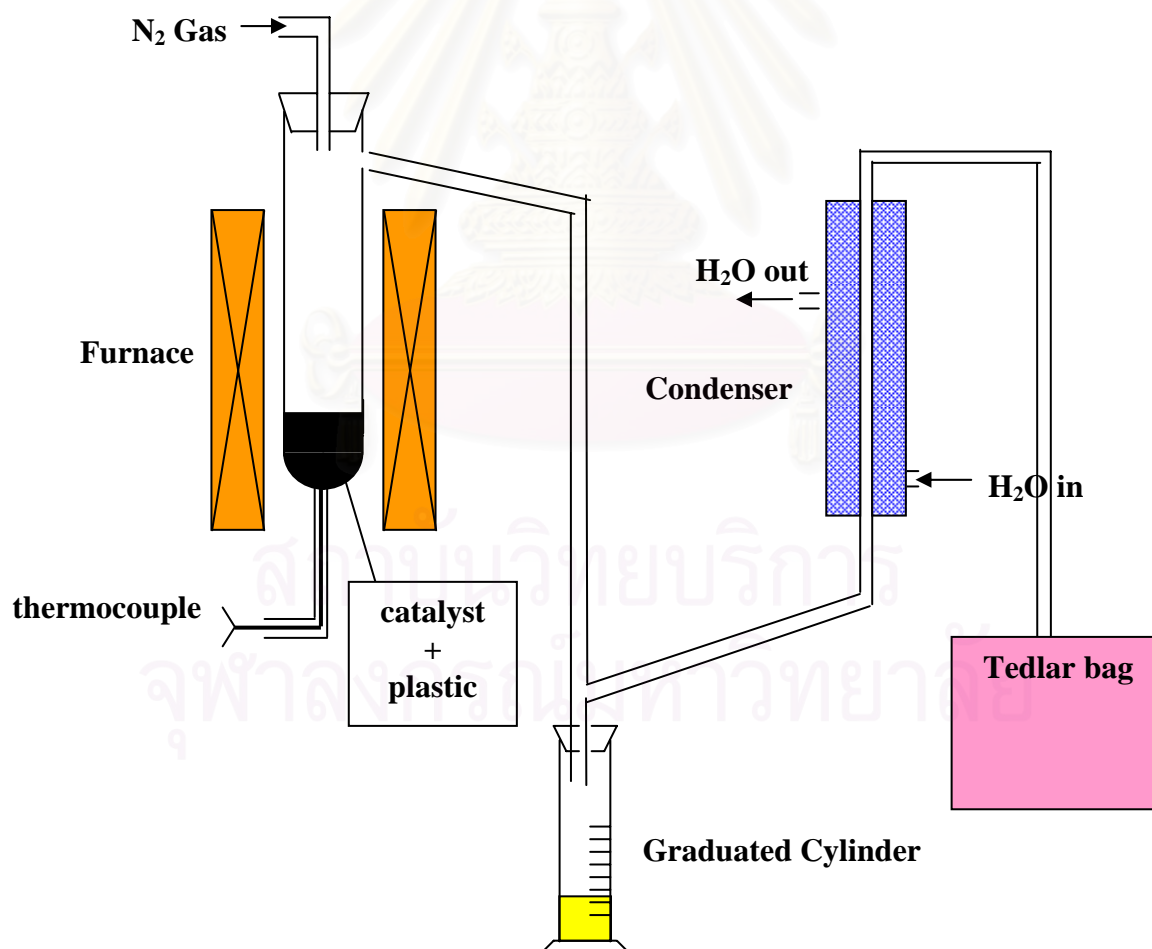


Figure 3.1 Apparatus for catalytic activity test in polymer degradation.

3.2 Chemical and Starting Materials

3.2.1 Clays

Clay (bentonite) was used as a raw material. Bentonite was kindly support by Cernic International Co., LTD. The composition of bentonite is summarized in Table 3.1.

Before being used for starting clay, the bentonite was purified because the natural compound contained impurities such as quartz, β -cristobalite and calcite that reduced the cationic exchange capacity of the clay. 20 g of the natural clay were dispersed into 1000 ml of distilled water under vigorous stirring for 2 h. After sedimentation, the suspension was separated out for further centrifuged step (at a speed of 4000 rpm for about 7 min) and dried at 100°C.

Table 3.1 Bentonite composition

Bentonite	
SiO ₂	63.60
Al ₂ O ₃	17.60
MgO	-
Fe ₂ O ₃	3.10
CaO	3.00
Na ₂ O	3.40

Information from Cernic International Co.,Ltd.

3.2.2 Chemicals

3.2.2.1 Sodium hydroxide, NaOH (Merk, reagent grade)

3.2.2.2 Sulfuric acid 95-97%, H₂SO₄ (Merk, reagent grade)

3.2.2.3 Aluminium chloride hexahydrate, AlCl₃.6H₂O (Ajax Finechemical, AR grade)

3.2.2.4 Zirconyl chloride, ZrOCl₂.8H₂O (Carlo Erba Reagenti, AR grade)

3.2.2.5 Silver nitrate, AgNO₃ (BHD, AR grade)

3.2.2.6 Standard gas mixture and liquid mixture for GC analysis were kindly obtained from PTT Chemical Public Company Limited.

3.2.2.7 Nitrogen gas, N_2 (Thai Industrial Gases (TIG), highly pure grade)

3.2.2.8 Ammonia gas, NH_3 (Linde Gas Thailand, highly pure grade)

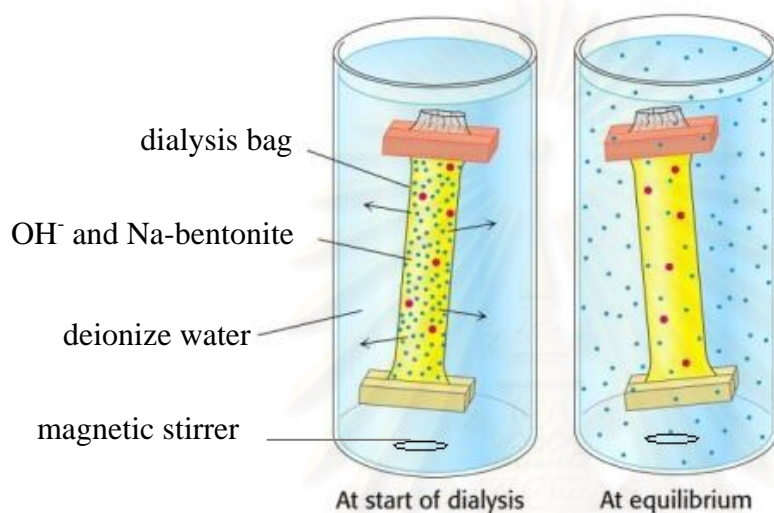
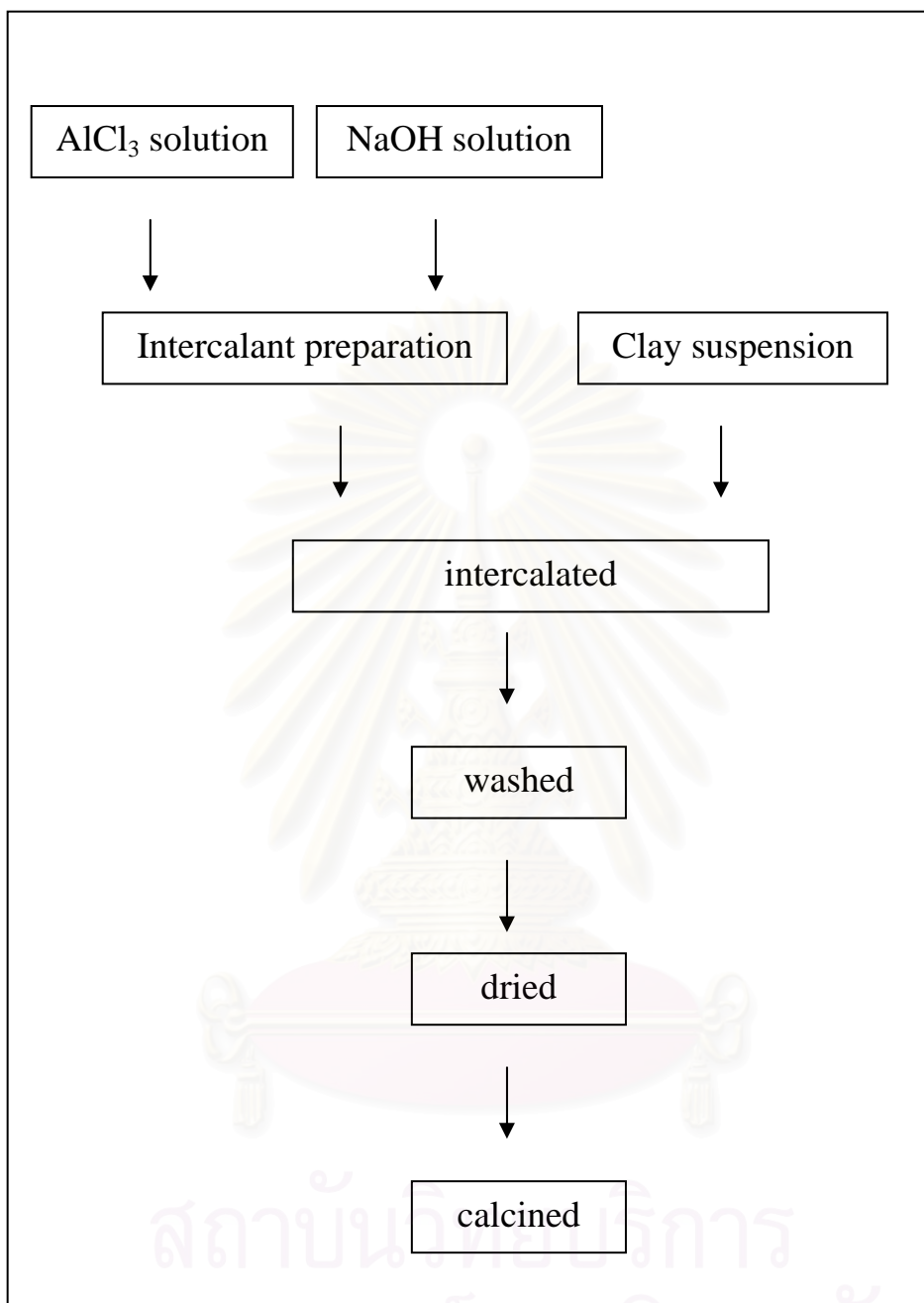


Figure 3.2 Dialysis apparatus.

3.3 Homoionic Clays

The natural exchange cation of the clay is Ca^+ and not Na^+ (more easily interchangeable), which was incorporated in the homoionization. Starting clay was dispersed into 5 M NaOH solution under vigorous stirring for 24 h at room temperature. The clay to NaOH solution ratio was 1 g : 50 ml. The Na-ion exchanged process was repeated for three times. The products were separated from solution by centrifuge and dialyzed until pH near 7 as shown in Scheme 3.6. The Na-bentonite was dried at $100^\circ C$.



Scheme 3.5 Main steps for preparation of aluminium oxide-pillared clay.

3.4 Synthesis of Aluminium Oxide – Pillared Clay [48]

A 0.2 wt.% of Na-clay was dispersed into water under stirring for 48 h at room temperature. An aqueous 0.2 M NaOH solution was added to a solution of 0.2 M AlCl₃ under vigorous stirring. In both cases the solutions remained standing for 24 h before titration. The final [OH]/[Al] ratio was 1.9. This solution was stirred for 24 h at

room temperature. The Al containing solution was slowly added at room temperature to clay suspension. The relative volume of the two solution was chosen to have a final Al to clay ratio equal 3.8 mol/kg. After the intercalation was completed, the flocculating clay was left in situ to age for 24 h before washing by distilled water until free Cl^- ions. The intercalated product was dried at 70 °C for 24 h and calcined with a heating rate of 5 °C /min, held for an hour at 500°C

3.5 Synthesis of Zirconium/Aluminium Oxide– Pillared Clay

The zirconium doped aluminium oxide-pillared clay was synthesized by slurry impregnation of aluminium oxide-pillared clay support with a solution of $\text{ZrOCl}_2 \cdot 8\text{H}_2\text{O}$ in acetone by vary percent of zirconium at 1.0, 2.0, 3.0 and 5.0 percent. After impregnation, the samples were dried at 120°C for 24 h and then calcined with heating rate of 5 °C /min, held for 4 h at 450°C.

3.6 Sample Preparation for ICP-AES

In a 100-ml teflon beaker, 0.0400 g of calcined catalysts was soaked with 10 ml of conc. HCl and subsequently with 10 ml of conc. hydrofluoric acid to get rid of silica form of volatile SiF_4 species. The solid was heated to dryness on a hot plate. The fluoride treatment was repeated twice. An amount of 10 ml of a mixture of 6 M HCl : 6 M HNO_3 at ratio 1 : 3 was added and further heated to dryness. An amount of 5 ml of 6 M HCl was added to the beaker and warmed for 5 min to dissolve the residue. The solution was transferred to a 50-ml pp volumetric flask and made to the volume by adding deionized water. The flask was capped and shaken thoroughly. If the sample was not analyzed immediately, the solution was then transfer into a dry plastic bottle with a treaded cap lined under with a polyethylene seal.

3.7 Activity of Aluminium Oxide-Pillared Clay Catalysts in PP cracking

3.7.1 Effect of Reaction Time

Degradation of plastic polymer was carried out in a glass reactor (4.4 cm. i.d. and 37 cm length) under atmospheric pressure by batch operation as show in Figure 3.2 and Scheme 3.6. Five grams of PP pellet and 0.5 g of catalyst were loaded into the reactor and inserted into a furnace split-tube. In a typical run, the reactor was set up, and purge with N_2 at flow rate of 20 ml/min to remove air. The reactor was heated

to 380°C in 20 min (20°C/ min) using the split-tube furnace equipped with a programmable temperature controller and a K-type thermocouple. The temperature was maintained constant at the reaction temperature for 0.5, 1.0, 1.5 and 2.0 h. The gas fraction which flowed from the reactor with the nitrogen stream was passed through a condenser cooled by cold water. The gas fraction was collected into a tedlar bag since the start of heating while the liquid fraction was condensed and collected in a 10-cm³ graduated cylinder. After completion of the reaction, the reactor was cooled down to room temperature and weighted. The values of % conversion and % yield were calculated based on the equations as follows:

$$\% \text{ conversion} = \frac{\text{mass of liquid fraction} + \text{mass of gas fraction}}{\text{mass of plastic}} \times 100$$

$$\text{mass of gas fraction} = \text{mass of the reactor with plastic and catalyst before reaction} - \text{mass of the reactor with residue and used catalyst after reaction} - \text{mass of liquid fraction}$$

$$\% \text{ yield} = \frac{\text{mass of product fraction}}{\text{mass of plastic}} \times 100$$

The degradation products were classified into three groups: gas fraction (products which were not condensed at water cooling temperature), liquid fraction and residue. The gas products were analyzed by a gas chromatography. The liquid fraction was distilled under vacuum as shown in Figure 3.3. The distillate oil was analyzed by a GC. The retention time of components in the distillate oil in the GC column was compared to the boiling point range of reference in form of n-paraffins. The value of % coke formed was determined by the weight loss upon calcinations of the used catalyst after leaching out of waxes by n-hexane. The heating program for de-coke was shown in Scheme 3.1

3.7.2 Effect of Reaction Temperature

The degradation of PP pellet was carried out using treated aluminium oxide-pillared clay catalyst at various temperatures. The reaction was performed in the similar way to what described in section 3.7.1 and the experiments were set up at the reaction temperature of 350, 380 and 410°C. The temperatures were maintained constant at the reaction temperature for 1.0 h.

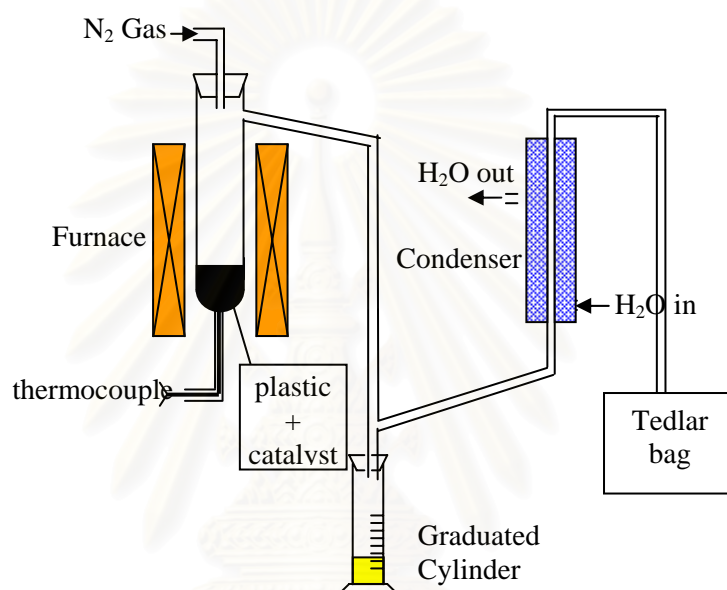
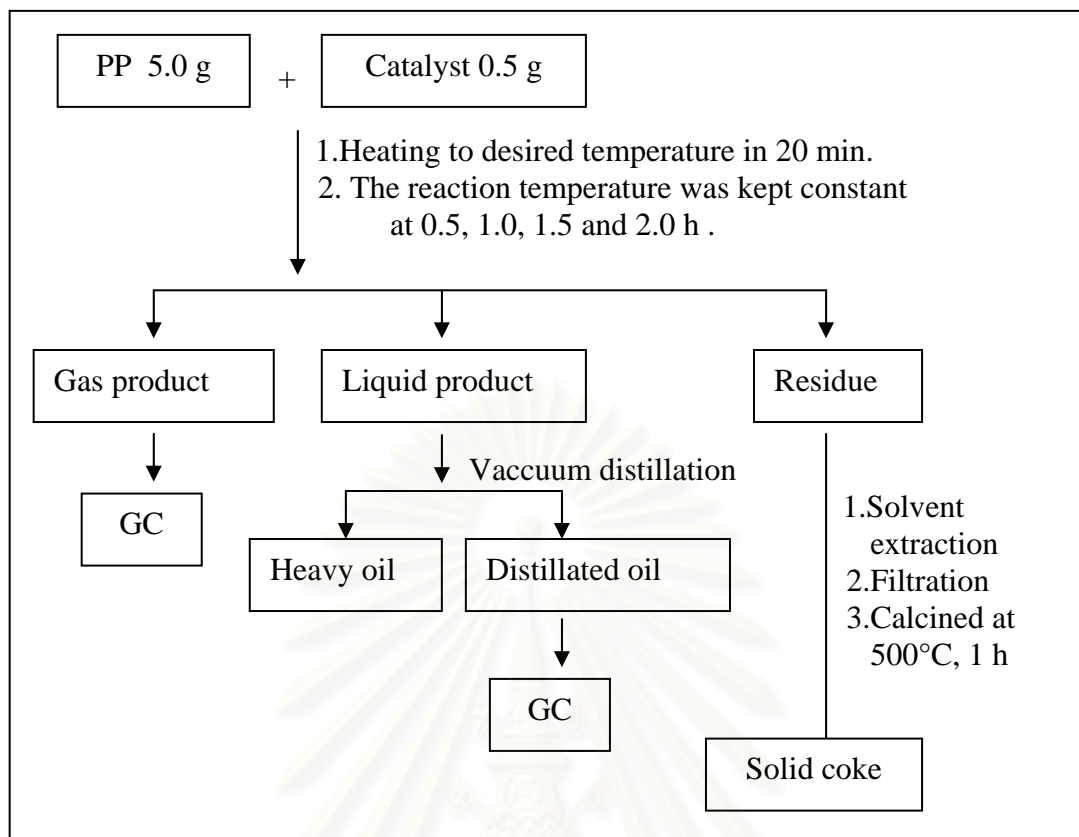


Figure 3.3 Apparatus for catalytic cracking.

3.7.3 Effect of Zirconium Doped Aluminium Oxide-Pillared Clay (Zirconium/Aluminium Oxide-Pillared Clay)

The degradation of PP pellet was carried out using treated zirconium/aluminium oxide-pillared clay catalyst with various concentration of zirconium (1.0, 2.0, 3.0 and 5.0 percent) by impregnation of $\text{ZrOCl}_2 \cdot 8\text{H}_2\text{O}$ on the calcined aluminium oxide-pillared clay. The reaction was performed in the similar way to what described in section 3.7.1 and the experiments were set up at 380°C for 1.0 h.



Scheme 3.6 Catalytic cracking of PP using aluminium oxide-pillared clay as catalyst.

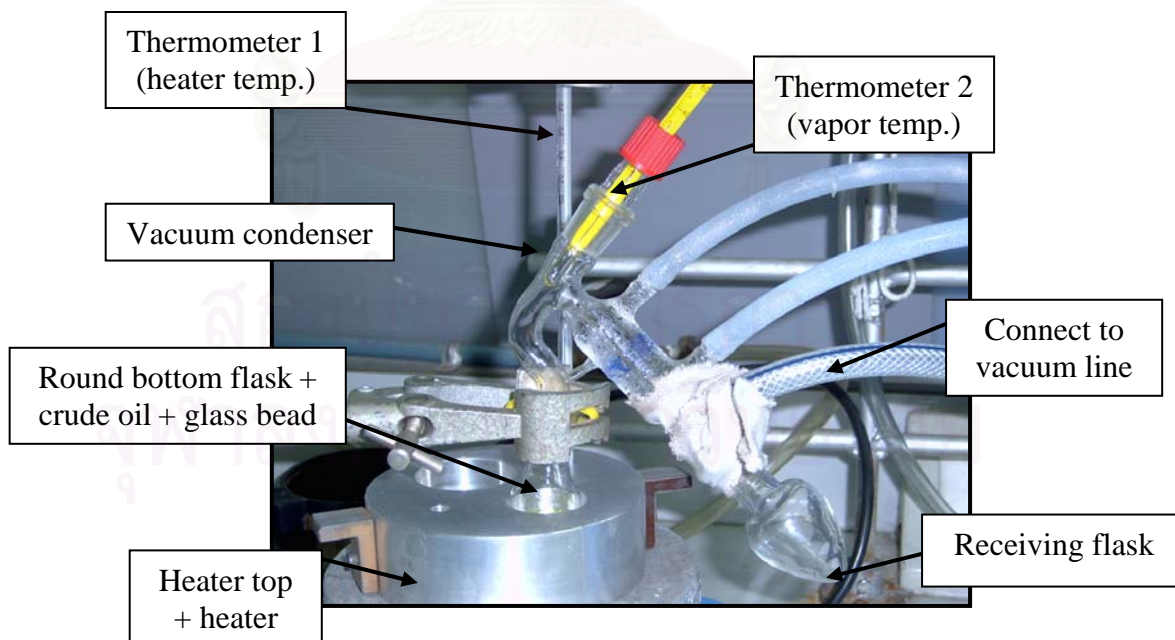


Figure 3.4 Apparatus for vacuum distillation.

3.7.4 Effect of catalyst per plastic ratio

The degradation of PP pellet was carried out using treated 2.0wt% zirconium/aluminium oxide-pillared clay catalyst with various catalyst per plastic ratio (5, 10, 20 and 30%). The reaction was performed in the similar way to what described in section 3.7.1 and the experiments were set up at the reaction temperature of 380 °C for 1.0 h.

3.8 Activity of Various Aluminium Oxide-Pillared Clays Catalyst in PE Cracking

3.8.1 Effect of Reaction Time

The degradation was performed in the similar way to what described in section 3.7.1 and the experiments were set up at the reaction time of 0.5, 1.0, 1.5, 2.0 and 3.0 h .

3.8.2 Effect of Reaction Temperature

The degradation of PE pellet was carried out using treated aluminium oxide-pillared clay catalyst with various temperature reactions. The reaction was performed in the similar way to what described in section 3.7.1 and the experiments were set up at the reaction temperature of 380, 410 and 440°C. The temperature was maintained constant at the reaction temperature for 1.5 h.

3.8.3 Effect of Zirconium Doped Aluminium Oxide-Pillared Clays

The degradation of PE pellet was carried out using treated zirconium/aluminium oxide-pillared clay catalyst with various percentages of zirconium (1.0, 2.0, 3.0 and 5.0 percent) by impregnation of $ZrOCl_2 \cdot 8H_2O$ on the aluminium oxide-pillared clay as catalyst. The reaction was performed in the similar way to what described in section 3.7.1 and the experiments were set up at the reaction temperature of 410°C. The temperature was maintained constant at the reaction temperature for 1.5 h.

3.8.4 Effect of catalyst per plastic ratio

The degradation of PE pellet was carried out using treated 2wt% zirconium doped aluminium oxide-pillared clay (zirconium/aluminium oxide-pillared clay) catalyst with various amount of a catalyst per plastic ratio (5, 10, 20 and 30%) as a

catalyst. The reaction was performed in the similar way to what described in section 3.7.1 and the experiments were set up at the reaction temperature of 410°C. The temperature was maintained constant at the reaction temperature for 1.5 h.



สถาบันวิทยบริการ
จุฬาลงกรณ์มหาวิทยาลัย

CHAPTER IV

RESULTS AND DISCUSSION

4.1 The characterization of clay catalysts

4.1.1 X – ray Diffraction (XRD)

This technique was used to investigate the changes of clay structure. The change in d-basal spacing in XRD patterns reflected to the change of sample structure such as an increased interlayer spacing of clay after pillaring process.

4.1.1.1 The characterization of raw clay.

Natural clay is not constituted from clay mineral only, but also other impurities. Bentonite is a phyllosilicate-typed clay, generally containing impurities such as calcite, quartz, feldspars and humic acids. Quartz is the major impurity of clay minerals. Its low surface area and acidic sites are the undesired properties of clay that reduce the catalytic efficiency of clay. The characteristic structure of raw bentonite was analyzed by X-ray diffraction technique as shown in Figure 4.1 The sample showed the sharpest peak at 6° , corresponding to the (001) plane of montmorillonite with the d-spacing of 14.8\AA . Another peak of montmorillonite showed at 19° , corresponding to the (100) plane [49]. The sharp peak at 27° was due to the present of quartz (SiO_2) [49].

4.1.1.2 The purification of purified-clay

The impurities could be removed by dispersion, centrifugation and decantation of clay suspension in water. The X-ray diffraction patterns of the raw material and purified-clay are shown in Figure 4.2. The d_{001} spacing of purified-clay was 12.8\AA . The quartz peak at 27° was disappeared from the XRD pattern of purified-clay collected from the centrifugal speed of 4000 rpm, suggesting quartz and other crystalline impurities were successfully removed from raw clay.

4.1.1.3 The preparation and characterization of Na-clay.

Layer structure of clay possesses negative charges which balance with additional interlayer cations such as Na^+ , K^+ and Ca^{2+} . Several interlayer

cations are difficult to be replaced by a large precursor during a pillaring process. Therefore, homoionic bentonite was prepared by ion exchange method. Bentonite treated with 5 M NaOH for three times, was chosen as a starting homoionic clay and designated as Na-clay. The XRD patterns of purified-clay and Na-clay are compared in Figure 4.3. The d_{001} peak of Na-clay was higher than purified-clay suggesting that Na ions intercalated into the clay layers and the NaOH treatment solution did not destroyed the clay layered structure. The d_{001} spacing of was 15.0 Å. The Na ion was chosen to intercalate between the clay layers because its high solvation energy and small electrostatic interaction between monovalent cations and negatively layered charge that are benefits for pillaring process.

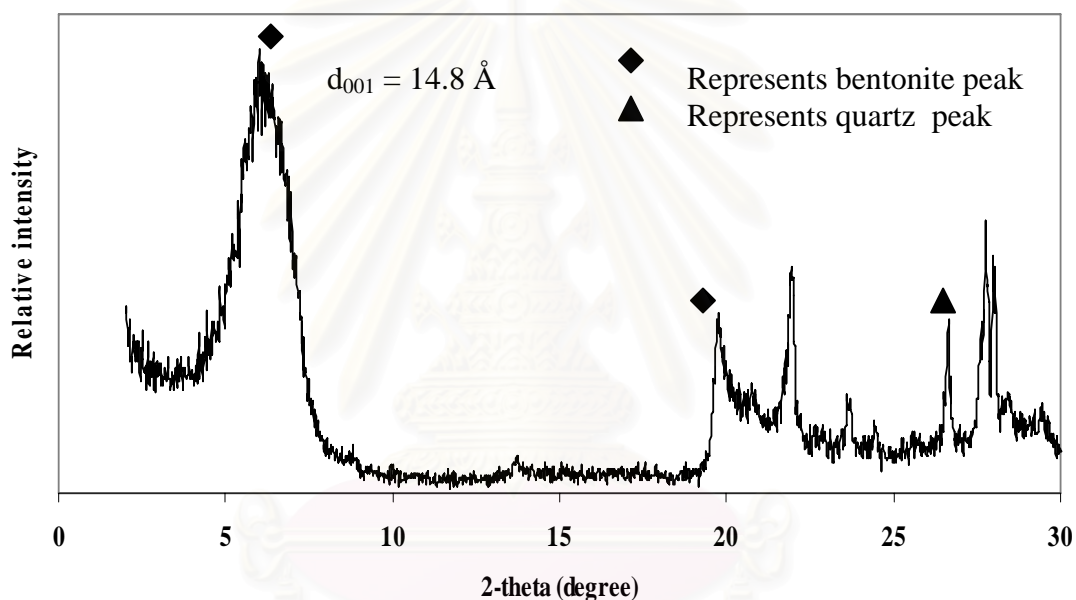


Figure 4.1 XRD pattern of raw clay.

4.1.1.4 The characterization of aluminium oxide-pillared clay by XRD

Aluminium oxide-pillared clay was synthesized by intercalation method. When Na ions was replaced by aluminium polycation and then was calcined at high temperature (500°C for 1h) [49]. Aluminium precursors between the clay layers converted to aluminium oxide (pillared form) and affected inter clay layer more expand. XRD patterns of aluminium-oxide pillared clay confirmed the changing of material structure. The characteristic peak of aluminium oxide-pillared clay showed peaks in the low 2-theta value when compared with Na-clay (starting

material). This was a clear indication of an increase in the basal spacing of the clay. The main 2-theta peak of aluminium oxide-pillared clay gives a basal spacing of 16.3 Å. The d_{001} spacing of aluminium oxide-pillared clay was higher than Na-clay (15Å).

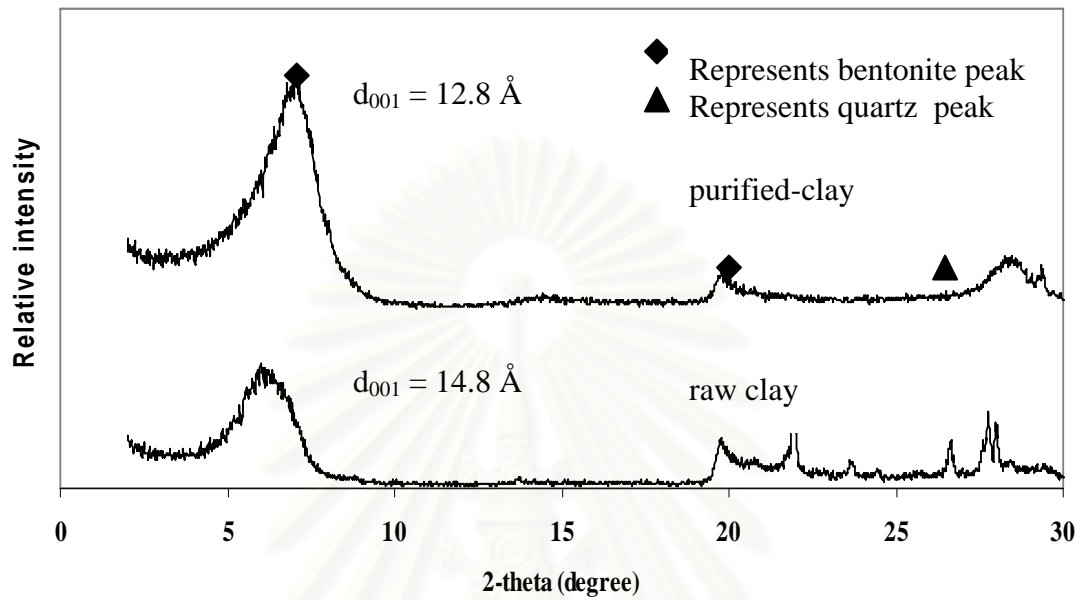


Figure 4.2 XRD patterns of raw clay and purified-clay.

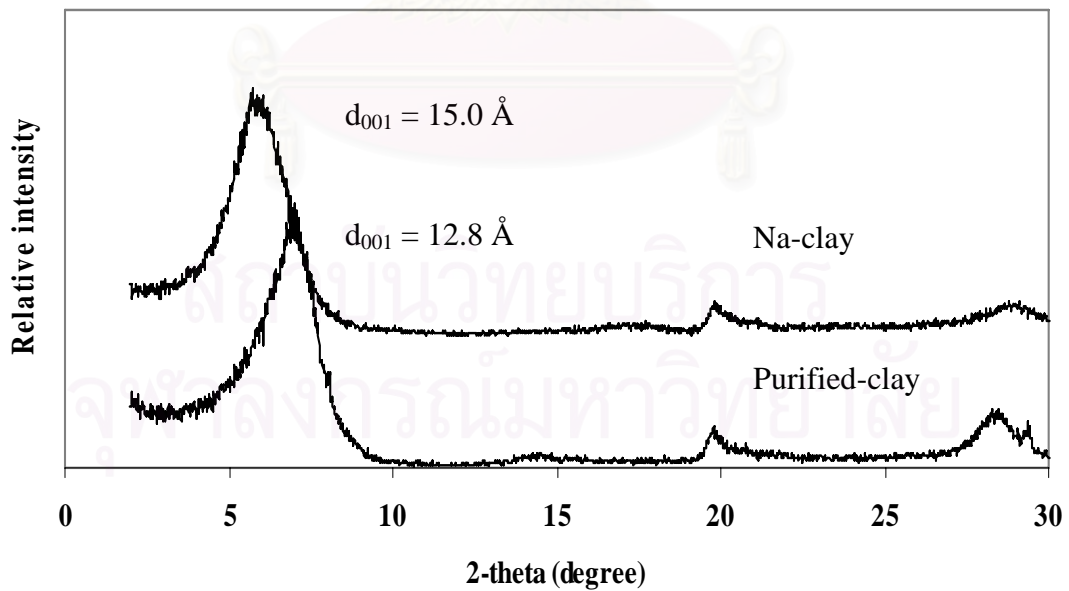


Figure 4.3 XRD patterns of purified-clay and Na-clay.

4.1.1.5 The preparation and characterization of zirconium/aluminium oxide-pillared clay

In order to investigate the effect of zirconium doped on the aluminium oxide-pillared clay, the amount of zirconium was varied between 0.0 to 5.0 wt% and all samples were calcined at 450°C for 4h. After calcination, the d_{001} spacing of all zirconium/aluminium oxide-pillared clays were lower than aluminium oxide-pillared clay as shown in Table 4.1, indicating that the second calcination in impregnation process caused the structure of the pillared catalyst collapse slightly. Their XRD patterns were shown in Figure 4.5 as compared to those of ZrO_2 and Al_2O_3 . The characteristic peaks of clay were observed in all samples, indicating that zirconium impregnation did not destroy the clay layered structure. The characteristic peaks of ZrO_2 were observed at 2-theta range 27° to 32° and the sharpest peak was observed at 2-theta of 30°. The characteristic peak of ZrO_2 [50] was found in the XRD pattern of 5.0wt% zirconium/aluminium oxide-pillared clay, indicating zirconium content excess and was presented in the outside of catalyst structure. Compared to the bulb Al_2O_3 , the aluminium oxide-pillared clay and 1.0wt% zirconium/aluminium oxide-pillared clay to 5.0wt% zirconium/aluminium oxide-pillared clay did not show the characteristic peak of Al_2O_3 at 14.5°, indicating that Al_2O_3 phase did not present outside of the layered structure.

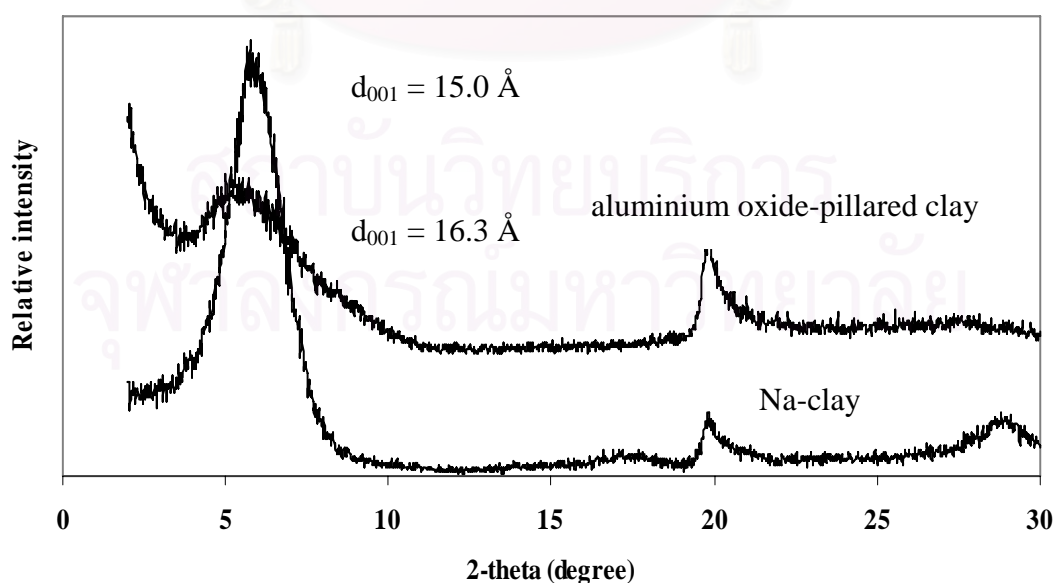


Figure 4.4 XRD patterns of Na-clay and aluminium oxide-pillared clay.

Table 4.1 The d_{001} spacing of aluminium oxide-pillared clay and 1.0wt% zirconium/aluminium oxide-pillared clay to 5.0wt% zirconium/aluminium oxide-pillared clay.

Sample	d_{001} (Å)
aluminium oxide-pillared clay	16.3
1.0wt% zirconium/aluminium oxide-pillared clay	15.8
2.0wt% zirconium/aluminium oxide-pillared clay	15.4
3.0wt% zirconium/aluminium oxide-pillared clay	15.4
5.0wt% zirconium/aluminium oxide-pillared clay	15.6



สถาบันวิทยบริการ
จุฬาลงกรณ์มหาวิทยาลัย

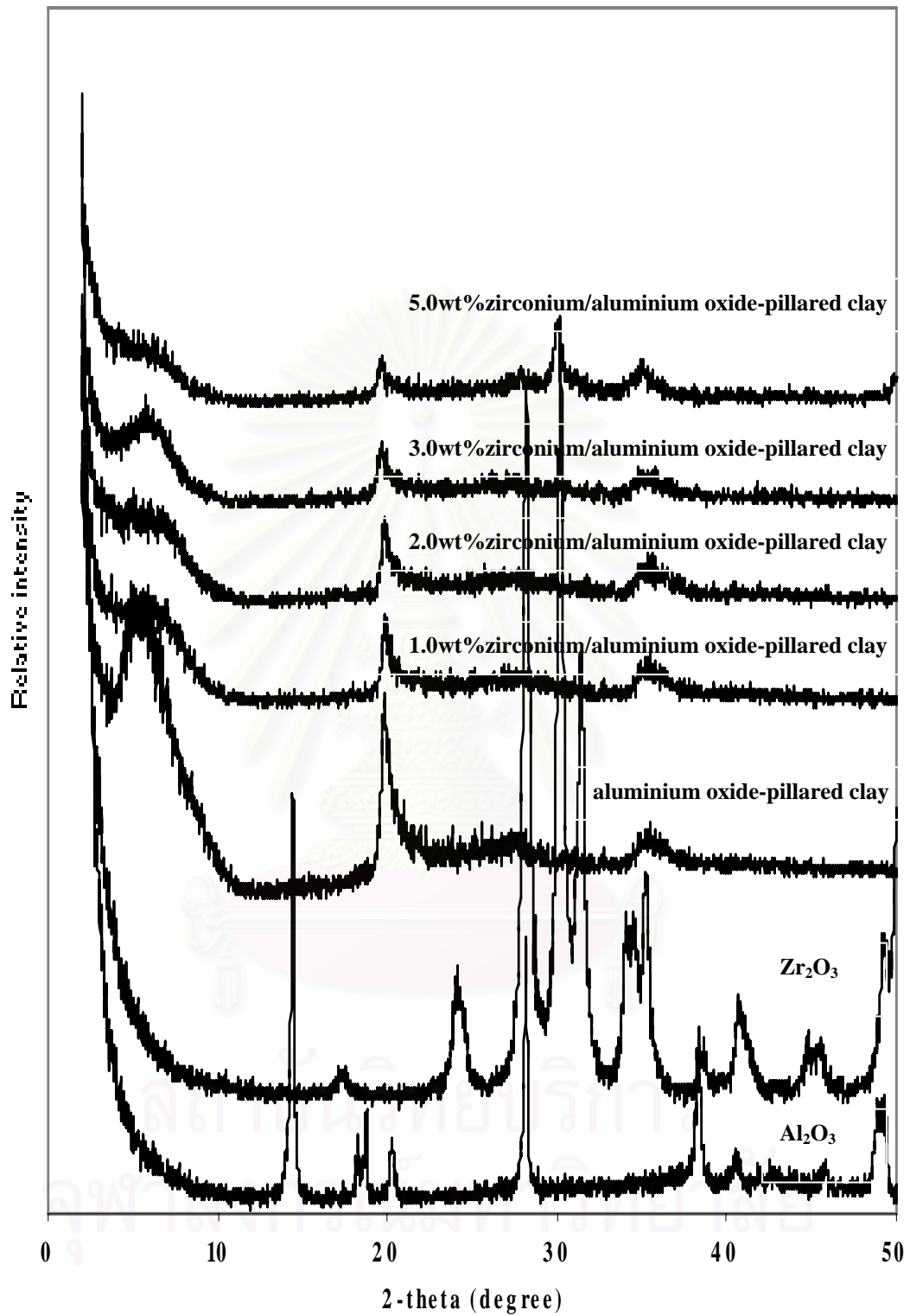


Figure 4.5 XRD patterns of Al₂O₃, ZrO₂, aluminium oxide-pillared clay and 1.0wt% zirconium/aluminium oxide-pillared clay to 5.0wt% zirconium/aluminium oxide-pillared clay.

4.1.2 Fourier Transform Infrared Spectroscopy (FT-IR)

Table 4.2 FTIR frequencies of major bands in raw clay, Na-clay and Al-pillared clay [51]-[55]

assignment	wave number (cm ⁻¹)		
	Raw clay	Na-clay	aluminium oxide-pillared clay
1.interlayer H ₂ O			
- stretching	3432.01	3436.1	34440.2
- bending	1634.05	1638.14	1634.05
2.framework OH			
- stretching	3624.06	3634.06	3636.32
- bending	1450.17	1429.74 (least intensity)	1429.74 (least intensity)
3.Si-O (Si-O-Si)			
- stretching	1029.28	1029.28	-
- shoulder	1113.04	1113.01	-
- bending	624.74	624.74	-
4.Si-O(O-Si-O) in framework			
- stretching	795.65,700	788.20,698.3 0	804.54,698.3
- bending	465.38	465.38	469.47
5.Si-O-Al			
- stretching	-	-	1052.17 (shift from Si-O)
- bending	518.5	522.59	526.09
6.Al-OH-Al			
- bending	914.87	914.87	930.43
7.Al-OH-Mg			
- bending	845.4	845.4	882.18

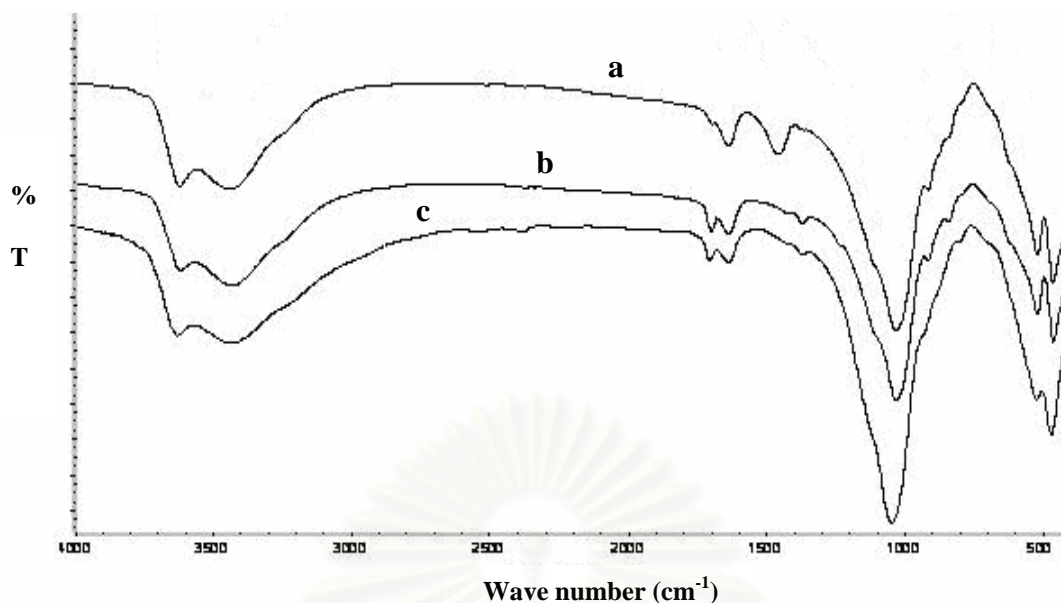


Figure 4.6 FTIR spectra of (a) raw clay, (b) Na-clay and (c) aluminium oxide-pillared clay.

The FTIR spectra of raw clay, Na-clay and aluminium oxide-pillared clay catalysts were shown in Figure 4.6 and Table 4.2 showed assign peak of them. As the framework vibrations of IR spectra contain information about the structural characteristics of materials, the similitude of the IR spectra as shown in raw clay (a) and Na-clay (b) clearly indicated that the basic clay layer structure remains unaffected on ion exchange process. Aluminium oxide-pillared clay showed the different IR spectra from each other. Stretching of Si-O-Si bond does not found in aluminium oxide-pillared clay but showed stretching and Si-O-Al bond around 1052 cm^{-1} . Suggested that effect from pillaring process to shift of Si-O-Si towards higher frequencies (1052 cm^{-1}). This fact has been related to a change in the symmetry of the surface Si-O-Si vibration perhaps associated to a change in the electric field near the Si groups due to the proximity of more positively charged aluminium groups. The bands at 910 and 840 cm^{-1} decrease with pillaring but no important differences among samples are visible, denoting a similar degree of exchange [54, 56].

4.1.3 Inductively Coupled Plasma-Atomic Emission Spectroscopy (ICP-AES)

The aluminium content in aluminium oxide-pillared clay was analyzed by ICP method. Thus, the aluminium content in aluminium oxide-pillared clay must be compared with that in the raw clay. Table 4.3 reports the aluminium contents in the form of Al_2O_3 . The large amount of aluminium in aluminium oxide-pillared clay,

exceeding the cation exchange capacity, suggests that aluminium would be in the pillared form within the interlayer. In addition, the XRD pattern of aluminium oxide-pillared clay shown in Figure 4.5 contains no peak of Al_2O_3 which indicates no significant amount of Al_2O_3 species outside the clay structure.

Table 4.3 The aluminium contents in clay and aluminium oxide-pillared clay

Samples	% Al_2O_3
raw clay	23.70
aluminium oxide-pillared clay	30.38

4.1.4 Nitrogen Adsorption-Desorption (BET)

The N_2 adsorption-desorption was the most widely technique used to determine the physical properties of mesoporous molecular sieves, such as the surface area, pore volume, pore diameter and pore-size distribution of solid catalysts. The surface area reported depends upon the method used, as well as the partial pressures at which the data are collected. The BET specific surface area of raw clay, purified-clay, Na-clay, aluminium oxide-pillared clay, ZrO_2 and Al_2O_3 are shown in Table 4.4. The modification from raw clay to aluminium oxide-pillared clay resulted to the increase of the specific surface area from 55 to $189 \text{ m}^2\text{g}^{-1}$, that could be related with the increase of d_{001} spacing from 14.5 to 16.3 \AA . It could be explain that the expanding of the interlayer of sample allowed the more access of nitrogen molecules. For increasing surface area of aluminium oxide-pillared clay also indicated that aluminium precursors are converted to the pillars of Al_2O_3 during calcinations process effect to expand inter layers structure and desegregation of clay particles largely contributes to the enhancement of surface area and porosity of the clay materials and easy for entering of nitrogen molecules [56]. The nitrogen adsorption-desorption isotherms of all sample revealed the type-IV isotherm as the example of Na-clay shown in Figure 4.7. The feature of type IV isotherm with H4 hysteresis loop was found, denoting a slit-shaped porosity between platelike particles. The first part of the isotherms, below $0.4p/p^0$, corresponding to adsorption in micropores, and in the last part, above $0.9 p/p^0$, corresponding to macropores [49].

The comparison of surface area of various zirconium doped amount shows that when the zirconium increased, the surface area decreased from $188 \text{ m}^2\text{g}^{-1}$ of

1.0wt% zirconium/aluminium oxide-pillared clay to $131 \text{ m}^2\text{g}^{-1}$ of 5.0wt% zirconium/aluminium oxide-pillared clay. The d_{001} spacings remain constant about 15.6 \AA , indicating that the high amount of zirconium did not degrade the pillared structure. The decrease in surface area resulted from ZrO_2 could block the cavity of catalysts, and reduced the passage of nitrogen. Especially for the 5.0wt% zirconium/aluminium oxide-pillared clay that contains the ZrO_2 outside the clay structure, the low surface area also results from the low surface area of bulb ZrO_2 of $28 \text{ m}^2\text{g}^{-1}$.

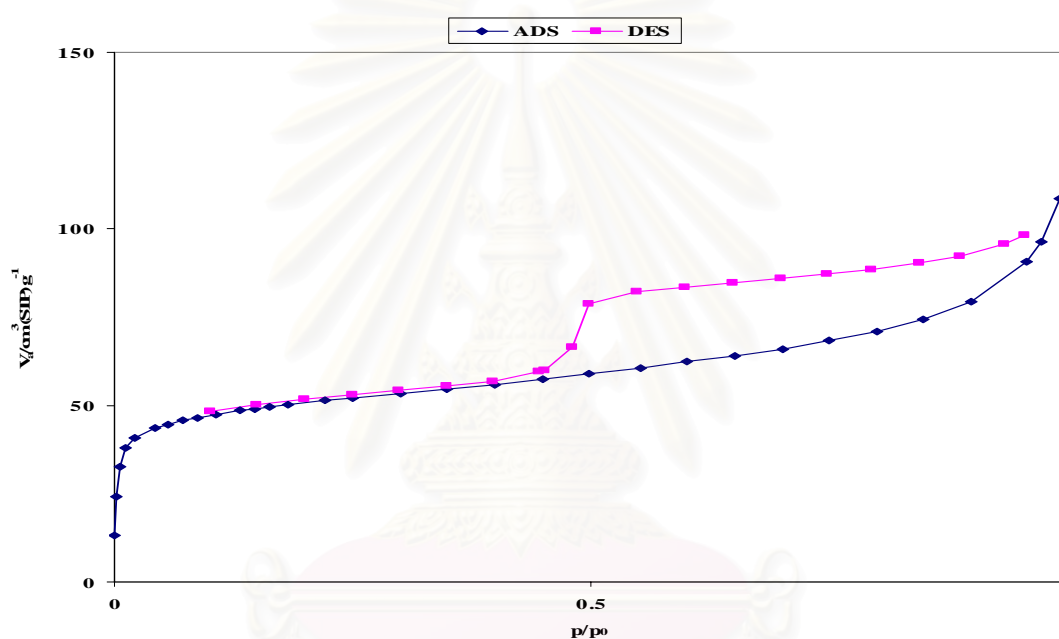


Figure 4.7 N_2 adsorption-desorption isotherm of Na-clay.

Table 4.4 The BET specific surface area of raw clay, purified-clay, Na-clay, aluminium oxide-pillared clay, ZrO_2 and Al_2O_3

Sample	surface area (m^2g^{-1})	d_{001} (\AA)
raw clay	55	14.5
Na-clay	118	15.0
aluminium oxide-pillared clay	189	16.3
Al_2O_3	138	-
ZrO_2	28	-

Table 4.5 The BET specific surface area of Al₂O₃, ZrO₂, aluminium oxide-pillared clay and 1.0wt% zirconium/aluminium oxide-pillared clay to 5.0wt% zirconium/aluminium oxide-pillared clay

Sample	surface area (m ² g ⁻¹)	d ₀₀₁ (Å)
aluminium oxide-pillared clay	189	16.3
1.0wt% zirconium/aluminium oxide-pillared clay	188	15.8
2.0wt% zirconium/aluminium oxide-pillared clay	183	15.4
3.0wt% zirconium/aluminium oxide-pillared clay	174	15.4
5.0wt% zirconium/aluminium oxide-pillared clay	131	15.6
Al ₂ O ₃	138	-
ZrO ₂	28	-

4.2 Activity of Aluminium Oxide-Pillared Clay Catalysts in PP Cracking

4.2.1 Effect of Reaction Time.

Reaction temperature at 380°C was chosen for studying the effect of reaction time on PP cracking over aluminium oxide-pillared clay catalyst. The values of conversion and the product yield for thermal and catalytic cracking are shown in Table 4.6. When the reaction time was increased, conversions of PP into liquid and gas fraction for thermal and catalytic cracking gave rising while residue decreased. This may be due to the reactant has more time to react and degrade into products. For a short period of reaction time, only small molecules can escape from the reaction with N₂ gas which results in high contact of gas fraction compared to liquid fraction.

When thermal and catalytic cracking were compared at the same reaction time, conversion of thermal cracking was lower than catalytic cracking because the acidity of catalyst accelerates the initial breakdown of the original macromolecules to product. With increasing reaction time, the difference between thermal and catalytic cracking conversion increased but after reaction time 1 h, the difference between thermal and catalytic cracking conversion decreased. This is because at higher reaction time, thermal cracking plays an important role than catalytic cracking. In addition, at reaction time 1 h, the reaction produced more liquid products than other

reaction time (The difference in liquid yield between cracking and thermal reactions was high). Thus, the reaction time at 1h was chosen for further studied in this work.

Table 4.6 %Conversion, %yield and %selectivity of liquid fraction obtained by thermal and catalytic cracking of PP over aluminium oxide-pillared clay catalyst with various reactions times.

	Catalytic cracking				Thermal cracking			
	0.5 h	1.0 h	1.5 h	2.0 h	0.5 h	1.0 h	1.5 h	2.0 h
% Conversion*	40.2	78.5	89.6	96.8	19.6	55.2	80.4	85.0
% yield* 1. gas fraction	16.7	31.1	36.8	39.7	14.6	26.4	36.0	39.6
2. liquid fraction	23.5	47.5	52.8	57.1	5.0	28.8	44.4	45.4
3. residue	59.8	21.5	10.4	3.2	80.4	44.8	19.6	15.0
% selectivity of liquid fraction								
1. distillate oil	23.0	24.2	14.2	22.4	19.4	14.1	20.4	18.5
2. heavy oil	77.0	75.8	85.8	77.6	80.6	85.9	79.6	81.5
Liquid fraction density (g/cm ³)	0.73	0.74	0.73	0.73	0.74	0.72	0.73	0.73

Condition: 10 wt% of catalyst to plastic ratio, N₂ flow of 20 cm³/min and reaction temperature of 380°C. *Deviation within ±0.4% for conversion, ±0.9% for yield of gas fraction, ±0.5% for yield of liquid fraction, and ±0.4% for yield of residue.

The comparison in accumulative volumes or fractional oil recovery of liquid products with lapse time between thermal and catalytic cracking at different reaction times, shown in Figure 4.8, indicates that catalytic cracking was faster than thermal cracking. When reaction time was increased, total volume of liquid fraction was increased. These results can be explained by catalyst acidity accelerates the cracking of PP. Proton from brønsted acid site of the catalyst leads to formation of carbenium ions by addition to the carbon-carbon double bond of polymer. Cracking of the adsorbed carbenium ion proceeds through the β -scission mechanism [57, 58]. And when the reaction time was increased thermal and catalytic cracking had more time to convert polymer into product such as liquid products.

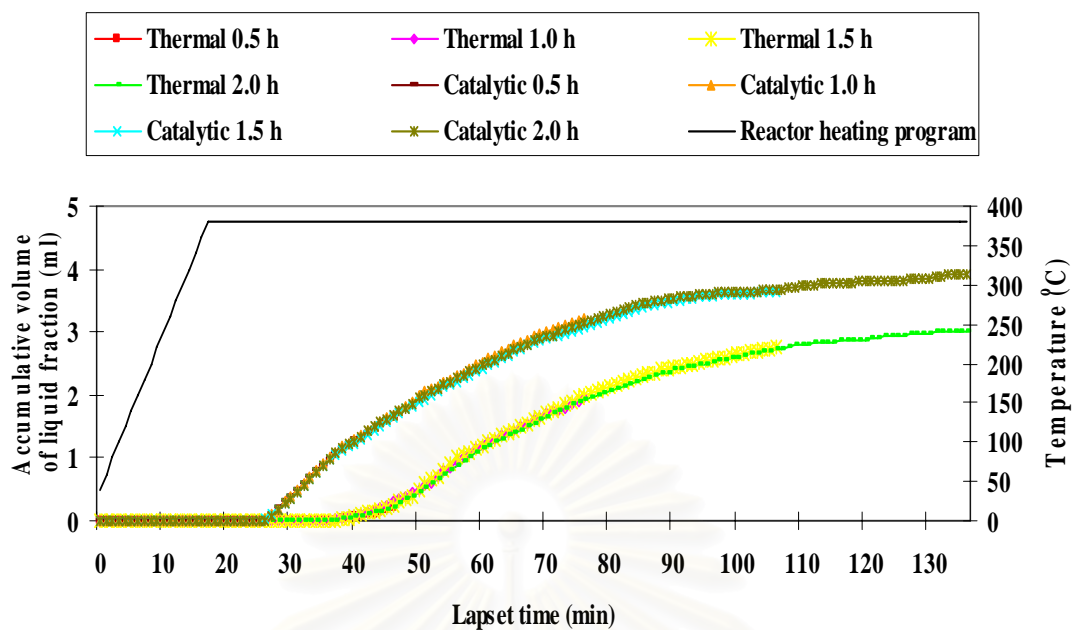


Figure 4.8 Accumulative volume of liquid fraction obtained by thermal and catalytic cracking of PP over aluminium oxide-pillared clay catalyst with various reaction times.

Figure 4.9 shows distribution of gas fraction for thermal and catalytic cracking. Considering only gases at ambient condition which were normally C_1 through C_5 . The product distribution of gas fraction obtained from thermal and catalytic cracking were not different and the reaction time was not affected the product distribution. For thermal cracking, the major product was C_3 (propene) and minor products were C_{5+} , C_5 (n-pentane), C_4 (i-butene) and C_2 (ethane). For catalytic cracking, major product was C_{5+} and minor products were C_3 (propene), C_1 (methane) and C_4 (i-butene). C_{5+} components were liquid vapors of C_6 (hexane) which had higher boiling point than that of C_5 (n-pentane). The difference in gas components between thermal and catalytic cracking is explained by the different cracking mechanism. Thermal cracking proceeds through free radical chain mechanism whereas catalytic cracking proceeded through carbocation mechanism [59, 60].

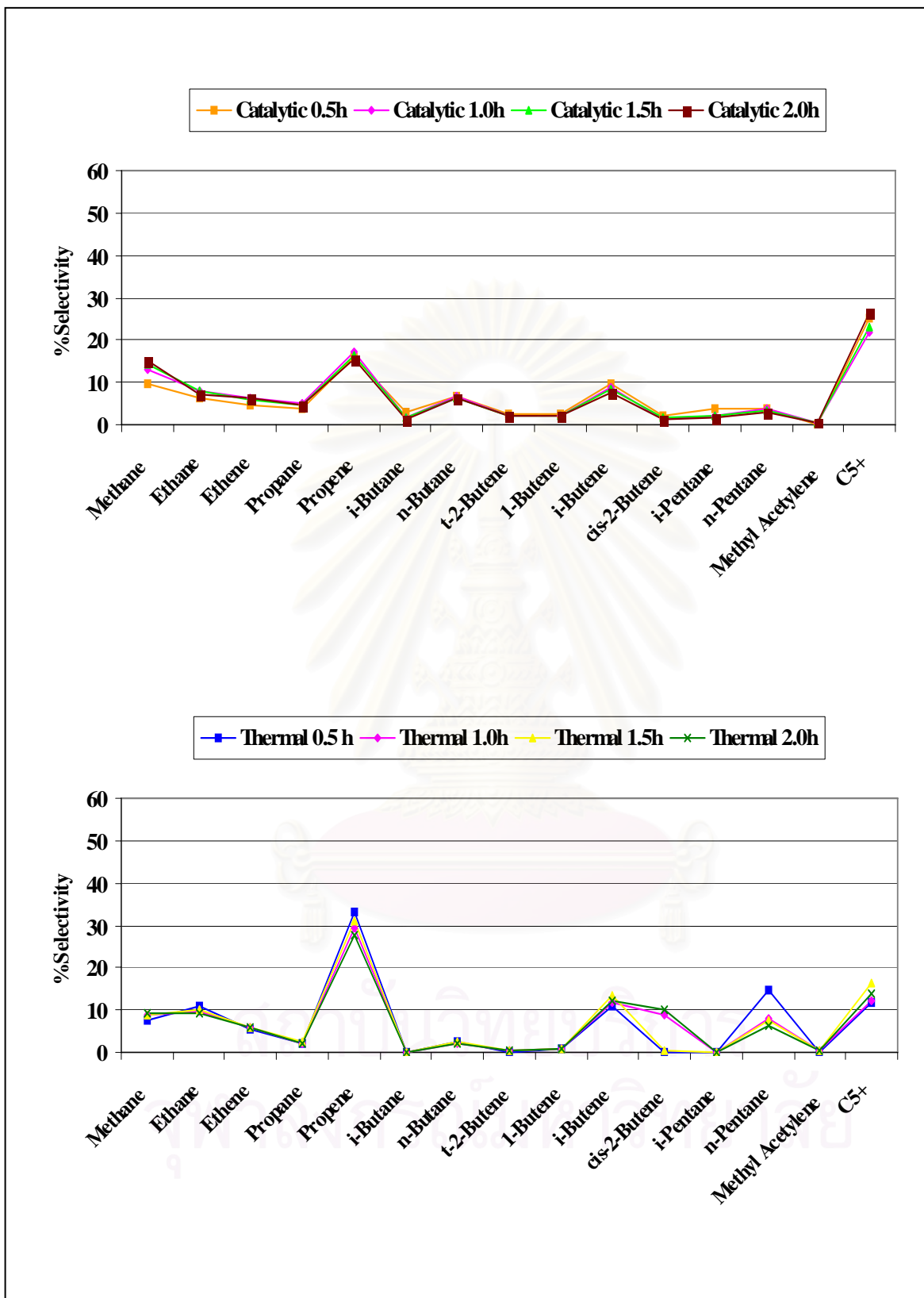


Figure 4.9 Distribution of gas fraction obtained by the thermal and catalytic cracking of PP with various reaction times.

The product distribution for distillate liquids has been shown in Figure 4.10. Thermal cracking showed product distribution in the range of C₆ to C₉ and the outstanding of major product was C₉. When reaction time was increased, the product distribution was not affected but the selectivity to C₉ was decreased because it has more time for large fragment to convert into small fragment. For catalytic cracking, the main products were C₇ to C₉. The major product for catalytic reaction was smaller than that of thermal reaction because of acidity and pore of catalyst.

Figure 4.11 shows the product distribution of SUPELCO standard gasoline fraction. It was found that the liquid distribution was in the range of C₇ to C₈, based on the boiling point range using n-paraffin. Hence, it can be conclude that catalytic cracking can be the good cracking catalyst for conversion PP to the valuable fraction of liquid hydrocarbon in the range of gasoline.

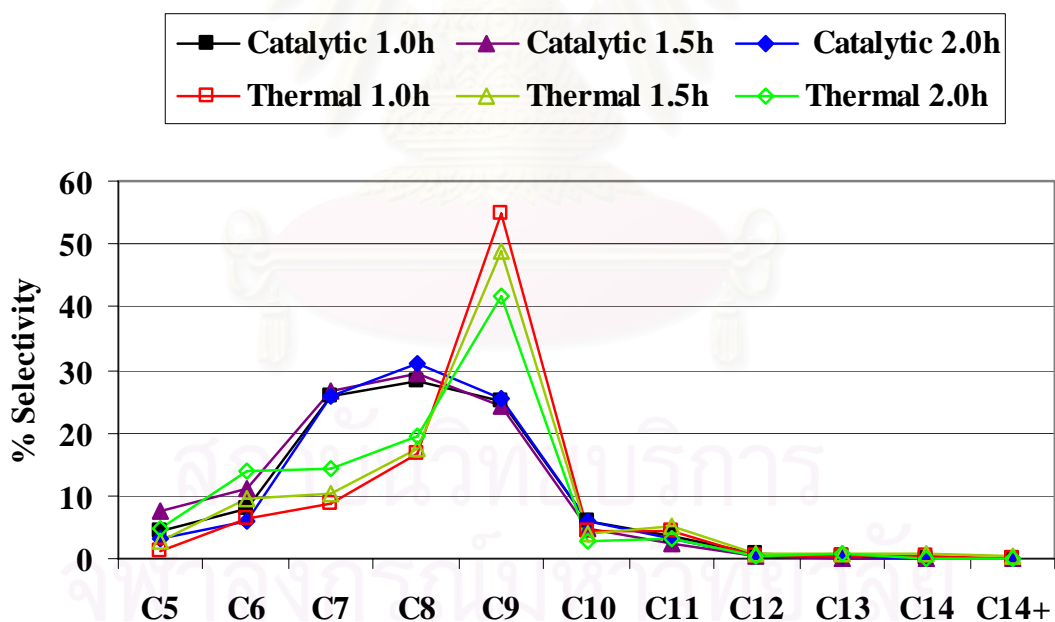


Figure 4.10 Carbon number distribution of distillate oil obtained by thermal and catalytic cracking of PP over aluminium oxide-pillared clay catalyst with various reaction times.

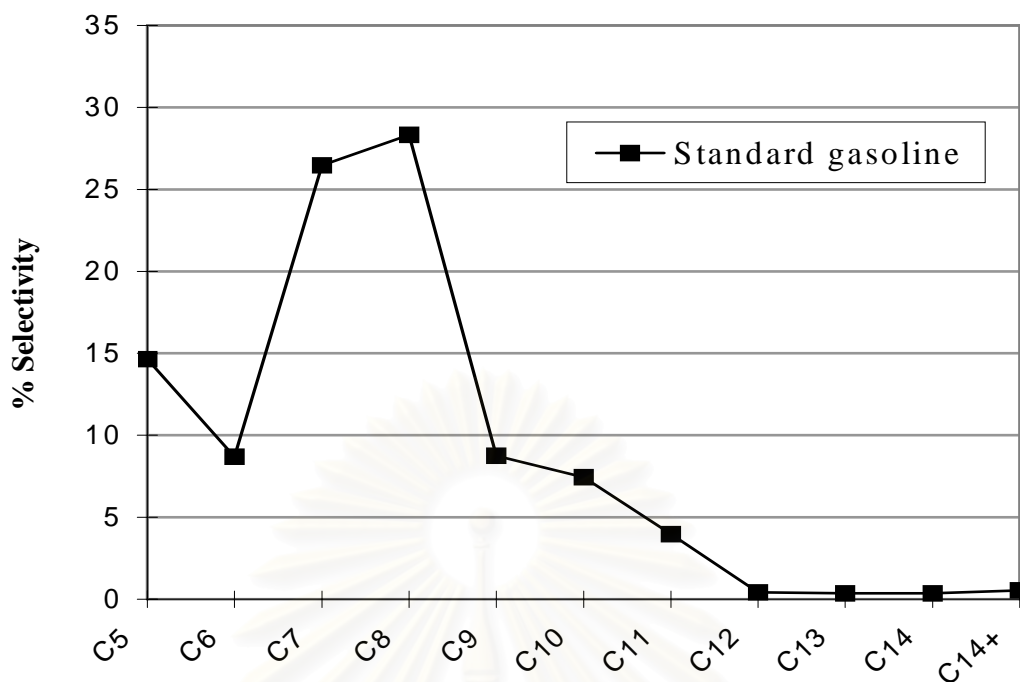


Figure 4.11 Carbon number distribution of commercial SUPELCO standard gasoline fraction.

4.2.2 Effect of Reaction Temperature

The value of conversion and the product yield for thermal and catalytic cracking of PP over aluminium oxide-pillared clay for 1 h at various temperatures are shown in Table 4.7. When the reaction temperatures were increased conversions of both cracking reactions were increased, suggesting the high temperature accelerated the cracking of PP. Thermal and catalytic cracking at reaction temperature 350°C showed gas fraction as main product and no liquid fraction was found in the graduated cylinder for thermal cracking at 350°C. Solid coke and wax values were not calculated because plastic was melted and combined with catalyst remaining in the reactor. Cracking temperatures at 380 and 410°C for thermal and catalytic reactions showed liquid fraction as main product. At low temperature, the scission of smaller chain hydrocarbon gave gas product as main product, while larger hydrocarbon demanded higher energies to break down at high temperatures and gave liquid product as main product. All of catalytic cracking temperatures showed amount of distillate oil around 25.0 wt% and for thermal cracking around 13.0 wt%. The reaction temperature was not affected the amount of distillate oil but acidity of catalyst did.

Table 4.7 %Conversion, %yield and %selectivity of liquid fraction obtained by thermal and catalytic cracking of PP over aluminium oxide-pillared clay with various reaction temperatures.

	Catalytic cracking			Thermal cracking		
	350 °C	380 °C	410 °C	350 °C	380 °C	410 °C
% Conversion *	21.7	78.5	93.9	4.0	55.2	91.6
% yield* 1. gas fraction	14.1	31.1	26.4	4.0	26.4	30.0
2. liquid fraction	7.5	47.5	67.5	0.0	28.8	61.6
3. residue	78.3	21.5	6.1	96.0	44.8	8.4
- wax	-	10.0	0.3	-	-	-
- solid coke	-	11.5	5.8	-	-	-
% selectivity of liquid fraction						
1. distillate oil	24.1	24.2	27.5	-	14.1	11.8
2. heavy oil	76.0	75.8	72.6	-	85.9	88.2
Liquid fraction density (g/cm ³)	0.71	0.74	0.76	-	0.72	0.75

Condition: 10 wt% of catalyst to plastic ratio, N₂ flow of 20 cm³/min, and reaction time 1.0 h. *Deviation within $\pm 0.4\%$ for conversion, $\pm 0.5\%$ for yield of gas fraction, $\pm 0.5\%$ for yield of liquid fraction, and $\pm 0.3\%$ for yield of residue.

The reaction temperature at 410°C showed the highest thermal effect that resulted in low value between thermal and catalytic cracking conversion. Therefore, it had been concluded that the reaction temperature at 380°C gave the highest catalyst efficiency. In this way, this condition (1.0 h, 380°C) was chosen for further study.

Figure 4.12 shows fractional oil recovery of liquid products derived from thermal and catalytic degradation with lapse time at various cracking temperatures. When the reaction temperatures were increased, rate of liquid fraction was increased indicating that reaction temperatures were affected liquid fraction rate.

Catalytic cracking of all reactions were look alike in selectivity of gas fraction. The major product was C₅₊ and minor products were C₃(propene), C₁(methane) and

C₄(i-butene). The selectivity of gas fractions for thermal reaction at 350°C was different from others. The major product was C₅(i-pentane) and minor products were C₄(cis-2-butene) and C₃(propene). Thermal reaction at 380 and 410°C showed that major product was C₃(propene) and minor products were C₄(i-butene), C₂(ethane), C₅(n-pentane) and C₅₊. During thermal cracking, a radical is formed through H-transfer reaction. The radical can also be form through chain isomerization reaction being n-alkane such as C₅(i-pentane) at mild condition (350°C). When temperature increases to 380-410°C, radicals decompose through the so-called “β scission” to form a smaller radical and an olefin (C₂(ethane) and C₃(propene)).

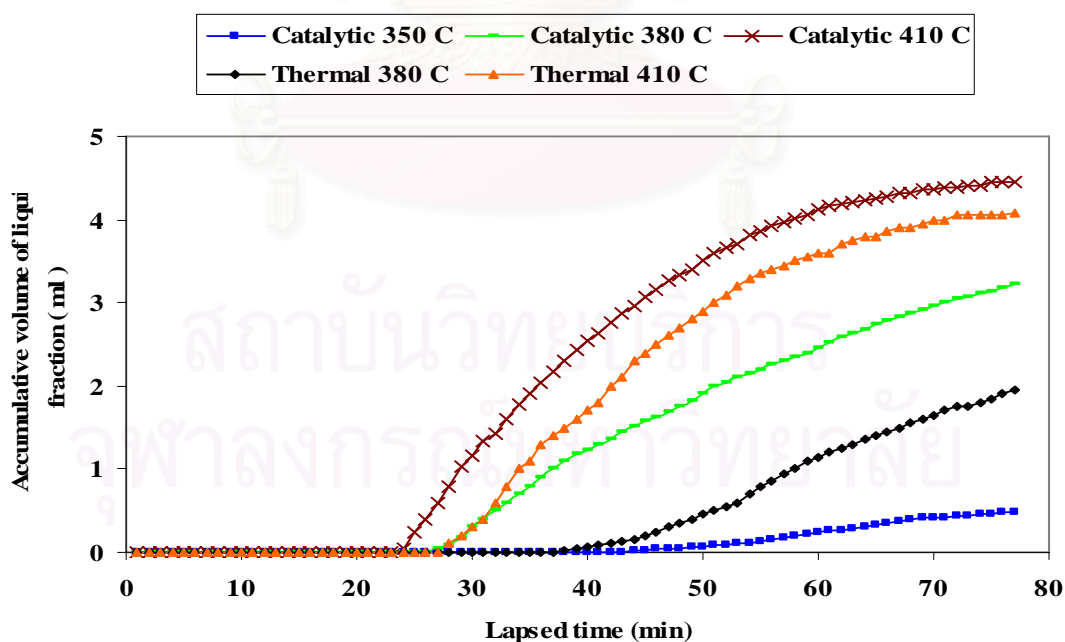
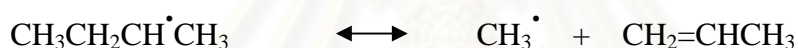


Figure 4.12 Accumulative volume of liquid fractions obtained by thermal and catalytic cracking of PP over aluminium oxide-pillared clay catalyst with various reaction temperatures.

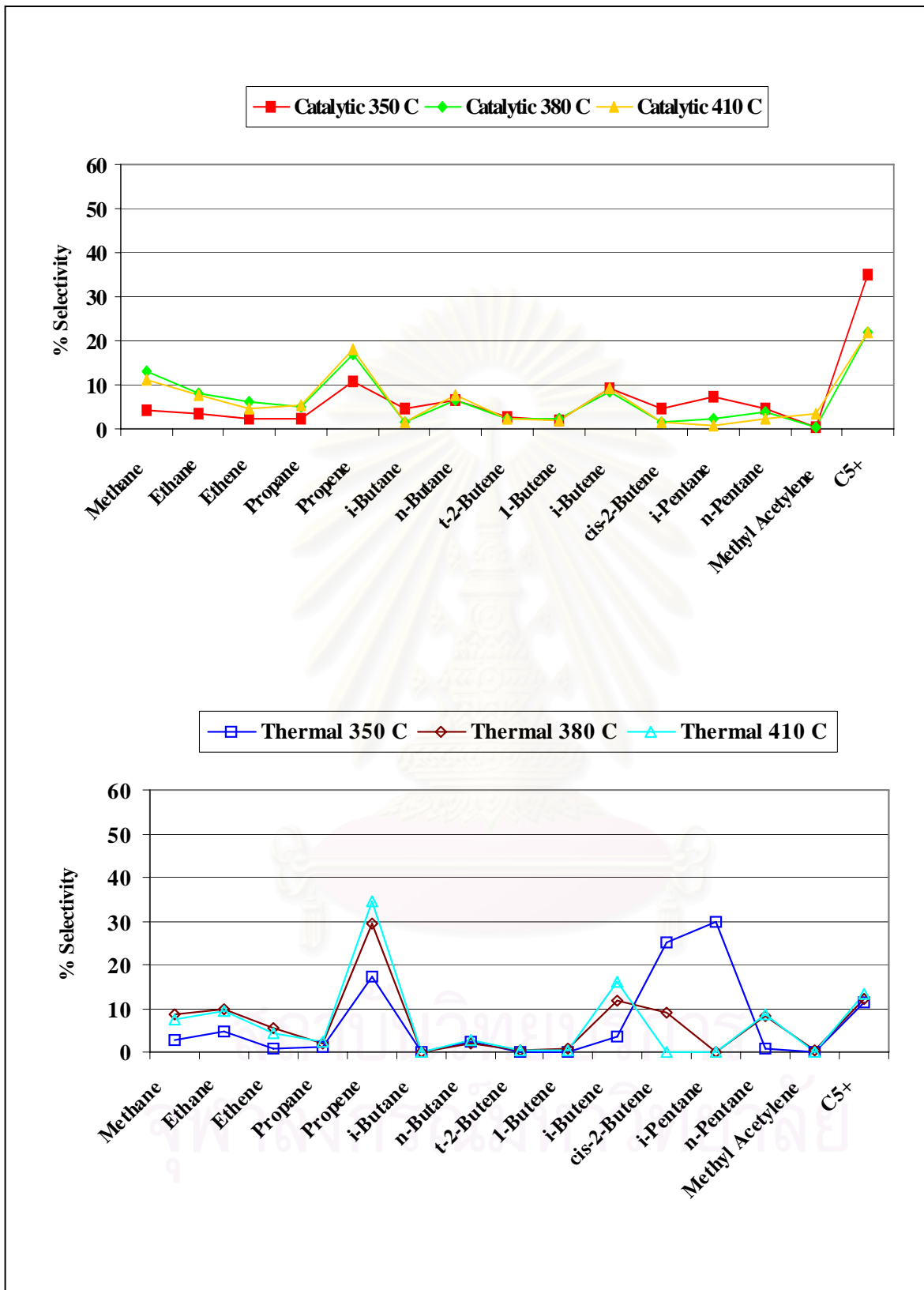


Figure 4.13 Distribution of gas fractions obtained by the thermal and catalytic cracking of PP over aluminium oxide-pillared clay with various reaction temperatures.

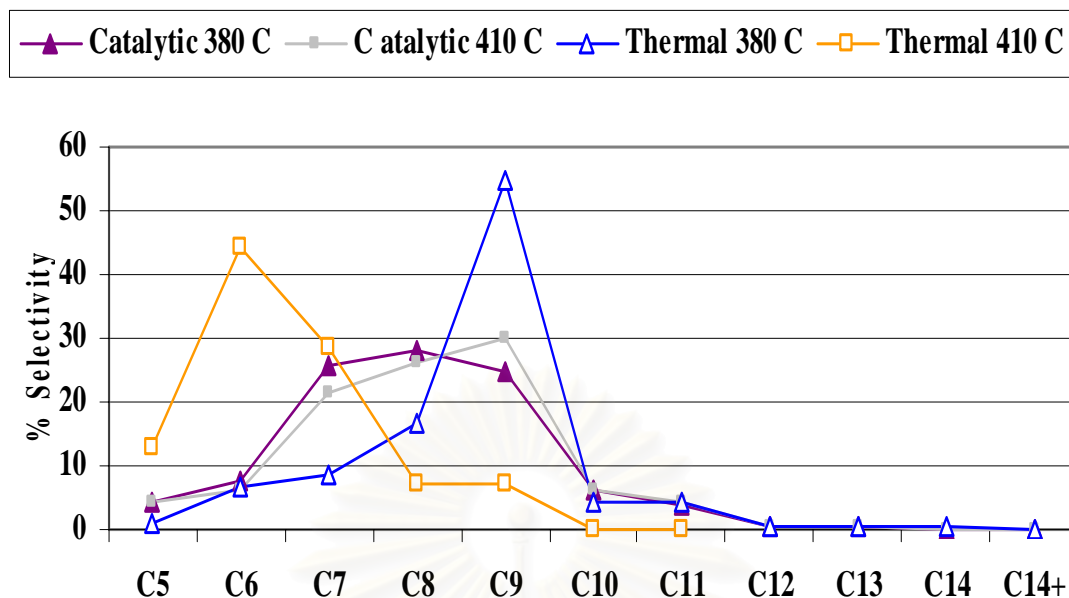


Figure 4.14 Carbon number distribution of distillate oil obtained by thermal and catalytic cracking of PP over aluminium oxide-pillared clay with various reaction temperatures.

Carbon number distribution of distillate oils showed in range of C₆ to C₉. C₉ and C₆ were the major product for thermal cracking at reaction temperature 380°C and 410°C respectively. Catalytic cracking at reaction temperature of 380°C and 410°C showed product distribution in range of C₇ to C₉. From this result, it was observed that reaction temperature was not affected on selectivity. When product distributions between thermal and catalytic cracking were compared, acidity of catalyst was not affected on selectivity of product but pore of catalyst did.

4.2.3 Effect of Zirconium Doped Aluminium Oxide-Pillared Clay (Zirconium/Aluminium Oxide-Pillared Clay).

To study the effect of zirconium doped aluminium oxide-pillared clay, the reaction was carried out by varying percent of zirconium impregnated on catalyst in the range of 0.0-5.0 wt%. Table 4.8 shows conversion and yield of catalytic cracking of PP over zirconium/aluminium oxide-pillared clay at various percent of zirconium. The increasing amount of zirconium affected %conversion and liquid fraction. The 2.0wt% zirconium/aluminium oxide-pillared clay showed the highest amount of %conversion and liquid fraction. When amount of zirconium was higher than 2.0 wt%, %conversion and liquid fraction were decreased because excess amount of

zirconium was decreasing surface area, acidity and active site of catalyst. For example 5.0wt% zirconium/aluminium oxide-pillared clay had the lowest conversion than others because excess amount of zirconium was observed on the catalyst support which blocked the catalytic cracking reaction. From this result, 2.0wt% zirconium/aluminium oxide-pillared clay was chosen for this reaction.

Table 4.8 %Conversion, %yield and %selectivity of liquid fraction obtained by thermal and catalytic cracking of PP over zirconium/aluminium oxide-pillared clay with various percent zirconium.

	Thermal	aluminium oxide- pillared clay	1.0wt% zirconium/ aluminium oxide- pillared clay	2.0wt% zirconium/ aluminium oxide- pillared clay	3.0wt% zirconium/ aluminium oxide- pillared clay	5.0wt% zirconium/ aluminium oxide- pillared clay
% Conversion*	55.2	79.0	82.4	89.8	81.3	56.9
% yield* 1.gas fraction	26.4	31.5	27.3	27.5	25.8	18.1
2.liquid fraction	28.8	47.5	55.1	62.3	55.5	38.8
3.residue	44.8	21.5	17.6	10.2	18.7	43.1
- wax	44.8	11.5	4.9	9.2	16.3	43.1
-solid coke	-	10.0	12.7	1.0	2.5	-
% selectivity of liquid fraction						
1.distillate oil	14.1	24.2	12.6	19.3	12.6	17.2
2.heavy oil	85.9	75.8	87.4	80.8	87.4	82.9
Liquid fraction density (g/cm ³)	0.72	0.74	0.76	0.75	0.79	0.78

Condition: 10 wt% of catalyst to plastic ratio, N₂ flow of 20 cm³/min and reaction time 1.0 h. *Deviation within $\pm 0.6\%$ for conversion, $\pm 0.1\%$ for yield of gas fraction, $\pm 0.5\%$ for yield of liquid fraction, and $\pm 0.3\%$ for yield of residue.

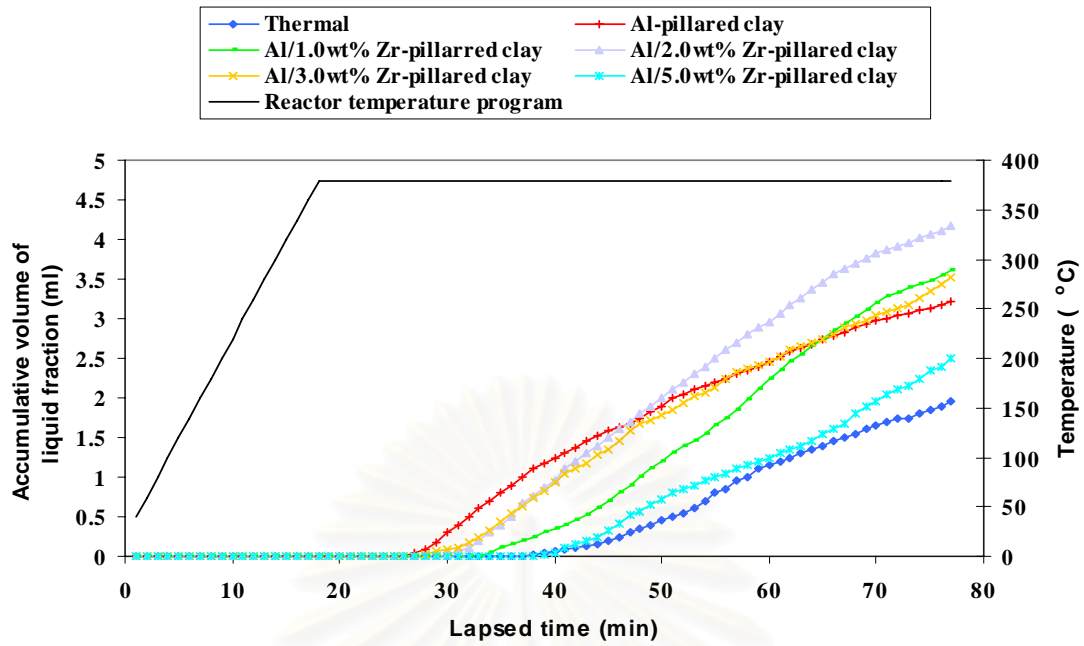


Figure 4.15 Accumulative volume of liquid fraction obtained by thermal and catalytic cracking of PP over zirconium/aluminium oxide-pillared clay with various percent zirconium.

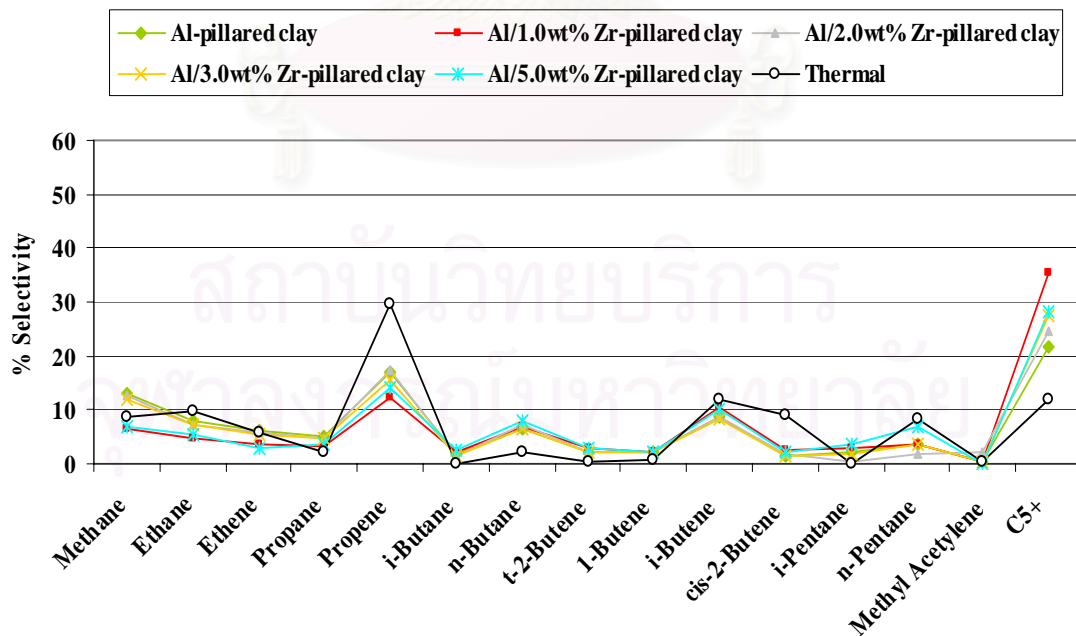


Figure 4.16 Distribution of gas fractions obtained by the thermal and catalytic cracking of PP over zirconium/aluminium oxide-pillared clay with various percent zirconium.

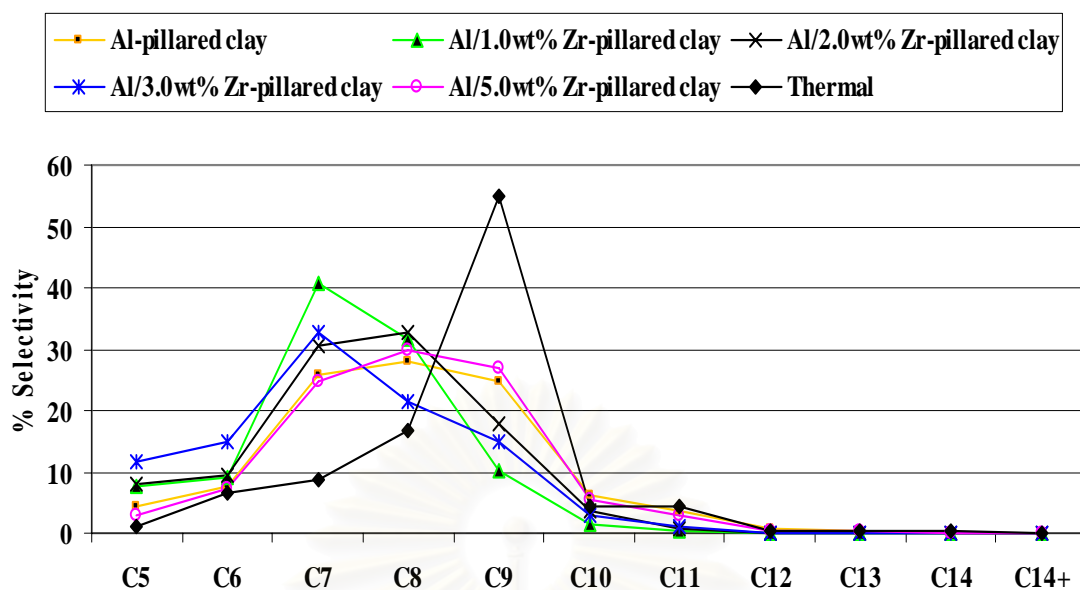


Figure 4.17 Carbon number distribution of distillate oil obtained by catalytic cracking of PP over zirconium/aluminium oxide-pillared clay with various percent zirconium.

Gas fraction for all catalytic reactions showed the major product was C_{5+} and minor product was C_3 (propene), C_1 (methane) and C_4 (i-butene). Thermal cracking showed C_3 (propene) as major product and minor products were C_{5+} , C_4 (i-butene), C_2 (ethane) and C_1 (methane). The reason has been explained in session 4.2.1.

Thermal and catalytic cracking with various percent zirconium showed products distribution in range of C_6 to C_9 . Thermal cracking showed the major product in C_9 and catalytic cracking showed high selectivity of C_7 to C_8 . Thermal cracking showed large hydrocarbon than catalytic cracking and acidity of catalyst breaks large molecules hydrocarbon into small hydrocarbon.

4.2.4 Effect of catalyst per plastic ratio

The 2.0wt% zirconium/aluminium oxide-pillared clay was used to study the effect of catalyst to plastic ratio on its activity. When the catalytic cracking was performed with increasing catalyst to plastic ratio, conversion of PP was increased while the decreased of residue was observed. It was suggested that the acidity of catalyst accelerated the cracking of PP into light hydrocarbons. A change in product yield was observed by an increased trend of gas products from 5.0 to 20.0 wt% of catalyst and a reduction of gas products at 30.0 wt% of catalyst. On the other hand,

with 30.0 wt% of catalyst showed the highest liquid fraction. This can be explained that the highest acidity by increasing amount of catalyst resulting in the increased in liquid fraction and the decreased of gas fraction. Amount of catalysts were not affected on distillate oil because all of reactions showed around 19 %.

Figure 4.18 shows the relationship between conversion and percent of catalyst. It was observed that conversion was quite constant after 10.0 wt. Increase in catalyst per plastic ratio means increasing acidity which affected total volume and rate of liquid fraction. The total volume of liquid fraction of 10.0, 20.0 and 30.0 wt% were slightly different (similar to %conversion). Therefore, 10.0 wt% of catalyst was the suitable amount of catalyst to plastic ratio in this work.

Table 4.9 %Conversion, %yield and %selectivity of liquid fraction obtained by thermal and catalytic cracking of PP over 2.0wt% zirconium/aluminium oxide-pillared clay with various percent catalyst per plastic ratios.

	5.0 % of catalyst to plastic ratio	10.0 % of catalyst to plastic ratio	20.0 % of catalyst to plastic ratio	30.0 % of catalyst to plastic ratio	Thermal
% Conversion*	57.5	89.8	93.9	94.0	55.2
% yield* 1. gas fraction	25.5	27.5	29.2	23.8	26.4
2.liquid fraction	32.0	62.3	64.7	70.2	28.8
3.residue	42.5	10.2	6.1	6.0	44.8
- wax	-	9.2	5.4	5.5	44.8
- solid coke	-	1.0	0.7	0.5	-
% selectivity of liquid fraction					
1.distillated oil	18.2	19.3	18.9	21.4	14.1
2. heavy oil	81.8	80.8	81.1	78.6	85.9
Liquid fraction density (g/cm ³)	0.75	0.75	0.74	0.75	0.72

Condition: 10 wt% of catalyst to plastic ratio, N₂ flow of 20 cm³/min and reaction time 1.0 h. *Deviation within $\pm 0.2\%$ for conversion, $\pm 0.2\%$ for yield of gas fraction, $\pm 0.2\%$ for yield of liquid fraction, and $\pm 0.2\%$ for yield of residue.

Figure 4.20 shows distribution of gas fraction for thermal and catalytic cracking. The product distribution of gas fraction obtained from thermal and catalytic were different and the variation of percent of catalyst to plastic ratio was not affected the product distribution. The selectivity of gas fraction for thermal cracking, major product was C_3 (propene) and minor product was C_{5+} . For catalytic cracking showed major product was C_{5+} and minor product was C_3 (propene). The difference in gas components between thermal and catalytic cracking has been explained in Session 4.2.1. When increased percent catalyst per plastic ratio, selectivity of C_{5+} increased while selectivity of C_3 (propene) decreased.

Carbon number distribution of distillate oil for thermal and catalytic cracking was in range of C_7 to C_{10} . Thermal cracking showed product distribution in range of C_8 to C_{10} and the outstanding of major product was C_9 . For catalytic cracking, the main products were C_7 to C_9 . Thermal cracking showed large hydrocarbon than catalytic cracking because of the different cracking mechanism as explain in Session 4.2.1. The increase in percent of catalyst to plastic ratio affected small hydrocarbon component in distillate oil, suggesting that high acidity and active site of catalyst lead to more carbenium ion by addition to the carbon-carbon double bond of polymer. Cracking of the adsorbed carbenium ion proceeds through the β -scission mechanism [57, 58].

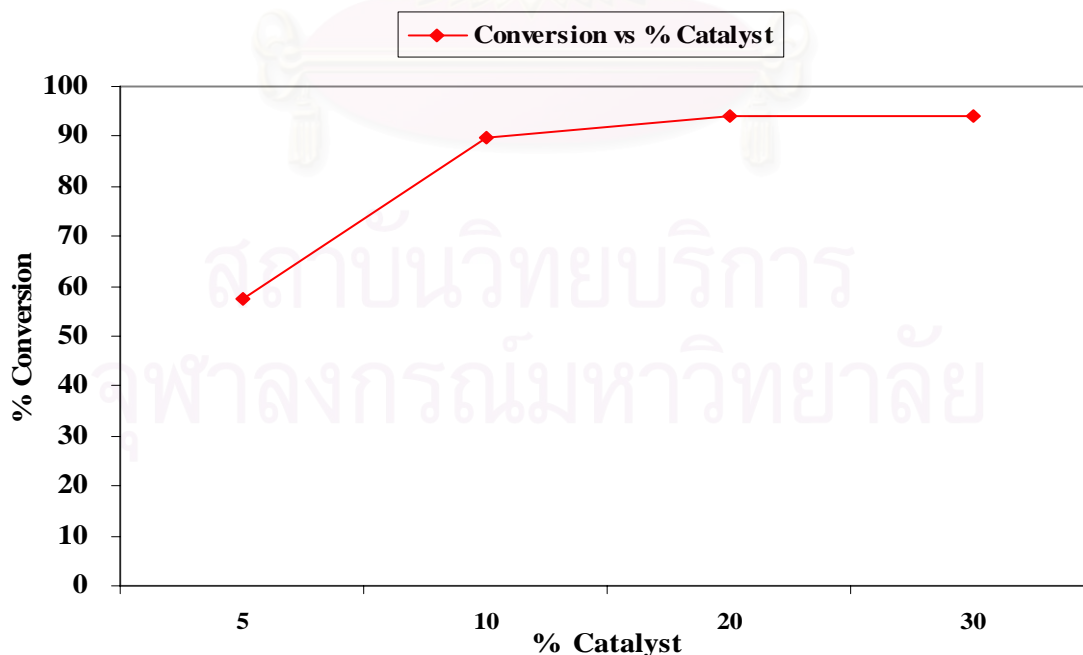


Figure 4.18 % Conversion at various percent catalyst to plastic ration.

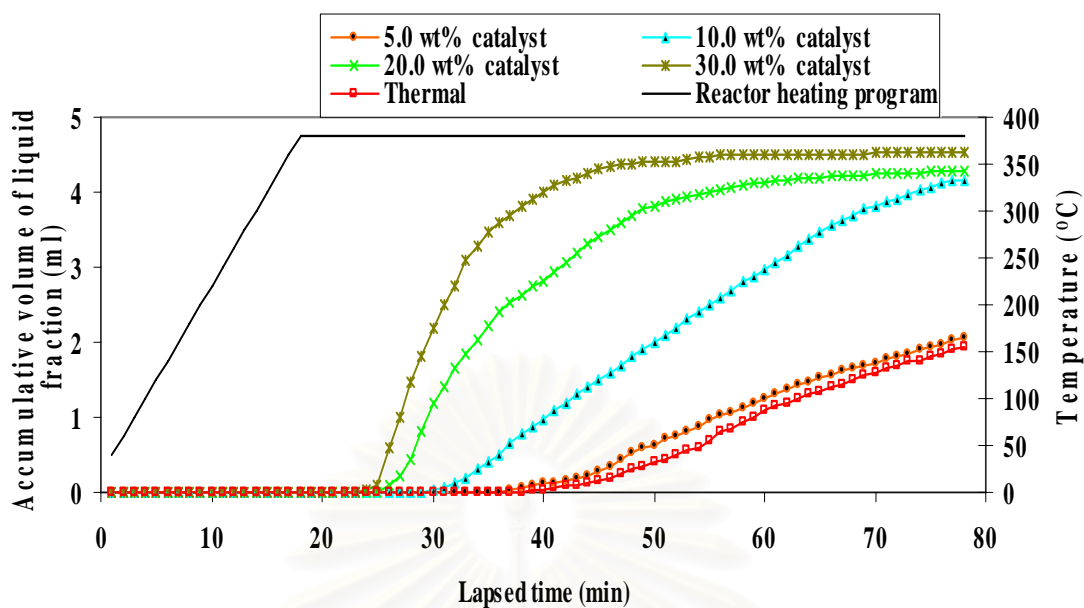


Figure 4.19 Accumulative volume of liquid fraction obtained by thermal and catalytic cracking of PP over 2.0wt% zirconium/aluminium oxide-pillared clay with various percent catalyst per plastic ratio.

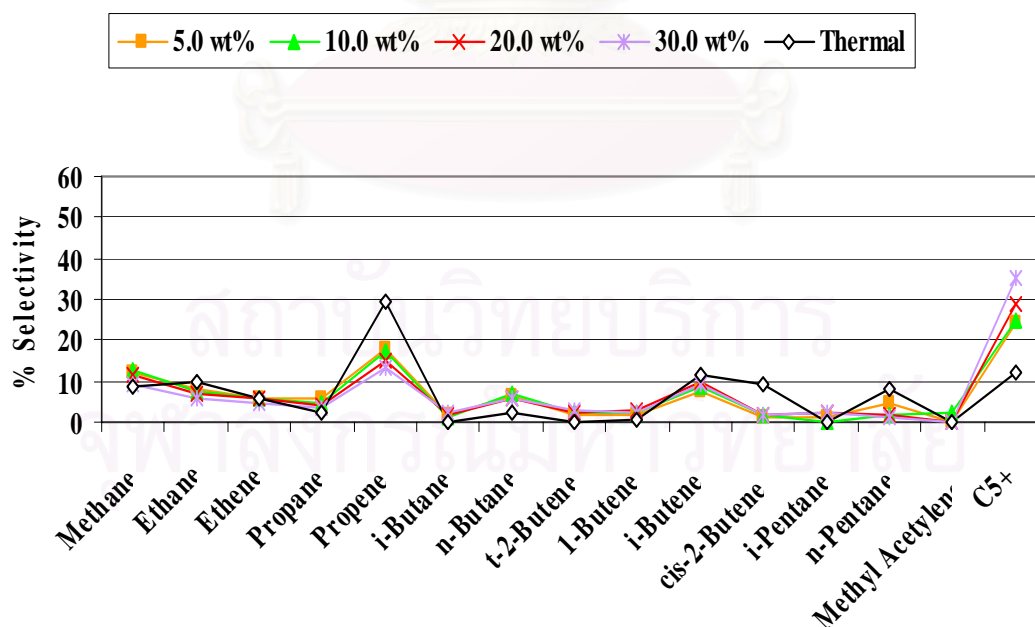


Figure 4.20 Distribution of gas fraction obtained by the thermal and catalytic cracking of PP over 2.0wt% zirconium/aluminium oxide-pillared clay with various percent catalyst per plastic ratio.

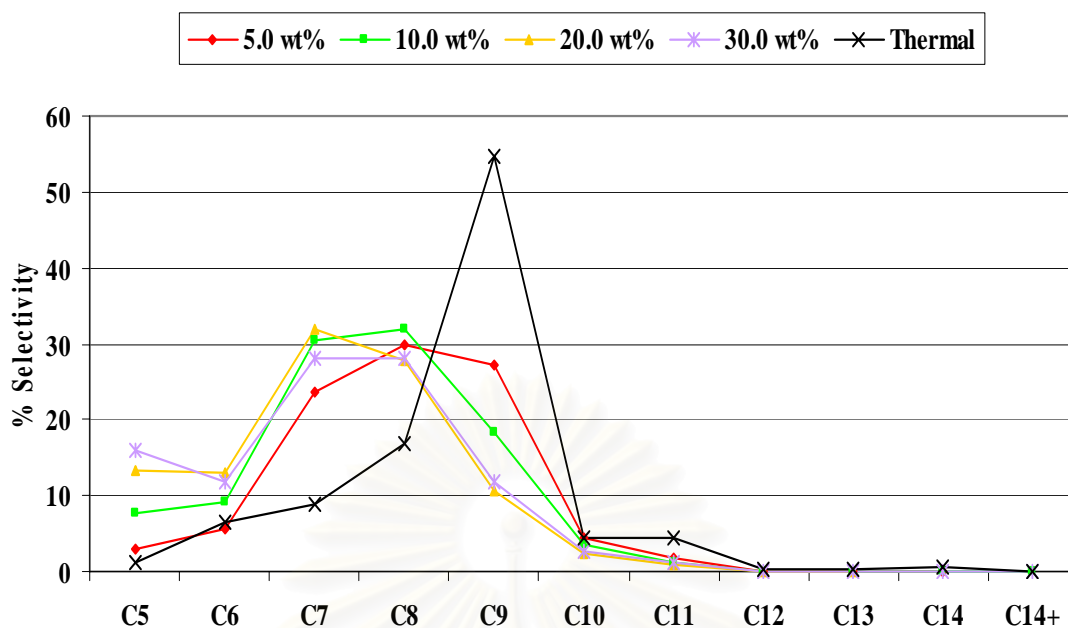


Figure 4.21 Carbon number distribution of distilled oil obtained by catalytic cracking of PP over 2.0wt% zirconium/aluminium oxide-pillared clay with various percent catalyst per plastic ratio.

4.3 Activity of Various Aluminium Oxide-Pillared Clay Catalysts in PE Cracking

4.3.1 Effect of Reaction Time.

To study the effect of time in PE cracking by vary reaction time in range of 0.5 to 3.0 h. Table 4.10 showed values of conversion and the product yield for thermal and catalytic cracking. Reaction temperature at 380°C was chosen for this study using aluminium oxide-pillared clay as catalyst. When the reaction time was increased, conversions of PE into light hydrocarbon for thermal and catalytic cracking gave rising while residue decreased. The reason has been explained in Session 4.2.1. Thermal and catalytic cracking showed gas fractions as major product. When conversions of PP and PE were compared at the same reaction time. PP cracking showed higher conversion than PE cracking and PE took longer period in cracking than PP. It was suggested that the difference in structure may be accounted for. PP proceeded through tertiary carbenium ion while secondary carbenium ion for PE. The stability of the carbenium ion decreased in the order tertiary > secondary > primary [43] and affected PP cracking reaction faster than PE.

When reaction time was increased, the difference between thermal and catalytic cracking conversion increased but after reaction time 1.5h, the difference between thermal and catalytic cracking conversion decreased. Thus, the reaction time at 1.5 h was chosen for further studied in this work. The comparison between thermal and catalytic cracking at the same reaction time found that conversion of catalytic cracking was higher than thermal cracking due to acidity of catalyst.

Figure 4.22 showed accumulative volume of liquid products with lapsed time of catalytic cracking. When reaction time was increased, total volume of liquid fraction was increased.

Reaction time was not affected on selectivity for gas products for catalytic and thermal cracking at reaction time less than 1.5h because product distribution of gas fraction of them were not different. They showed C₅₊ as major product and C₄(n-butane) as minor product. However reaction time affected on selectivity of thermal cracking after 1.5h. C₅₊ was still major product but minor products were different, which was C₂(ethene) and C₃(propene). The difference in gas components between thermal and catalytic cracking at longer time period has already been explained in Session 4.2.1.

Table 4.10 %Conversion, %yield and %selectivity of liquid fraction obtained by thermal and catalytic cracking of PE over aluminium oxide-pillared clay catalyst with various reactions times.

	Catalytic cracking					Thermal cracking				
	0.5 h	1.0 h	1.5 h	2.0 h	3.0 h	0.5 h	1.0 h	1.5 h	2.0 h	3.0 h
% Conversion*	6.8	12.8	17.6	18.7	29.4	0.8	1.0	2.4	4.2	18.4
% Yield* 1.gas fraction	6.8	10.2	12.4	11.6	19.0	0.8	1.0	2.4	4.2	18.4
2.liquid fraction	0.0	2.6	5.2	7.1	10.4	0.0	0.0	0.0	0.0	0.0
3.residue	93.2	87.2	82.4	81.3	70.6	99.2	99.0	97.6	95.8	81.6
Liquid fraction density (g/cm ³)	-	0.87	0.87	0.88	0.87	-	-	-	-	-

Condition: 10 wt% of catalyst to plastic ratio, N₂ flow of 20 cm³/min, and reaction temperature of 380°C. *Deviation within ±0.2% for conversion, ±0.2% for yield of gas fraction, ±0.2% for yield of liquid fraction, and ±0.2% for yield of residue.

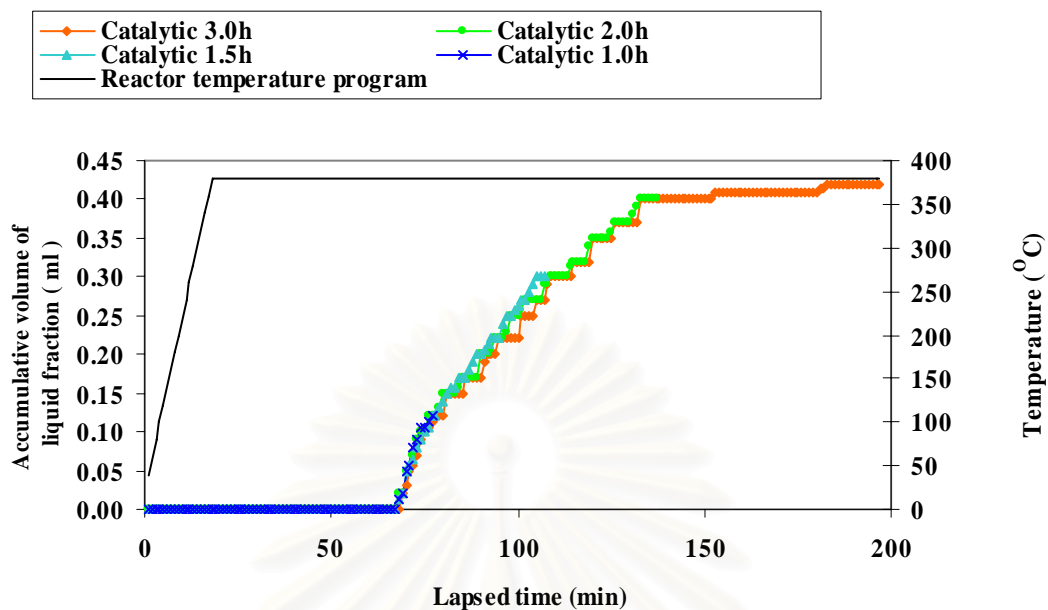


Figure 4.22 Accumulative volume of liquid fraction obtained by thermal and catalytic cracking of PE over aluminium oxide-pillared clay catalyst with various reaction times.

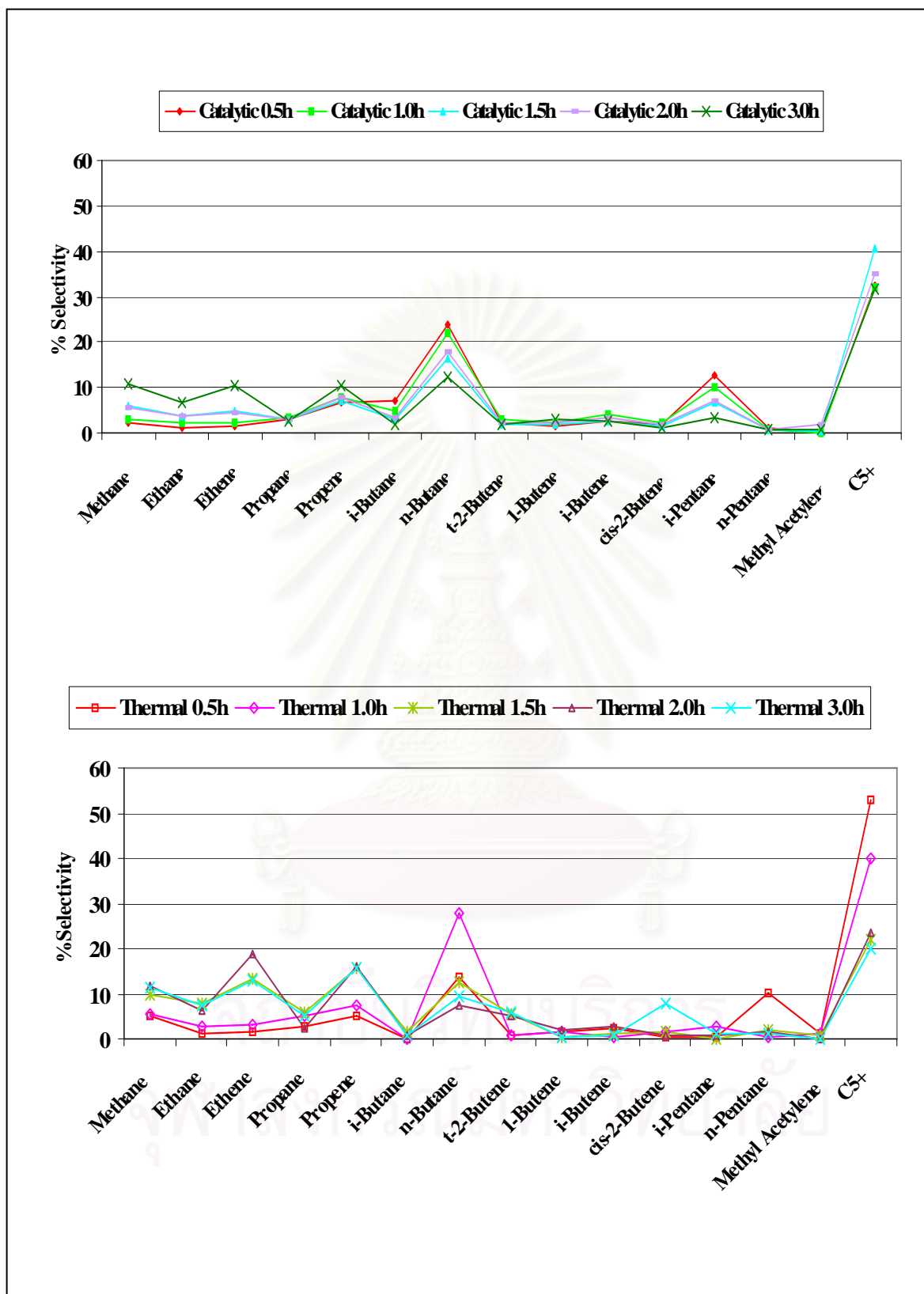


Figure 4.23 Distribution of gas fraction obtained by the thermal and catalytic cracking of PE with various reaction times.

4.3.2 Effect of Reaction Temperature

Table 4.11 %Conversion, %yield and %selectivity of liquid fraction obtained by thermal and catalytic cracking of PE over aluminium oxide-pillared clay with various reaction temperatures.

	Catalytic cracking			Thermal cracking		
	380°C	410°C	440°C	380°C	410°C	440°C
% Conversion*	17.6	62.0	89.7	2.4	20.2	76.4
% Yield* 1. gas fraction	12.4	32.6	39.6	2.4	20.2	33.4
2. liquid fraction	5.2	29.4	50.1	0.0	0.0	43.0
3. residue	82.4	38.0	10.3	97.6	79.8	23.6
- wax	82.4	34.6	9.9	-	-	-
- solid coke	-	3.4	0.3	-	-	-
% selectivity of liquid fraction						
1. distillate oil	-	14.0	14.9	0.0	0.0	27.7
2. heavy oil	-	86.0	85.1	0.0	0.0	72.3
Liquid fraction density (g/cm ³)	0.87	0.74	0.74	0.00	0.00	0.77

Condition: 10 wt% of catalyst to plastic ratio, N₂ flow of 20 cm³/min and reaction time 1.5 h. *Deviation within $\pm 0.2\%$ for conversion, $\pm 0.2\%$ for yield of gas fraction, $\pm 0.2\%$ for yield of liquid fraction, and $\pm 0.2\%$ for yield of residue.

Table 4.11 showed the value of conversion and the product yield for thermal and catalytic cracking of PE over aluminium oxide-pillared clay at various reaction temperature. In this session, reaction time at 1.5h was selected for studying effect of reaction temperature in PE cracking. Conversions of PE into liquid and gas product for thermal and catalytic cracking gave rising while residue decreased, when the reaction temperatures were increased. Cracking temperatures at 380 and 410°C for thermal and catalytic crackings showed gas fraction as main product. Thermal and catalytic crackings at reaction temperature 440°C showed liquid fraction as main product and lowest solid coke and wax values. Thermal cracking at 440°C showed

amount of distillate oil around 28.0 wt% and for all catalytic cracking showed around 14.45 wt%. It has been explained in Session 4.2.2.

When reaction temperature was increased from 380 to 410°C, the difference between thermal and catalytic cracking conversion decreased and after 410°C the difference between thermal and catalytic cracking conversion decreased. The reaction temperature at 440°C showed the lowest different between thermal and catalytic cracking conversion because highest thermal affect. Therefore, it has been concluded that the reaction temperature at 410°C gave the highest catalyst efficiency. In this way, this condition (1.5 h, 410°C) was chosen for further study.

The comparison in fractional oil recovery of liquid products derived from thermal and catalytic degradation with lapse time at different cracking temperatures, shown in Figure 4.24, indicates that catalytic cracking was faster than thermal cracking. Reaction temperature affected on cracking reaction because when the reaction temperatures were increased, total volume and rate of liquid fractions increased.

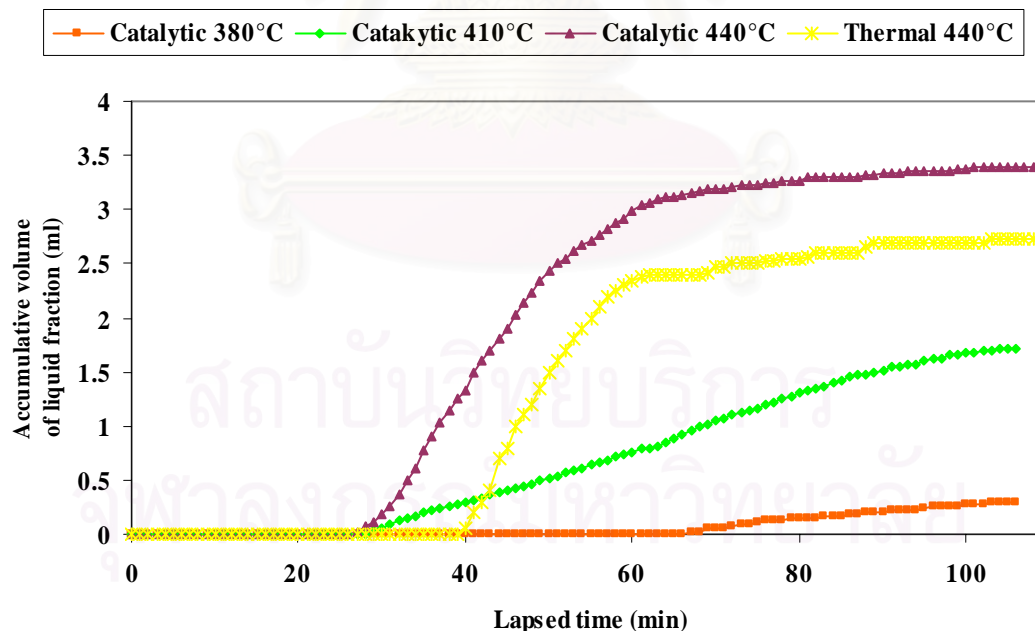


Figure 4.24 Accumulative volume of liquid fractions obtained by thermal and catalytic cracking of PE over aluminium oxide-pillared clay catalyst with various reaction temperatures.

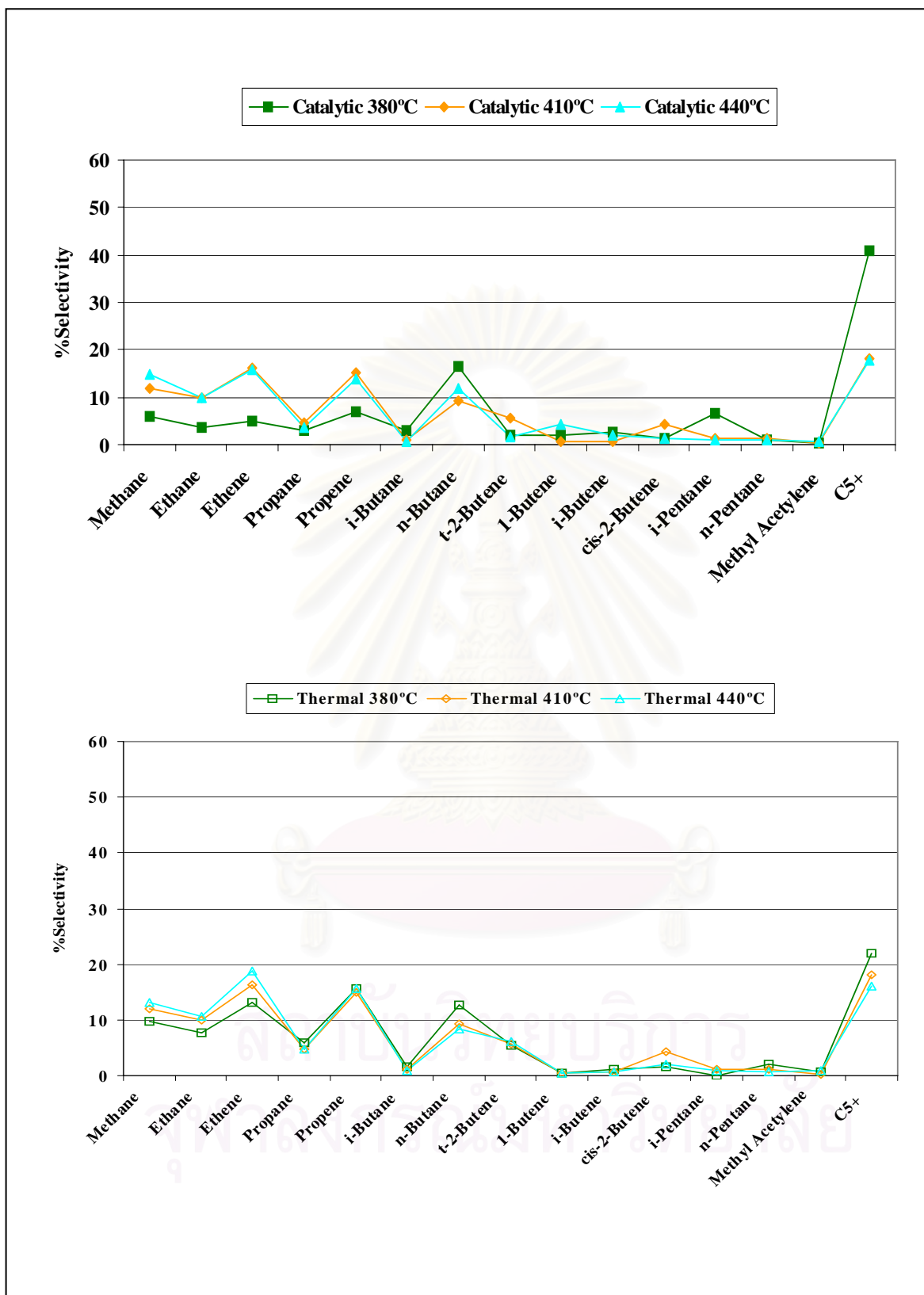


Figure 4.25 Distribution of gas fractions obtained by the thermal and catalytic cracking of PE over aluminium oxide-pillared clay with various reaction temperatures.

Figure 4.25 shows distribution of gas fraction for thermal and catalytic cracking.

The product distribution of gas fraction obtained from catalytic and thermal cracking at 380 and 410°C were not different in selectivity of gas fraction. C₅₊ was major product and C₃(propene), C₁(methane), C₂(ethene), C₂(ethane) and C₄(n-butane) were minor products. The selectivity of gas fractions for thermal reaction at 440°C was different from other. The major product was C₂(ethene) and minor products were C₅₊, C₁(methane) and C₃(propene). During thermal cracking, a radical was formed through H-transfer reaction. The radical can also be form through chain isomerization reaction being n-alkane such as C₅₊ at mild condition (380 and 410°C). When temperature increased to 440°C, radicals can decompose through the so-called “β scission” to form a smaller radical and an olefin C₂(ethene) and C₃(propene).

Figure 4.26 showed carbon number distribution of distillate oil. The selectivity of distillate oil showed in range of C₆ to C₁₀. C₈ was the major product for thermal cracking at reaction temperature of 440°C and C₇ to C₈ were the major product for catalytic cracking. From this result, it was observed that reaction temperature was not affected on selectivity.

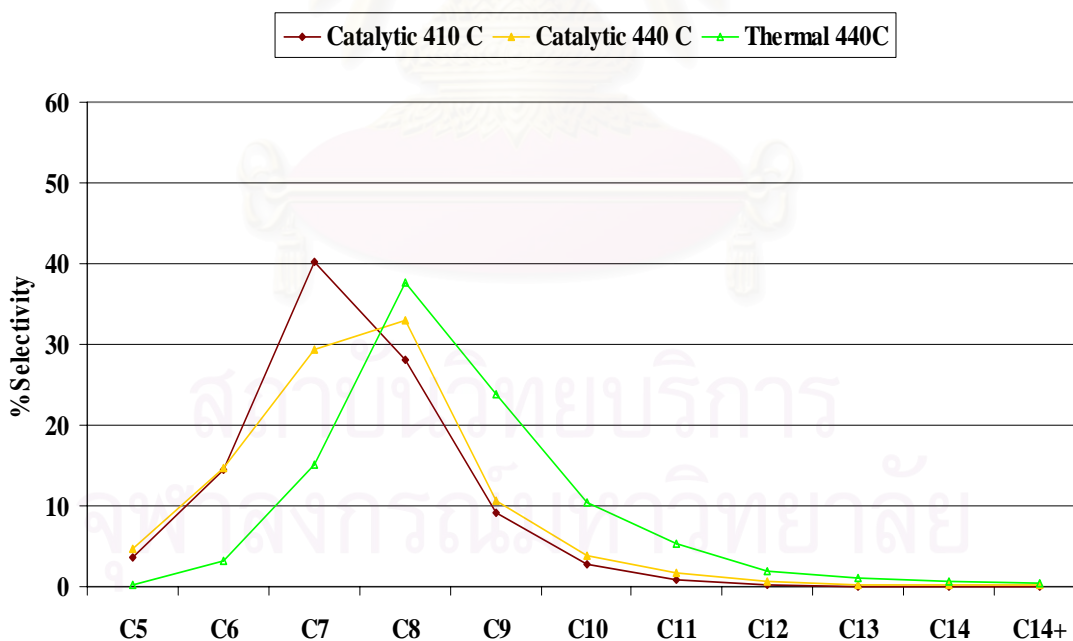


Figure 4.26 Carbon number distribution of distillate oil obtained by thermal and catalytic cracking of PE over aluminium oxide-pillared clay with various reaction temperatures.

4.3.3 Effect of Zirconium Doped Aluminium Oxide-Pillared Clay (Zirconium/Aluminium Oxide-Pillared Clay).

To investigate the effect of zirconium doped aluminium-pillared clay for PE cracking. The reaction was performed in the same way as PP cracking. The value of conversion and yield of catalytic cracking of PE over zirconium/aluminium oxide-pillared clay at various percent of zirconium were shown in Table 4.12. Increasing the percent of zirconium from 0.0-2.0 wt%, conversion and liquid fraction were increased and when zirconium content was increased from 2.0-5.0wt%, conversion and liquid fraction were decreased. The 2.0wt% zirconium/aluminium oxide-pillared clay showed the highest conversion and was chosen for further studied.

Table 4.12 %Conversion, %yield and %selectivity of liquid fraction obtained by thermal and catalytic cracking of PE over zirconium/aluminium oxide-pillared clay with various percent zirconium.

	Thermal	aluminium oxide-pillared clay	1.0wt% zirconium/aluminium oxide-pillared clay	2.0wt% zirconium/aluminium oxide-pillared clay	3.0wt% zirconium/aluminium oxide-pillared clay	5.0wt% zirconium/aluminium oxide-pillared clay
% Conversion*	20.2	62.0	67.2	72.4	68.0	63.3
% Yield* 1. gas fraction	20.2	32.6	40.5	39.2	39.5	35.9
2. liquid fraction	0.0	29.4	26.7	33.2	28.5	27.3
3. residue	79.8	38.0	32.7	27.6	32.0	36.7
- wax	-	34.6	31.0	21.4	28.7	34.1
- solid coke	-	3.4	1.8	6.2	3.3	2.6
% selectivity of liquid fraction						
1. distillate oil	0.0	14.0	34.0	40.8	32.1	58.7
2. heavy oil	0.0	86.0	66.0	59.2	67.9	41.3
Liquid fraction density (g/cm ³)	0.0	0.74	0.74	0.77	0.77	0.80

Condition: 10 wt% of catalyst to plastic ratio, N₂ flow of 20 cm³/min, and reaction time 1.5 h. *Deviation within $\pm 0.2\%$ for conversion, $\pm 0.2\%$ for yield of gas fraction, $\pm 0.2\%$ for yield of liquid fraction, and $\pm 0.2\%$ for yield of residue.

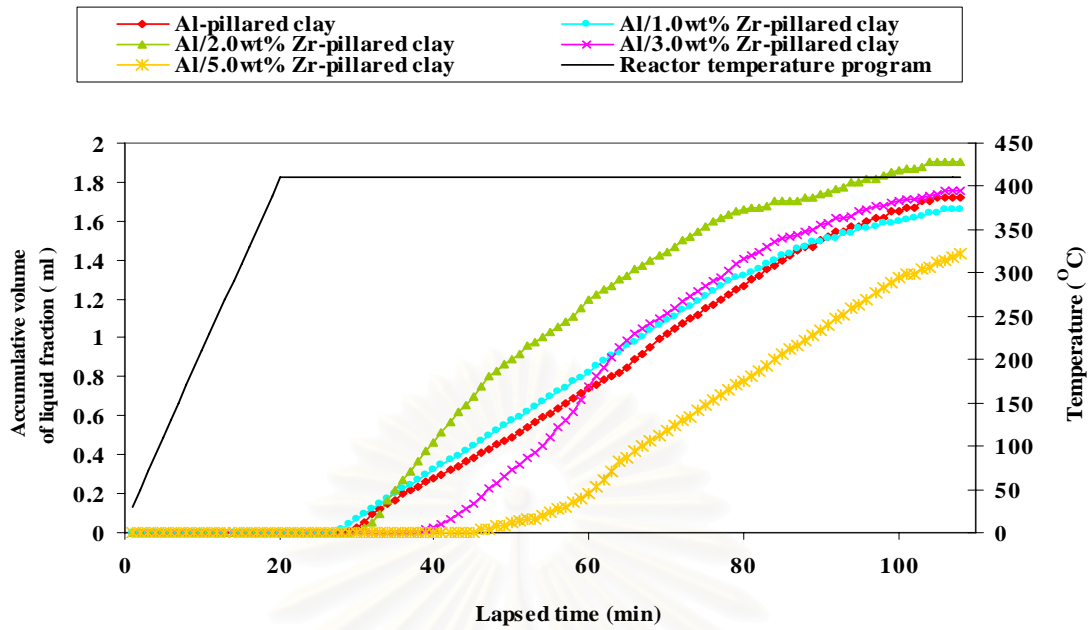


Figure 4.27 Accumulative volume of liquid fraction obtained by thermal and catalytic cracking of PE over zirconium/aluminium oxide-pillared clay with various percent zirconium.

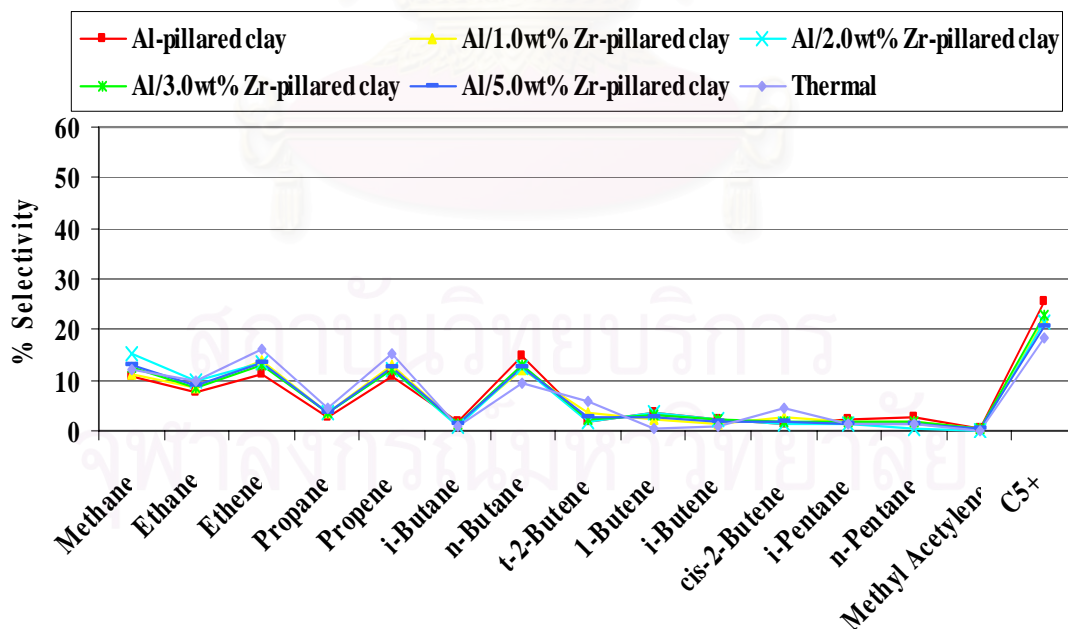


Figure 4.28 Distribution of gas fractions obtained by the thermal and catalytic cracking of PE over zirconium/aluminium oxide-pillared clay with various percent zirconium.

Figure 4.27 shows fractional oil recovery of liquid products derived from thermal and catalytic cracking with lapsed time at various percent of zirconium. The 5.0wt% zirconium/aluminium oxide-pillared clay showed the lowest rate and total volume of liquid fraction. The 2.0wt% zirconium/aluminium oxide-pillared clay showed the highest rate and total volume of liquid fraction.

Gas fraction for all of catalytic and thermal reactions showed the major product in C_{5+} and minor product were C_3 (propene), C_1 (methane), C_2 (ethene), C_2 (ethane) and C_4 (n-butane). From the result, it was observed that variation of zirconium and acidity of catalyst were not affected on selectivity.

The 1.0-5.0wt% zirconium/aluminium oxide-pillared clay showed products distribution in range of C_7 to C_{11} and major product was C_9 . Aluminium oxide-pillared clay showed products distribution in range of C_6 to C_7 and major product was C_7 . From this result, it was observed that aluminium oxide-pillared clay consisted of small hydrocarbon molecules than others.

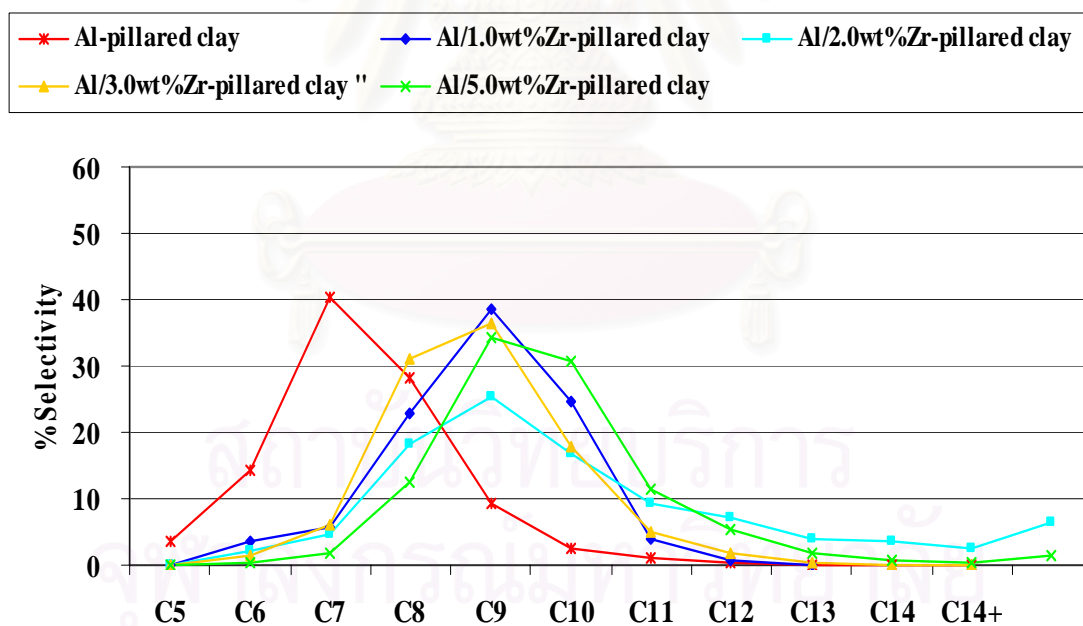


Figure 4.29 Carbon number distribution of distillate oil obtained by catalytic cracking of PE over zirconium/aluminium oxide-pillared clay with various percent zirconium.

4.3.4 Effect of catalyst per plastic ratio

Table 4.13 %Conversion, %yield and %selectivity of liquid fraction obtained by thermal and catalytic cracking of PE over 2.0wt% zirconium/aluminium oxide-pillared clay with various percent catalyst per plastic ratios.

	5.0 % of catalyst to plastic ratio	10.0 % of catalyst to plastic ratio	20.0 % of catalyst to plastic ratio	30.0 % of catalyst to plastic ratio	Thermal
% Conversion *	56.7	72.4	82.4	84.3	20.2
% Yield* 1. gas fraction	36.5	39.2	47.3	35.9	20.2
2. liquid fraction	20.2	33.2	35.1	48.2	0.0
3. residue	43.3	27.6	17.6	15.9	79.8
- wax	25.5	21.4	10.0	13.5	-
- solid coke	17.9	6.2	7.6	2.4	-
% selectivity of liquid fraction					
1. distillate oil	45.2	40.8	32.1	30.8	0.0
2. heavy oil	54.8	59.2	67.9	69.2	0.0
Liquid fraction density (g/cm ³)	0.72	0.77	0.75	0.74	0.00

Condition: 10 wt% of catalyst to plastic ratio, N₂ flow of 20 cm³/min and reaction time 1.5 h. *Deviation within $\pm 0.2\%$ for conversion, $\pm 0.2\%$ for yield of gas fraction, $\pm 0.2\%$ for yield of liquid fraction, and $\pm 0.2\%$ for yield of residue.

To study effect of catalyst to plastic ratio for PE cracking, the cracking reaction was performed as PP cracking. From Session 4.3.3, 2.0wt% zirconium/aluminium oxide-pillared clay was chosen as catalyst in this studied. With increasing catalyst to plastic ratio, conversion of PE increased while residue was decreased. From Table 4.13, it could be observed that liquid products increased from 5.0 to 30.0 wt%. That effect 30.0 wt% of catalyst showed the highest liquid fraction. Gas products increased from 5.0 to 20.0 wt% of catalyst and reduction at 30.0 wt% of catalyst. It has been explained in Session 4.2.4.

The relationship between conversion and percent of catalyst to plastic ratio is presented in Figure 4.30. It was observed that conversion was not much change 10.0 wt%. The yields of distillate oil calculated from yield of liquid fraction and selectivity

of distillate oil were not much different. Thus, 10.0 wt% of catalyst was the suitable amount of catalyst to plastic ratio in this work.

Total volume and rate of liquid fraction increased when percent catalyst per plastic ratio was increased. That effect 30.0 wt% of catalyst showed the highest total volume and rate of liquid fraction. The reason has been explained in Session 4.2.4.

Acidity of catalyst and variation of catalyst to plastic ratios were not affected on product distribution of gas fraction. Similar distribution of gas fraction between thermal and catalytic cracking were confirmed. Major product was C_{5+} and minor products were C_3 (propene), C_4 (n-butane), C_2 (ethane), C_2 (ethene) and C_1 (methane). It has been explained in Session 4.2.4

Carbon number distribution of distillate oil for catalytic cracking in range of C_7 to C_9 and major product was C_8 . The C_7 was the smallest hydrocarbon between product distribution and increased follow as raising amount of catalyst. Suggest high acidity and active site of catalyst led to more carbenium ion by addition to the carbon-carbon double bond of polymer. Cracking of the adsorbed carbenium ion proceeds through the β -scission mechanism [57, 58].

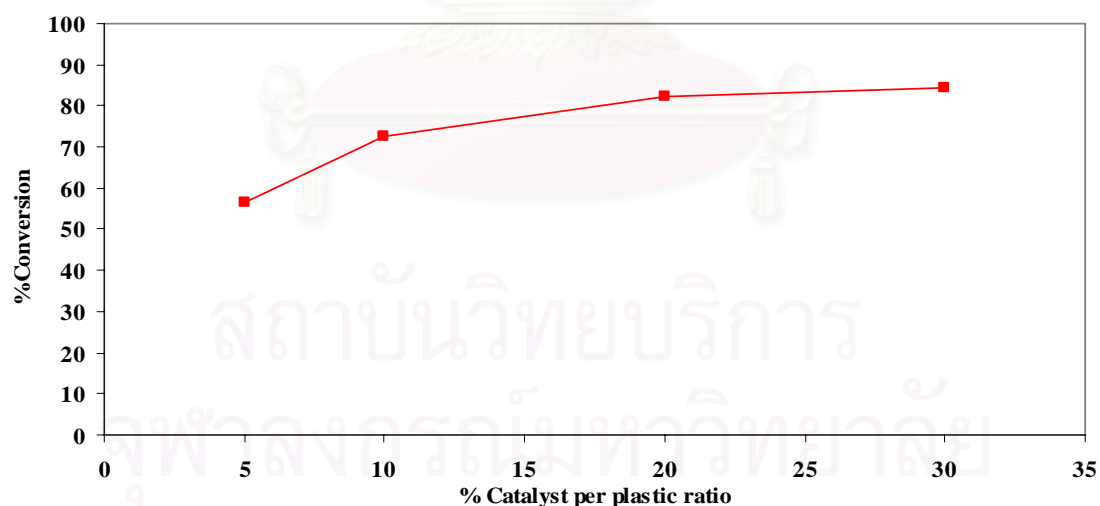


Figure 4.30 %Conversion at various percent catalyst to plastic ratio.

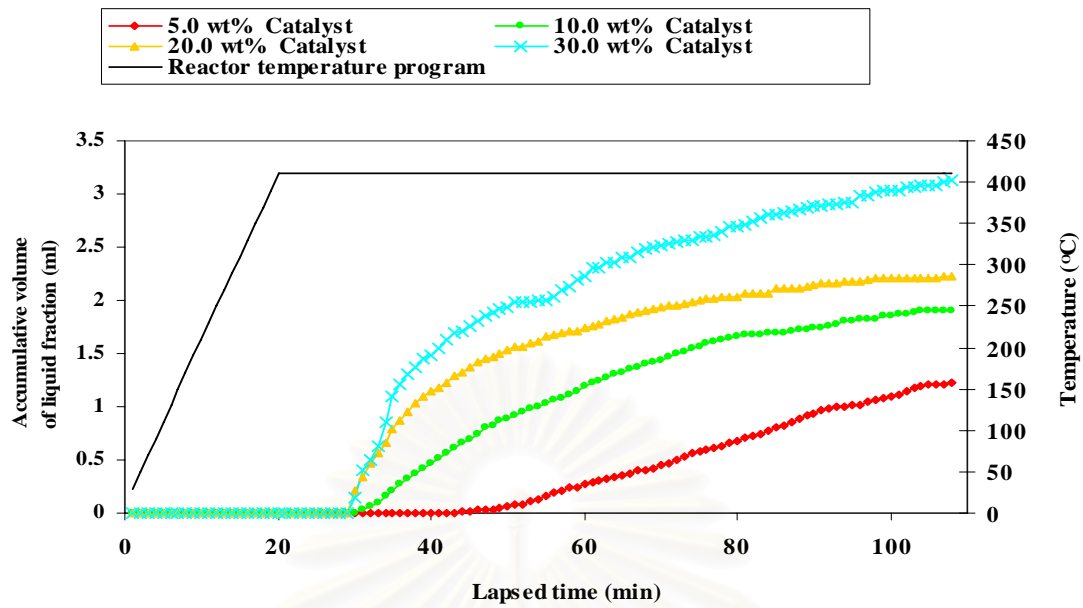


Figure 4.31 Accumulative volume of liquid fraction obtained by thermal and catalytic cracking of PE over 2.0wt% zirconium/aluminium oxide-pillared clay with various percent catalyst per plastic ratio.

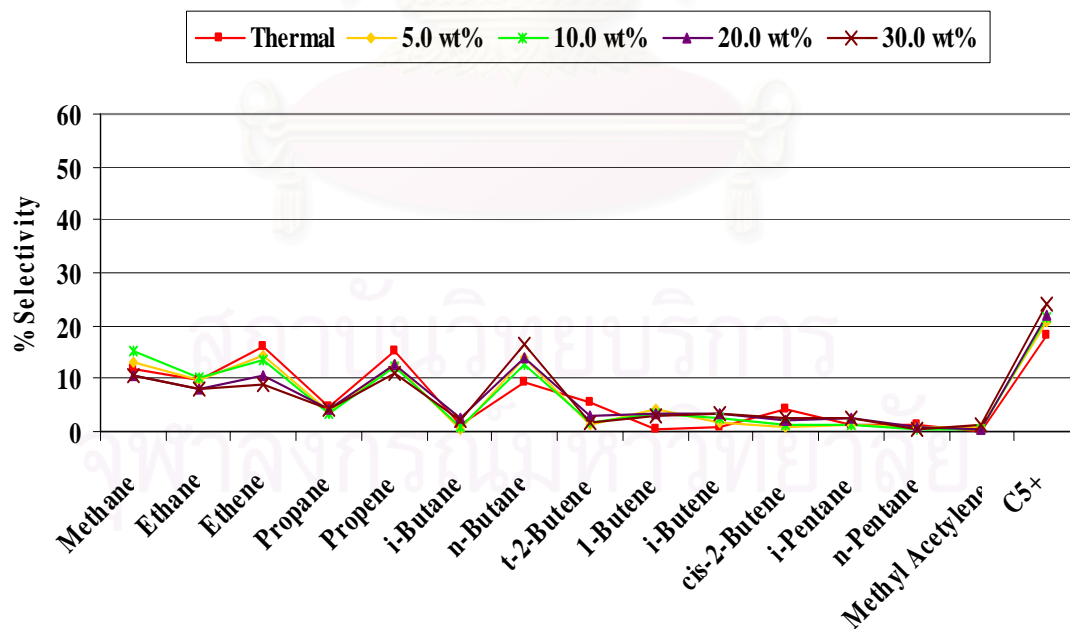


Figure 4.32 Distribution of gas fraction obtained by the thermal and catalytic cracking of PE over 2.0wt% zirconium/aluminium oxide-pillared clay with various percent catalyst per plastic ratio.

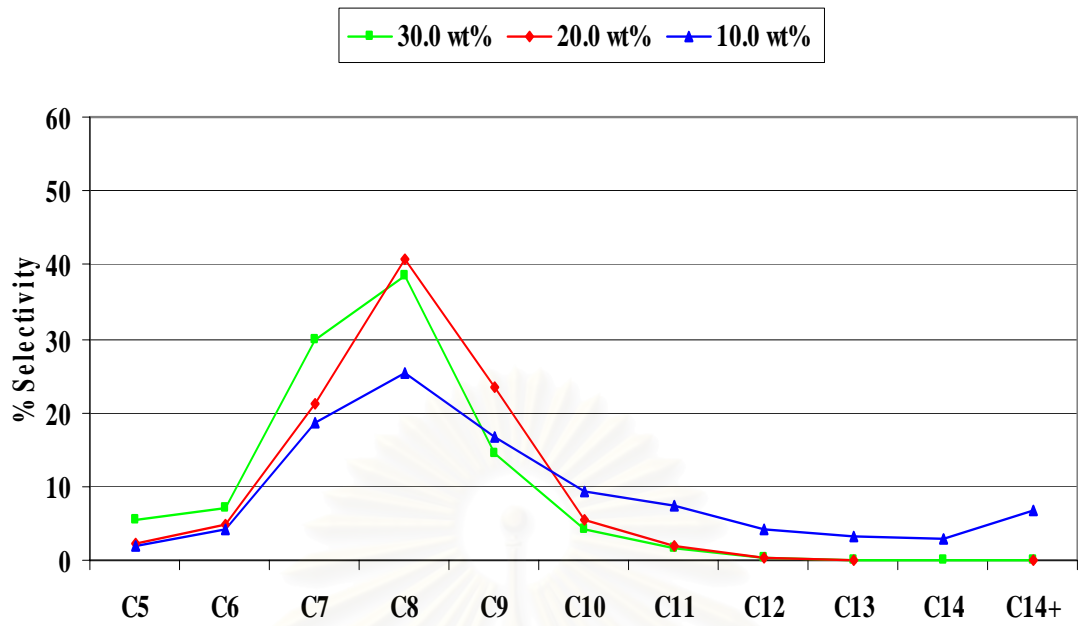


Figure 4.33 Carbon number distribution of distilled oil obtained by catalytic cracking of PE over 2.0wt% zirconium/aluminium oxide-pillared clay with various percent catalyst per plastic ratio.

CHAPTER V

CONCLUSIONS

Aluminium oxide-pillared clay was prepared by intercalation between ionic precursors and raw clay suspensions. The intercalated product was calcined at 500°C for 1h. After that catalyst was impregnated with various amounts of zirconium (from 0.0 to 5.0 wt%) by slurry method and calcined at 450°C for 4h. The basal spacing, the surface area, the aluminium contents and the vibrational modes of chemical bonds in different environments were determined by XRD, BET, ICP-AES and IR respectively. XRD pattern of aluminium oxide-pillared clay showed the characteristic peaks at 2-theta range of 6 and 19 degree, and the d_{001} spacing of 16.3 Å. The expansion of interlayer structure in aluminium oxide-pillared clay promotes the surface area to approximately 189 m²g⁻¹. The aluminium content in aluminium oxide-pillared clay (30.38 %) exhibits higher aluminium content than raw clay (23.70 %). Si-O-Si stretching shifted towards higher frequencies (1052 cm⁻¹). Zirconium/aluminium oxide-pillared clay catalysts with 0.0 to 5.0 wt% zirconium have the d_{001} spacing of 15.6 Å which is lower than aluminium oxide-pillared clay. XRD pattern of 5.0wt% zirconium/aluminium oxide-pillared clay showed characteristic peak of ZrO₂ at 2-theta range 30°, suggesting that, ZrO₂ phase was found outside a catalyst structure. When the amount of zirconium increased, surface area zirconium/aluminium oxide-pillared clay decreased from 188 to 131 m²g⁻¹.

Aluminium oxide-pillared clay and zirconium/aluminium oxide-pillared clays were used as catalysts for cracking PP and PE. The cracking reaction was carried out in a glass reactor with a mixture of catalyst and plastic at 350-450°C. Gaseous and liquidous hydrocarbon products were analysed by GC. The effects of reaction temperature, reaction time, type of catalyst and catalyst per plastic ratio were discussed. Conversion increased follow by increasing of reaction time, reaction temperature and percent catalyst to plastic ratio. Thermal cracking showed lower conversion than catalytic cracking under similar condition. It was explained by acidity of catalyst in catalytic cracking accelerated cracking reaction. Reaction temperature, reaction time, type of catalyst and catalyst per plastic ratio were not affected in selectivity of gas and liquid fraction. Selectivity of gas and liquid fraction between

thermal and catalytic cracking were different. It was suggested that the difference cracking. Catalytic cracking proceeds through carbenium ion mechanism while thermal cracking proceeds through free radical mechanism. The optimal condition for PP cracking was reaction time for 1.0 h, reaction temperature at 380°C, 2.0wt% zirconium/aluminium oxide-pillared clay as a catalyst and 10.0 wt% catalyst per plastic ratio. The major components of gas fraction were C₅₊ and C₃ (propene). Liquid fractions were in the range of C₇ to C₉. The optimal condition for PE cracking was reaction time for 1.5 h, reaction temperature at 410 °C, 2.0wt% zirconium/aluminium oxide-pillared clay and 10.0 % catalyst per plastic ratio. The major components of gas fractions were C₅₊, C₄(n-butane), C₃ (propene), C₂(ethane) and C₁(methane). Liquid fractions were in the range of C₇ to C₁₀. Boiling point distribution of liquid fraction derived from PP and PE cracking was in the range of standard gasoline.

The suggestions for future work

1. To investigate the hydrocarbon component of liquid fraction such as aromatic, alkenes and alkanes
2. To compare aluminium oxide-pillared clay with zeolite or other pillared clay catalyst for catalytic cracking of HDPE and PP under the similar condition

REFERENCES

- [1] Plastic [Online] Available from : <http://www.rexam.com/files/reports/2005cpr/index.asp?pageid=6>
- [2] Plastic [Online] Available from ; www.plasticconverters.eu/images/markets/packaging/graphic2/gif
- [3] Applied Market Information Ltd. [Online] Available from : www.amiplastics.com/ami/Assers/press/releases-P158-graphic_jpg [2009]
- [4] Manos, G.; and Gobin, K. Polymer degradation to fuels over microporous catalyst as a novel tertiary plastic recycling method. *Polymer Degradation and Stability* 83 (2004): 267.
- [5] Aguado, J.; Serrano, D.P.; Miguel, G. S.; Escola, J.M.; and Rodriguez, J. Catalytic activity of zeolite and mesostructured catalysts in the cracking of pure and waste polyolefins. *Journal of Analytical and Applied Pyrolysis*. 78 (2007): 153.
- [6] Kerdsa, N. Gasoline Preparation from Polypropylene Waste Using MCM-22 Zeolite as Catalyst. Master's Thesis, Department of Petrochemistry and Polymer Science, Faculty of Science, Chulalongkorn University, 2007.
- [7] Gobin, K.; and Manos, G. Polymer degradation to fuels over microporous catalysts as a novel tertiary plastic recycling method. *Polymer Degradation and Stability*. 83 (2004): 267-279.
- [8] Manos, G.; Yusof, I.; Papayannakos, N.; and Gangas, N. Catalytic cracking of polyethylene over clay catalysts. Comparison with an Ultrastable Y zeolite. *Industrial and Engineering Chemistry* 40 (2001): 2220-2225.
- [9] Gobin, K.; and Manos, G. Thermogravimetric study of polymer catalytic degradation over microporous materials. *Polymer Degradation and Stability*. 86 (2004): 225-231.
- [10] Manos, G.; Yusof, I.; Gangas, N.; and Papayannakos, N. Tertiary recycling of polyethylene to hydrocarbon fuel by catalytic cracking over aluminum pillared clays. *Energy & Fuels* 16 (2002): 485-489.
- [11] Tae, J.; Jang, B.; Kim, J.; Kim, I.; and Park, D. Catalytic degradation of polystyrene using acid-treated halloysite clays. *Solid State Ionics* 172 (2004): 129-133.

- [12] Yang, h.; Wilson, M.; Fairbridge, C.; and Ring, Z. Mild hydrocracking of synthetic crude gas oil over Pt supported on pillared and delaminated clays. *Energy & Fuels* 16 (2002): 855-863.
- [13] Manos, G.; Gaefort, A.; and Dwyer, J. Catalytic degradation of HDPE over different zeolitic structures. *Industrial and Engineering Chemistry* 39 (2000): 1198.
- [14] Gonzaaleza, F.; Pesqueraa, C.; Benitoa, I.; Herreroa, E.; Ponciob, C.; and Casuscellib, S. Pillared clays: catalytic evaluation in heavy oil cracking using a microactivity test. *Applied Catalysis A: General*. 181 (1999): 71±76.
- [15] Moreno, S.; Sou Kou, P.; Molina, R.; and Poncelert, G. Al-, Al,Zr-, and Zr-pillared montmorillonites and saponites: preparation, characterization, and catalytic activity in heptane hydroconversion. *Journal of Catalysis*. 182 (1999): 174-185.
- [16] Uddin, M.; Aguado, J.; and Escola, J. Catalytic conversion of polystyrene over HMCM-41, HZSM-5 and amorphous SiO₂-Al₂O₃: comparison with thermal cracking. *Applied Catalysis B* 25 (2000): 181.
- [17] Aguado, J.; Sotelo, J.; D., P.; Callers, J.; and Escola, J. Catalytic conversion of polyolefins into liquid fuels over MCM-4: Comparison with ZSM-5 and amorphous SiO₂-Al₂O₃. *Energy & Fuels* 11 (1997): 1225.
- [18] Grieken, R.; Serrano, D.; Aguado, J.; Garcia, R.; and Rojo, C. Thermal and catalytic cracking of PE under mild conditions. *Journal of Analytical and Applied Pyrolysis*. 58-59 (2001): 127.
- [19] Fernandes, J.; Araujo, A.; and Fernandes, G. Catalytic degradation of high density polyethylene by HZSM-5 zeolite. *Studies in Surface Science and Catalysis*. 105 (1997): 941.
- [20] Shichi, T.; and Takagi, K. Clay minerals as photochemical reaction fields. *Journal of Photochemistry and Photobiology C: Photochemistry Previews I*, (2000): 113-130.
- [21] Moore, D.M.; Reynolds, Jr.R.C. X-RAY Diffraction and the Identification and Analysis of Clay Minerals. New York, USA, Oxford University Press, 1989.
- [22] Michael, R.; Grace, S.T.; and Vishnu, K. The many ways of making anionic clays. *Indian Academy of Sciences(Chemical Science)*. 113 (2001): 671-680.
- [23] Varma, R. Clay and clay-supported reagents in organic synthesis. *Tetrahedron*. 58 (2002): 1235.

- [24] Jean, F.; and Grace, P. Acidity in pillared clays: origin and catalytic manifestations. *Topic in Catalysis*. 4 (1997): 43.
- [25] Bruce, W.; and O'Hare, D.; *Inorganic material*, 2nd ed., New York, John Wiley & Sons, Inc., 1997.
- [26] Robert, A.; Tom, P.; Gerhard, L.; and Nick, G. Pillared clays and pillared layered solids (technical report). *Pure and Apply Chemistry* 71 (1999): 2367.
- [27] Gonzaaeza, F.; Pesqueraa, C.; Blanco, C.; Benito, I.; and Mendioroz, S. Synthesis and Characterization of Al-Ga Pillared Clays with High Thermal and Hydrothermal Stability. *Inorganic Chemistry* 31 (1992): 727-731.
- [28] Sawangkam, P. Synthesis of Tungsten Containing MCM-41 Catalyst and Their Activity for Olefin Metathesis. Master's Thesis, Department of Petrochemistry and Polymer Science, Faculty of Science, Chulalongkorn University, 2005.
- [29] Dialysis method for removing small molecules from a solution. [Online] Available from : [http:// course.cm.utexas.edu/jrobertus/ch339k/overheads-1/ch5_dialysis.jpg](http://course.cm.utexas.edu/jrobertus/ch339k/overheads-1/ch5_dialysis.jpg)
- [30] Basic Operating Principle of the Sorptomatic. 1970. Available from : [http:// saf.chem.ox.ac.uk/Instruments/BET/sorptoprin](http://saf.chem.ox.ac.uk/Instruments/BET/sorptoprin).
- [31] Skoog, D.A. *Principles of Instrumental Analysis*, 4th ed., Harcourt Brace College Publishers, New York, 1997, 363.
- [32] Analysis Software User's Manual, BELSORP, BEL JAPAN, INC.57
- [33] Basic operating principles of the Sorptomatic 1990 [Online] Available from : <http://saf.chem.ox.ac.uk/Instruments-BET/isotherms/jpg>
- [34] Brunauer, S.; Emmett, P.M.; and Teller, E. Adsorption of gases in multimolecular layers. *The Bureau of chemistry and solids and george Washington University*, 60 (1938): 309.
- [35] Songninluck, J. Development of Al-MCM-41 Catalyst for Cracking of High Density Polyethylene and Polypropylene Wastes. Master's Thesis, Department of Petrochemistry and Polymer Science, Faculty of Science, Chulalongkorn University, 2005.
- [36] Infrared Analysis Inc. [Online] Available from : <http://www.forumsci.co.il/HPLC/FTIR/inst/jpg>
- [37] Nelson, W.L. *Petroleum Refinery Engineering*, 4th ed., Singapore: Mcgraw-hill, 1987, 759-818.

- [38] Serge Raseev *Thermal and Catalytic Process in Petroleum Refining*. Maecel Dekker New York, 2003, 293-403.
- [39] Ali, S.; Garforth, A.A.; Harris, D.H.; Rawlence, D.J.; and Uemichi, Y. Polymer waste recycling over used catalyst. *Catalysis Today*. 75 (2002): 247-41
- [40] Oil refinery: Cracking [Online] Available from : <http://www.schoolscience.co.uk/content4/chemistry/petroleum/knowl/4/cracking.html>,2006
- [41] George Odian *Principle of Polymerization*, 4th ed., Canada: Wiley & Sons, 2004, 209.
- [42] Yury, V.K. Chemical mechanism of catalytic cracking over solid acid catalyst: alkanes and alkenes. *Taylor&Francis* 48 (2001): 85
- [43] Scherzer, J. Octane-enhancing, zeolite FCC catalyst: science and technical aspect. *Science and Engineering*. 31 (1989): 8
- [44] Greensfelder, B.S.; and Voge, H.H.; Good, G.M. Catalytic and thermal cracking of pure hydrocarbons. *Industrial and engineering chemistry* 41 (1949): 2573.
- [45] Thomas, C.L. Chemistry of cracking catalyst. *Industrial and engineering chemistry* 41 (1949): 2564.
- [46] Wojciechowski, B.; and Abbot, J. The mechanism of catalytic cracking of n-alkanes on ZSM-5 zeolite. *Chemical Engineering Journal*. 63 (1985): 462.
- [47] Makkee, M.; Wissink, M.; and Moulijn, J. Gasoline conversion: reactivity towards cracking with equilibrated FCC and ZSM-5 catalysts. *Applied Catalysis A.: General*. 223 (2002): 85.
- [48] Kaloidas, V.; Koufopoulos, C.; Gangas, N.; and Papayannakos, N. Scale-up studies for the preparation of pillared layered clays at 1 kg per batch. *Microporous Materials*. 5 (1995): 97-106
- [49] P. Salerno, S.; Mendioroz, A.; and López, A. Al-pillared montmorillonite-based NiMo catalysts for HDS and HDN of gas oil: influence of the method and order of Mo and Ni impregnation. *Applied Catalysis A*. 259 (2004): 17-28
- [50] Ribeiro, N.; Mendes, F.; Perez, C.; Souza, M.; and Schmal, M. Selective CO oxidation with nano gold particles-based catalysts over Al₂O₃ and ZrO₂. *Applied Catalysis A*. 347 (2008): 62-71.
- [51] Tunc, S.; and Duman, O. The effect of different molecular weight of poly(ethylene glycol) on the electrokinetic and rheological properties of Na-bentonite suspensions. *Colloids and Surfaces A*. 317 (2008): 93-99.

- [52] Nunes, C.; Pires, J.; Carvalho, A.; Calhorda, M.; and Ferreira, P. Synthesis and characterisation of organo-silica hydrophobic clay heterostructures for volatile organic compounds removal. *Microporous and Mesoporous Materials*. 111 (2008): 612–619.
- [53] Manohar, D.; Noeline, B.; and Anirudhan, T. Adsorption performance of Al-pillared bentonite clay for the removal of cobalt(II) from aqueous phase. *Applied Clay Science*. 31 (2006): 194–206.
- [54] Pan, J.; Wang, C.; Guo, S.; Li, J.; and Yang, Z. Cu supported over Al-pillared interlayer clays catalysts for direct hydroxylation of benzene to phenol. *Catalysis Communications*. 9 (2008): 176–181.
- [55] Hrachova, J.; Madejova, J.; Billik, P.; Komadel, P.; and Fajnor, V. Dry grinding of Ca and octadecyltrimethylammonium montmorillonite. *Journal of Colloid and Interface Science*. 316 (2007): 589–595.
- [56] Sowmiya, M.; Sharma, A.; Parsodkar, S.; and Mishra, B. Dubey, A. Nanosized sulfated SnO₂ dispersed in the micropores of Al-pillared clay as an efficient catalyst for the synthesis of some biologically important molecules. *Applied Catalysis*. 333 (2007): 272–280.
- [57] Sie, S. Acid-catalyzed cracking of paraffins Part2. Evidence for the protonated cyclopropane mechanism from catalytic cracking experimentals. *Industrial Engineering and Chemistry*. 32 (1993): 397.
- [58] Williams, B.; Babiz, S.; Miller, J.; Snurr, R.; and Kung, H. The role of acid strength and pore diffusion in the enhanced cracking activity of steamed zeolite Y. *Applied Catalysis A*. 32 (1999): 161.
- [59] Scherzer, J. Octane-enhancing, zeolite FCC catalyst: scientific and technical aspect. *Science and Engineering*. 31 (1989): 83.
- [60] Yury, V. Chemical mechanisms of catalytic cracking over solid acidic catalyst: alkanes and alkenes. *Taylor & Francis*. 48 (2001): 85.



APPENDICES

สถาบันวิทยบริการ
จุฬาลงกรณ์มหาวิทยาลัย

Appendix

A-1 % Selectivity Of gas fraction and liquid fraction

$$\% \text{ Selectivity of X} = \frac{\text{concentration of X} \times 100}{\text{total concentration of fraction}}$$

$$\text{Concentration of X} = \frac{b \times c}{a}$$

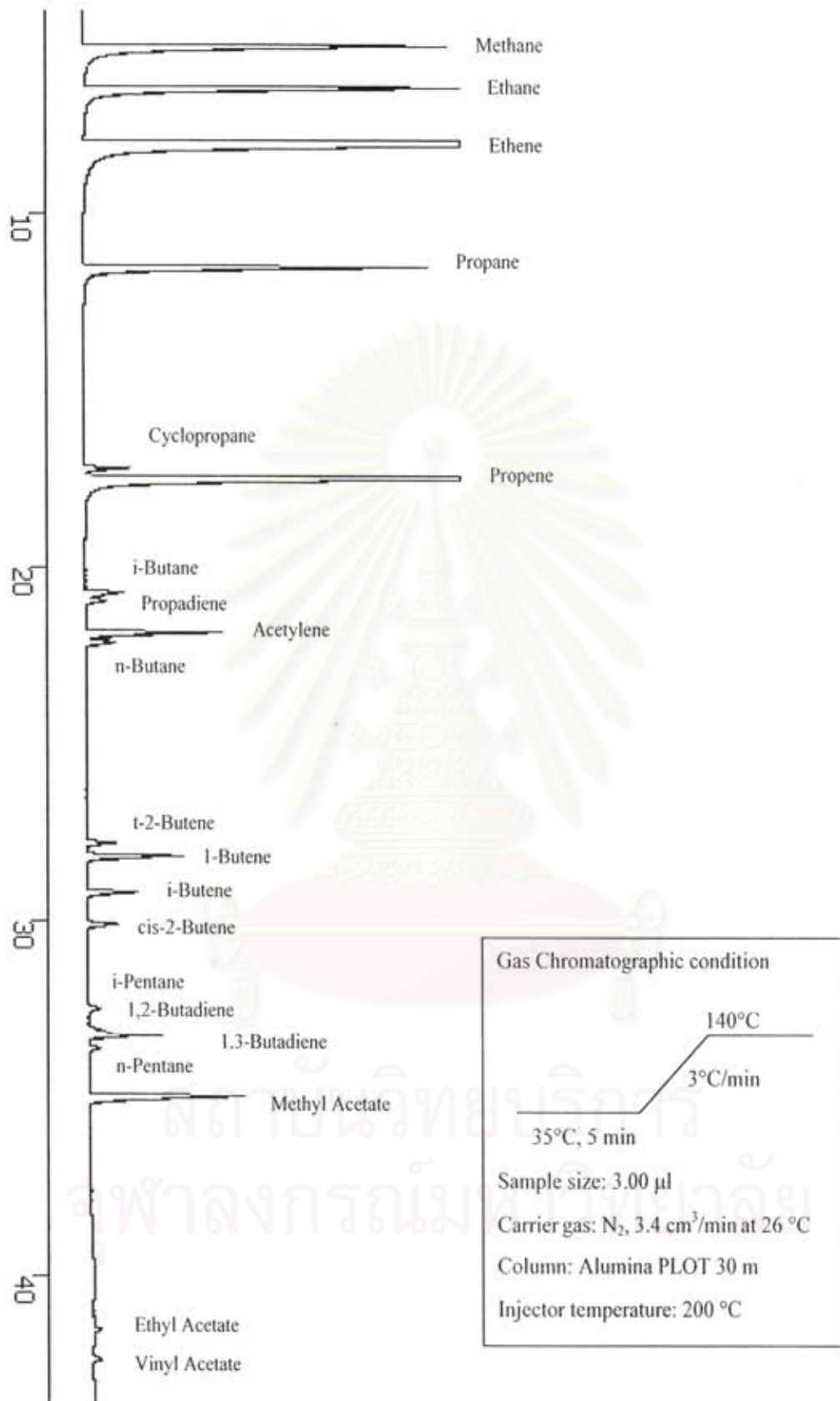
a = Peak area of X in standard gas or liquid fraction

b = % molar of X in standard gas or liquid fraction

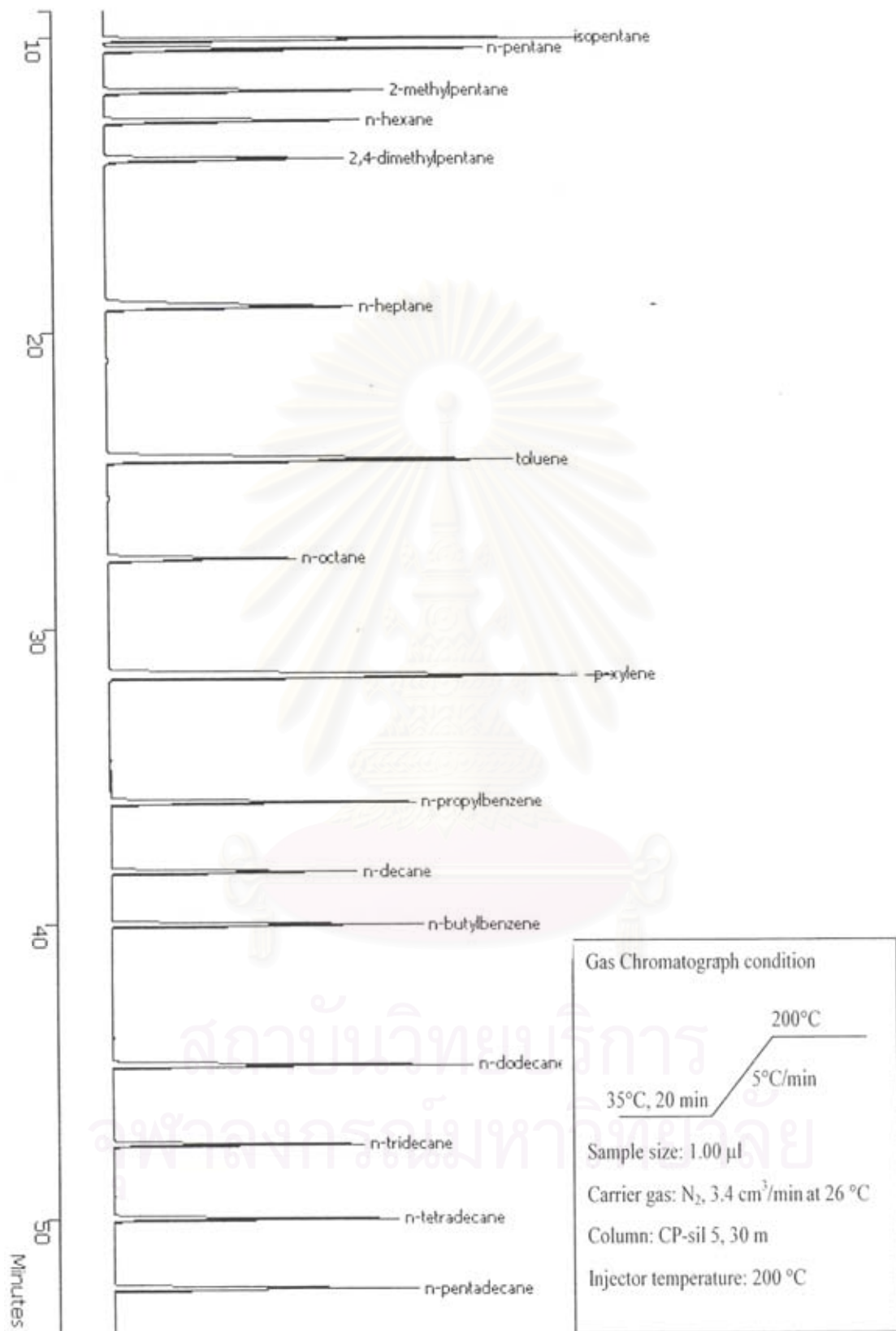
c = Peak area of X in sample products



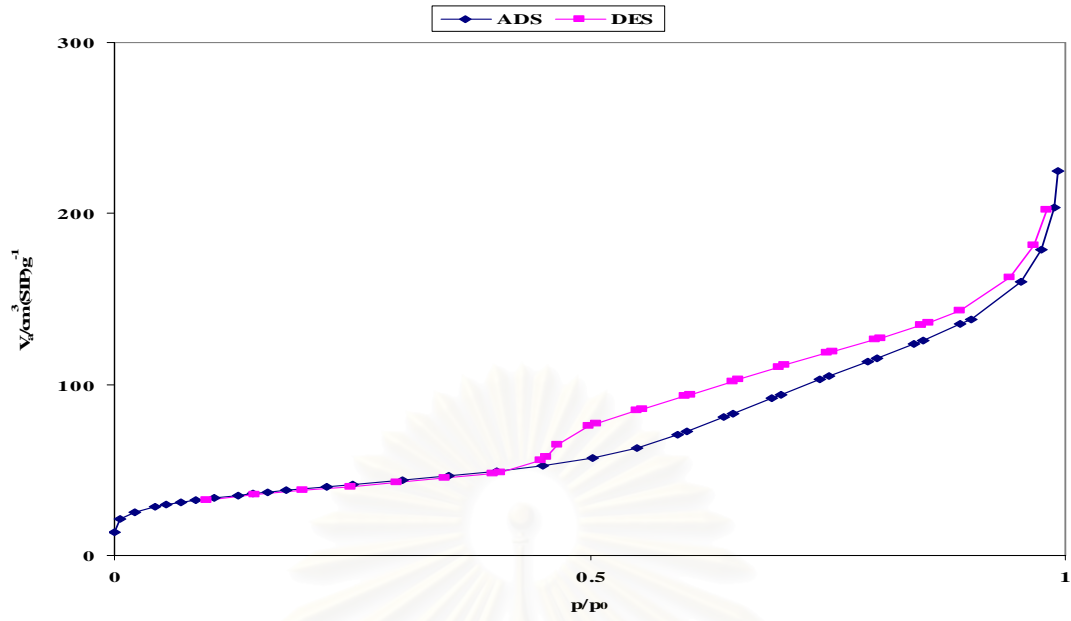
สถาบันวิทยบริการ
จุฬาลงกรณ์มหาวิทยาลัย



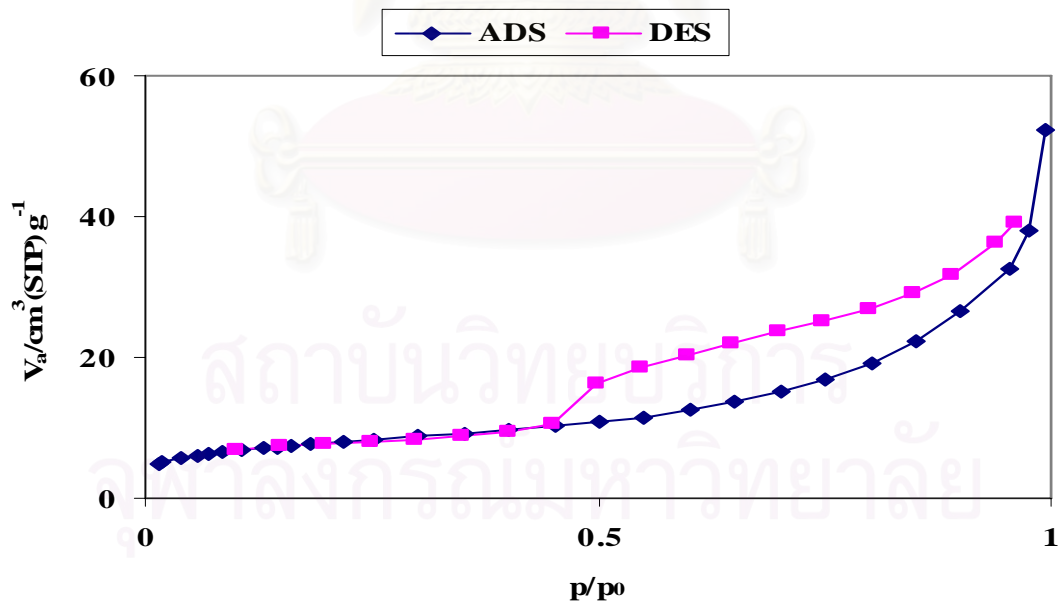
FigureA-1 Gas chromatogram of standard mixture gas



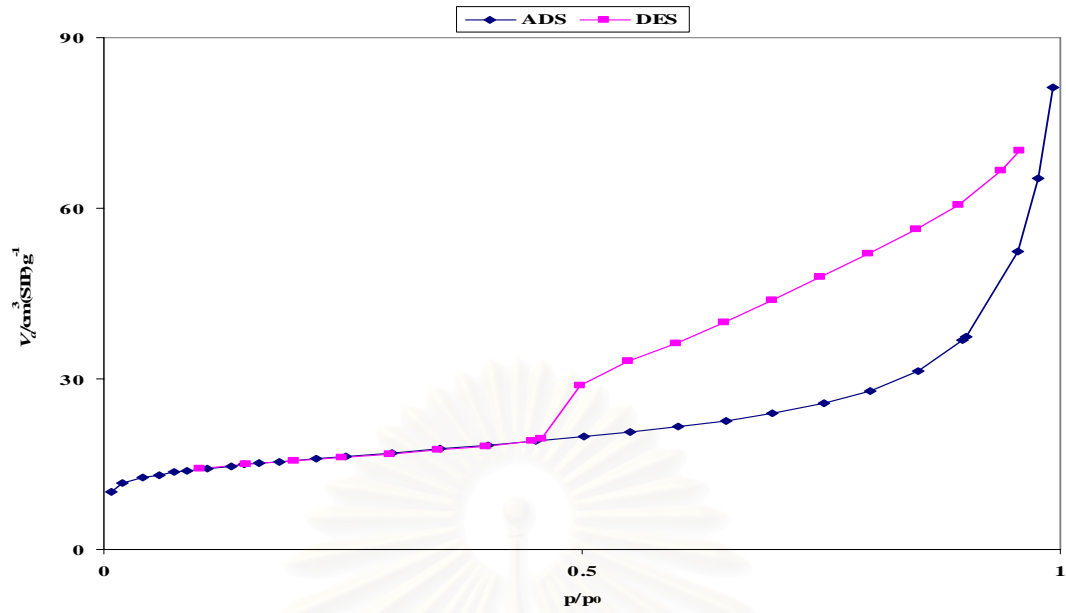
FigureA-2 Liquid chromatogram of standard gasoline (SUPELCO)



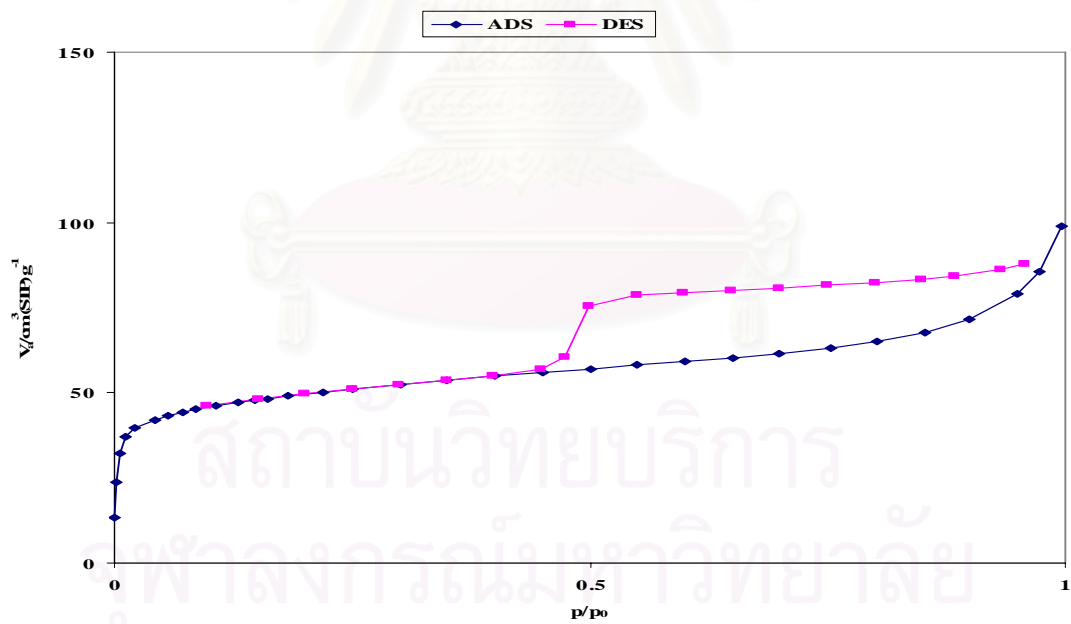
FigureA-3 N₂ adsorption-desorption isotherm of Al₂O₃



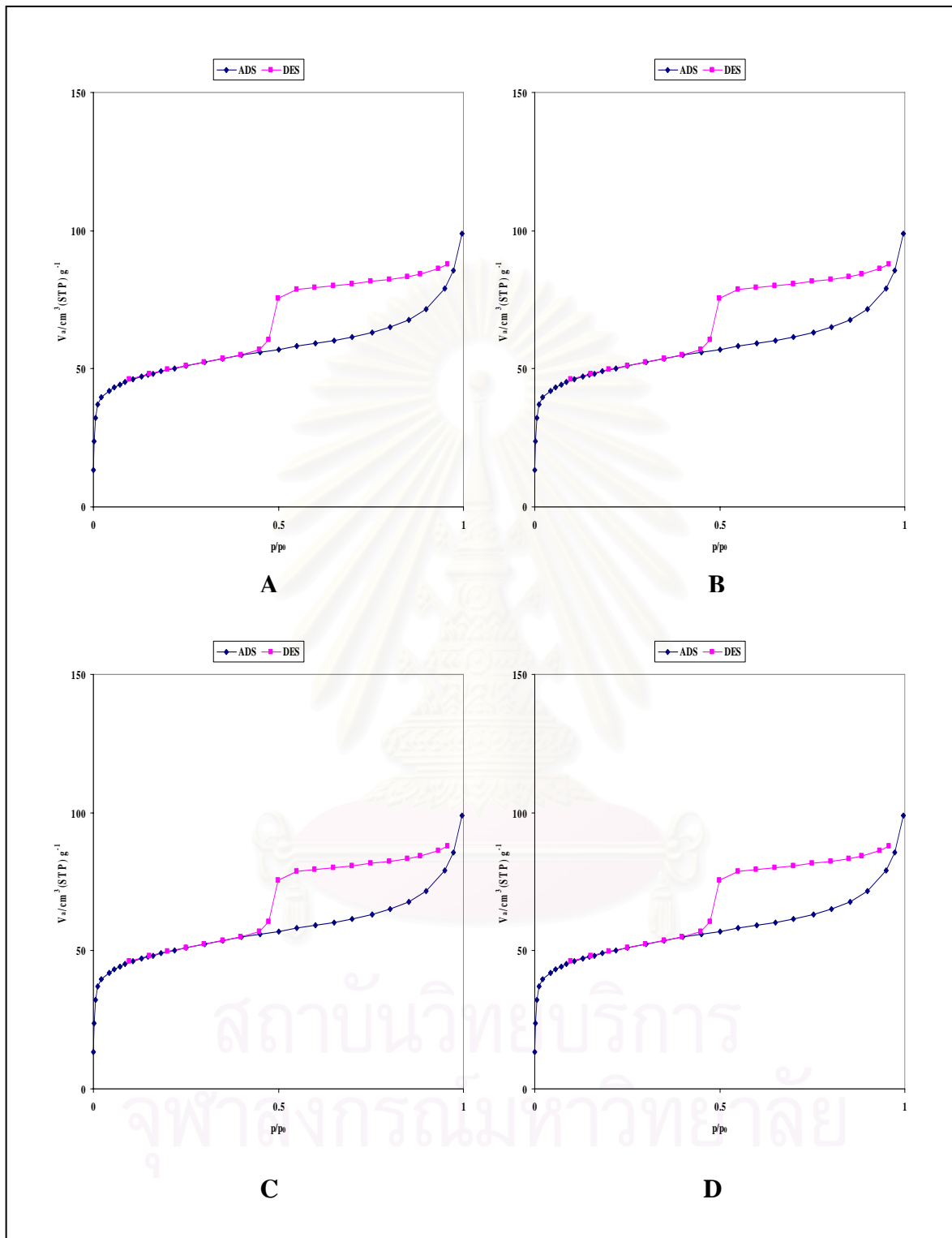
FigureA-4 N₂ adsorption-desorption isotherm of ZrO₂



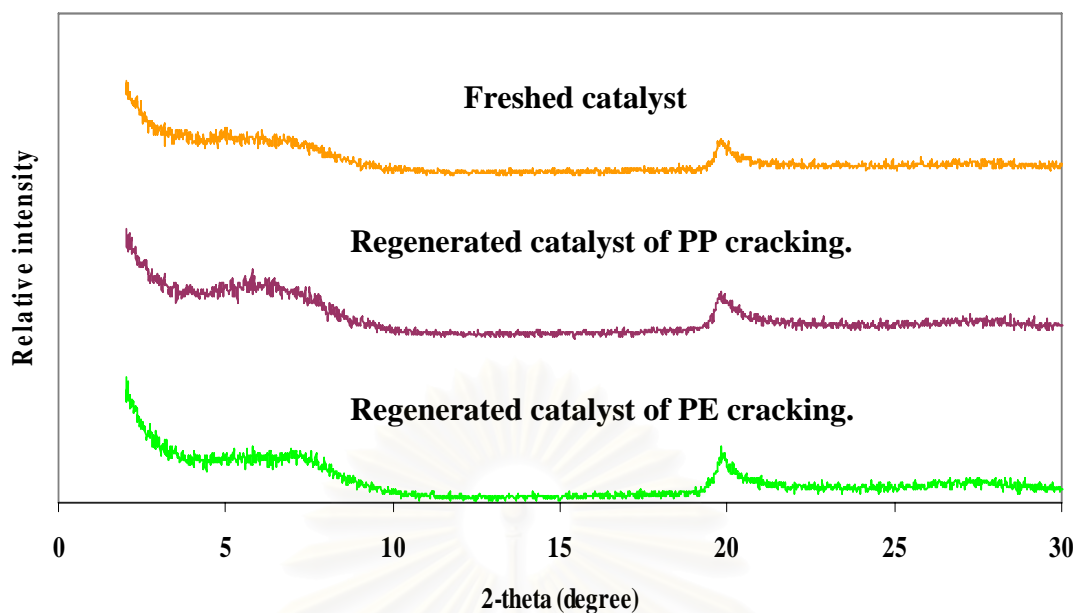
FigureA-5 N_2 adsorption-desorption isotherm of raw clay



FigureA-6 N_2 adsorption-desorption isotherm of aluminium oxide-pillared clay



FigureA-7 N_2 adsorption-desorption isotherm of
A). 1.0wt% zirconium/aluminium oxide-pillared clay
B). 2.0wt% zirconium/aluminium oxide-pillared clay
C). 3.0wt% zirconium/aluminium oxide-pillared clay
D). 1.0wt% zirconium/aluminium oxide-pillared clay

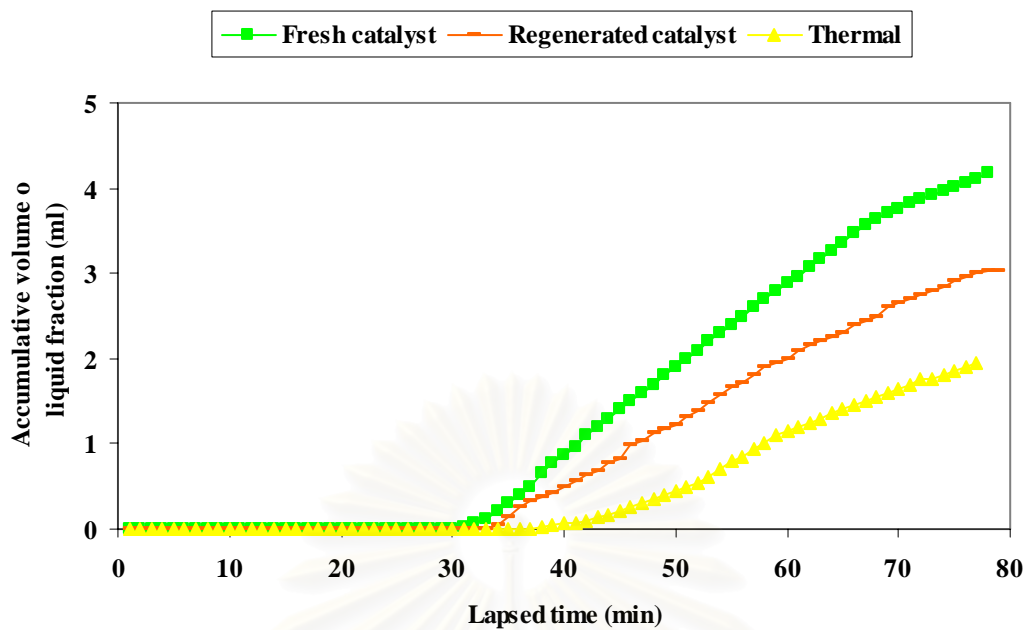


FigureA-8. XRD pattern of freshed and regenerated 2.0 wt% zirconium/aluminium oxide-pillared clay.

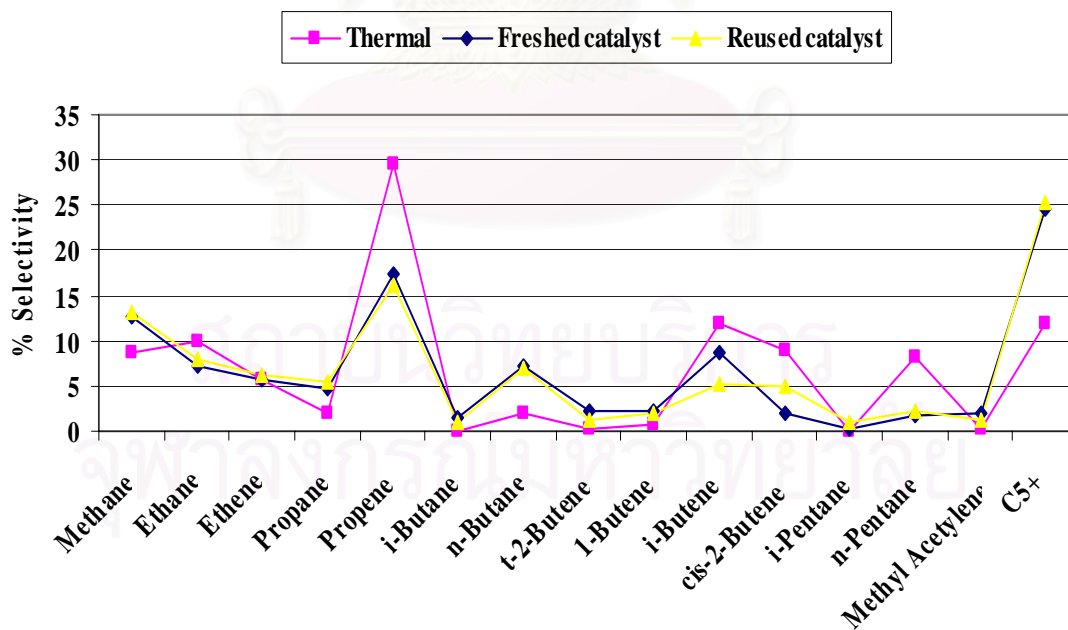
Table A-1. Value of %conversion and %yield obtained by catalytic cracking of PP over sample fresh and regenerated 2.0 wt% zirconium/aluminium oxide-pillared clay.

	Thermal	Freshed catalyst	Regenerated catalyst
% Conversion *	42.86	89.8	78.9
% Yield* 1. gas fraction	26.40	27.53	29.5
2. liquid fraction	28.80	62.27	49.4
3. residue	44.80	10.20	21.1
Liquid fraction density (g/cm ³)	0.72	0.75	0.75

Condition: 10 wt% of catalyst to plastic ratio, N₂ flow of 20 cm³/min and reaction time 1.0 h. *Deviation within $\pm 0.2\%$ for conversion, $\pm 0.2\%$ for yield of gas fraction, $\pm 0.2\%$ for yield of liquid fraction and $\pm 0.2\%$ for yield of residue.



FigureA-9. Accumulative volume of liquid fraction obtained by thermal and catalytic cracking of PP over freshed and regenerated 2.0wt% zirconium/aluminium oxide-pillared clay with various percent catalyst per plastic ratio.



FigureA-10. Distribution of gas fraction obtained by the thermal and catalytic cracking of PP over freshed and regenerated 2.0wt% zirconium/aluminium oxide-pillared clay .

Table A-2. Value of %conversion and %yield obtained by catalytic cracking of PE over sample fresh and regenerated 2.0 wt% zirconium/aluminium oxide-pillared clay.

	Thermal	Freshed catalyst	Regenerated catalyst
% Conversion*	20.20	72.40	64.80
% Yield* 1. gas fraction	20.20	39.20	35.70
2. liquid fraction	-	33.20	29.10
3. residue	79.80	27.60	35.20
Liquid fraction density (g/cm ³)	-	0.77	0.76

Condition: 10 wt% of catalyst to plastic ratio, N₂ flow of 20 cm³/min and reaction time 1.0 h. *Deviation within $\pm 0.2\%$ for conversion, $\pm 0.2\%$ for yield of gas fraction, $\pm 0.2\%$ for yield of liquid fraction and $\pm 0.2\%$ for yield of residue.

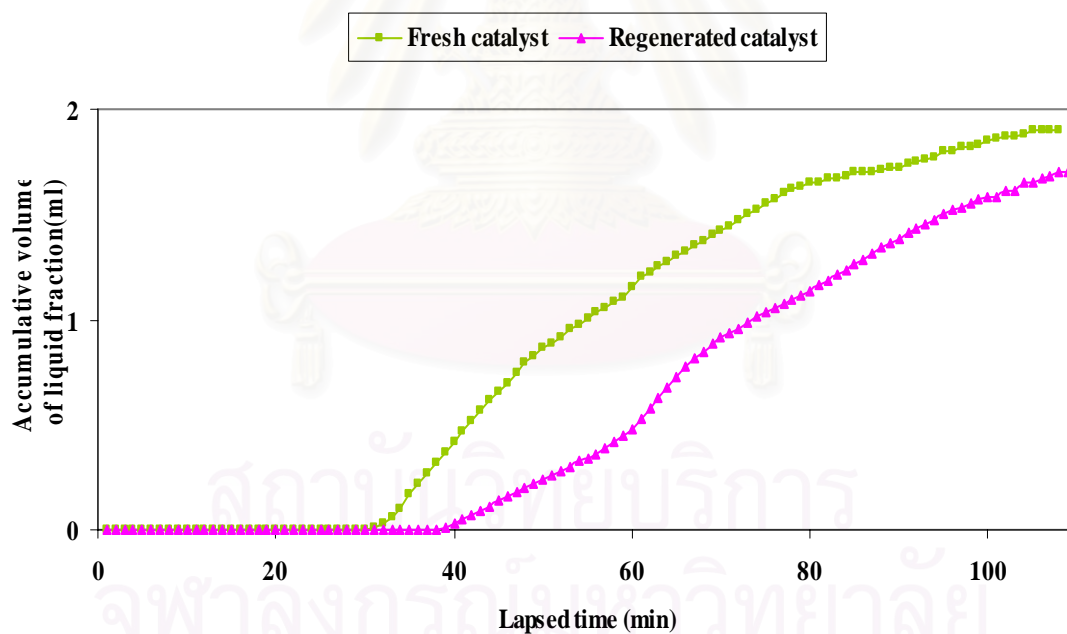
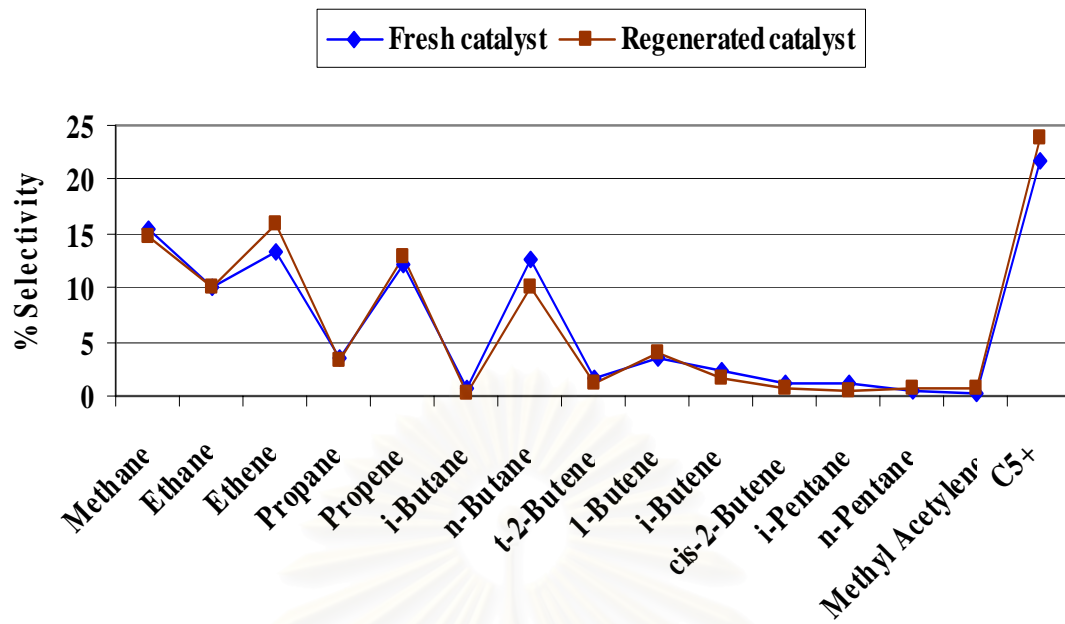


Figure A-11. Accumulative volume of liquid fraction obtained by catalytic cracking of PE over freshed and regenerated 2.0wt% zirconium/aluminium oxide-pillared clay with various percent catalyst per plastic ratio.



FigureA-12. Distribution of gas fraction obtained by the thermal and catalytic cracking of PE over fresh and regenerated 2.0wt% zirconium/aluminium oxide-pillared clay

VITAE

Miss Mahfuzah Masalaeh was born on January 23, 1982 in Pattani, Thailand. She graduated with Bachelor's Degree in Chemistry from Faculty of Science, Srinakharinwirot University in 2005. She continued her study in Petrochemistry and Polymer Science Program, Faculty of Science, Chulalongkorn University in 2005 and completed in 2008. During her graduate studies towards the Master's Degree, she also joined the international conferences and presents her thesis work in the poster form.

Poster Topics

1. Masaleh, M.; Chaianansutcharit, S. Sukpirom, N.; CATALYTIC CRACKING OF POLYPROPYLENE AND POLYETHYLENE USING Al- AND Al/Zr-PILLARED CLAYS. Pure and Applied Chemistry International Conference 2009 (PACCON) Faculty of Science, Naresuan University, Phitsanulok, Thailand, 2009.

Her present address is 130 Moo.1 Sakam, Mayo, Pattani, Thailand 94140

สถาบันวิทยบริการ
จุฬาลงกรณ์มหาวิทยาลัย